

UNCLASSIFIED

AD 411806

DEFENSE DOCUMENTATION CENTER

FOR

SCIENTIFIC AND TECHNICAL INFORMATION

CAMERON STATION, ALEXANDRIA, VIRGINIA



UNCLASSIFIED

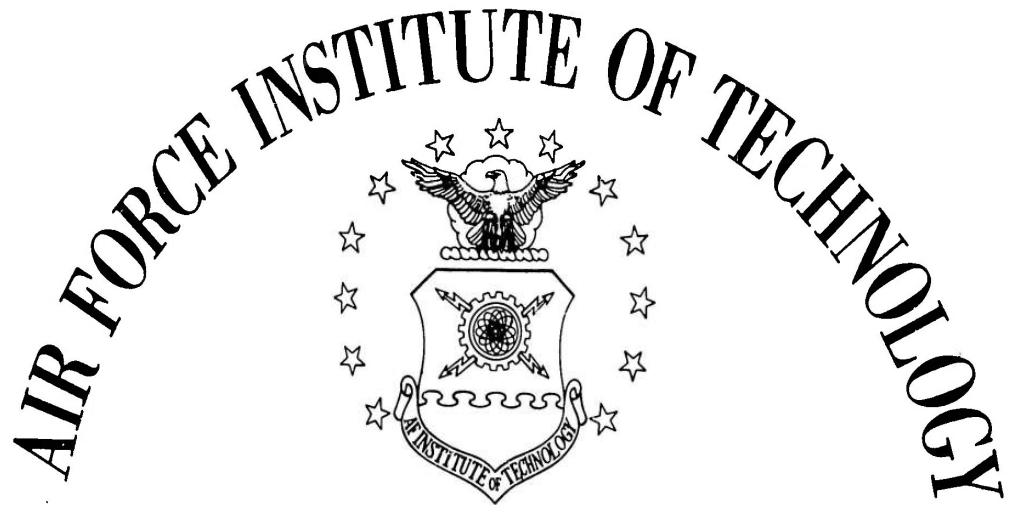
NOTICE: When government or other drawings, specifications or other data are used for any purpose other than in connection with a definitely related government procurement operation, the U. S. Government thereby incurs no responsibility, nor any obligation whatsoever; and the fact that the Government may have formulated, furnished, or in any way supplied the said drawings, specifications, or other data is not to be regarded by implication or otherwise as in any manner licensing the holder or any other person or corporation, or conveying any rights or permission to manufacture, use or sell any patented invention that may in any way be related thereto.

63-4-4

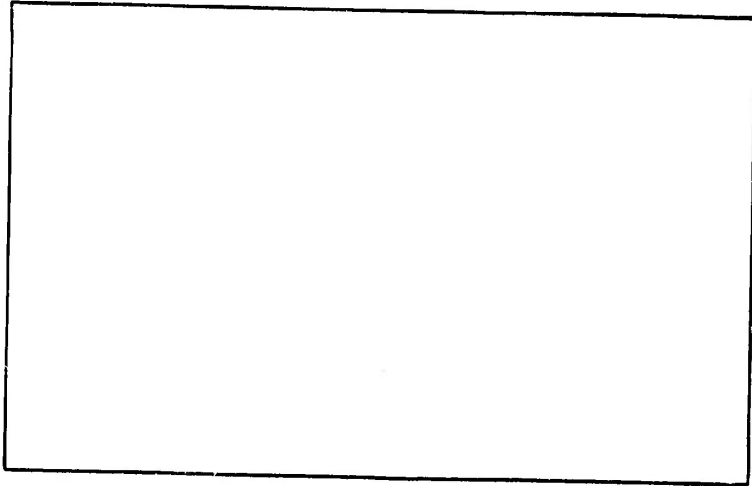
411806

CATALOGED BY DDC 411806

AS AD No. _____

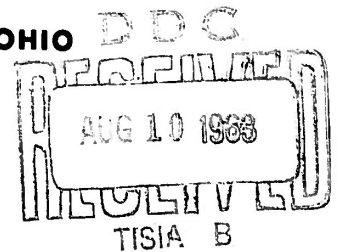


AIR UNIVERSITY
UNITED STATES AIR FORCE



SCHOOL OF ENGINEERING

WRIGHT-PATTERSON AIR FORCE BASE, OHIO



Presented to the Faculty of the School of Engineering
of the Air Force Institute of Technology
Air University
in Partial Fulfillment of the
Requirements for the Degree of
Master of Science

COMPARISON OF HIGH-GAIN-LINEAR AND SELF-
ADAPTIVE FLIGHT CONTROL SYSTEMS FOR A
TYPICAL WINGED RE-ENTRY VEHICLE

Thesis

GGC/EE/63-2

ROBERT E. BEALE
Capt., USAF

FRAZIER J. HELTINGS
Capt., USAF

Graduate Guidance and Control

May 1963

Preface

This report is the result of our comparison of a high-gain-linear design and a self-adaptive design which were applied to a flight-control system of a winged re-entry vehicle. The investigation entailed a linear analysis of the systems when subjected to command and disturbance inputs to the pitch-rate-control loop.

Our purpose was to select a system based on the comparison of the design techniques, the resulting designs, and the performance of the two systems in the presence of vehicle-parameter variations.

We wish to express our gratitude to Lt. Edwin B. Stear of the Flight Control Laboratory, Aeronautical Systems Division, and to I. M. Horowitz of Hughes Research Laboratory, Hughes Aircraft Company, for their assistance during the study. We would further like to acknowledge the support and help given us by Lt. Col. John H. Blakelock, our Faculty Thesis Advisor.

Frazier J. Hellings

Robert E. Beale

Contents

| | Page |
|---|------|
| Preface | ii |
| List of Figures. | v |
| Abstract | viii |
| I. Introduction. | 1 |
| II. Vehicle Dynamics and System Hardware. | 7 |
| Vehicle Dynamics | 7 |
| Hardware | 8 |
| Assembled Components | 12 |
| Response Criteria. | 14 |
| III. The Self-Adaptive System. | 16 |
| Principles of Design | 16 |
| Design Analysis. | 20 |
| Computer Simulation. | 35 |
| IV. The High Fixed-Gain Linear System | 48 |
| Design Principles. | 48 |
| Root-Locus Method. | 53 |
| Frequency-Response Method. | 71 |
| Computer Simulation. | 76 |
| V. Comparison of the Systems and Conclusions | 94 |
| Comparison of the Systems. | 94 |
| Conclusions and Recommendations. | 101 |
| Bibliography | 103 |
| Appendix A: Bode's Fundamental Feedback Theorems Using Control Theory Terminology | 104 |
| Appendix B: Analog Computer Circuits for Simulation of Vehicle Characteristics. | 108 |
| Appendix C: Analog Computer Circuit for Simulation of the Self-Adaptive Pitch-Rate Control System. | 112 |
| Appendix D: Location of Dominant Closed-Loop Poles for the Fixed-Gain Design. | 115 |

| | Page |
|--|------|
| Appendix E: Analog Computer Circuit for Simulation of the High-Gain-Linear System from the Root-Locus Method of Design | 118 |
| Appendix F: Analog Computer Circuit for Simulation of the High-Gain-Linear System from the Frequency-Response Method of Design | 120 |
| Vita (Hellings). | 122 |
| Vita (Beale) | 123 |

List of Figures

| Figure | Page |
|---|------|
| 1 Pole-Zero Plot of Vehicle Dynamics. | 9 |
| 2 Block Diagram Showing Disturbance Input | 10 |
| 3 Block Diagram of Uncompensated System | 12 |
| 4 Uncompensated System Pole-Zero Plot | 13 |
| 5 Region of Exclusion for a Dominant Pair of Poles. | 15 |
| 6 Feedback System with Model Prefilter. | 17 |
| 7 Root Locus Diagram of Self-Adaptive System for Condition Three | 21 |
| 8 Root Locus Plot of Self-Adaptive System at Flight-Condition Six. | 22 |
| 9 Log-Magnitude Diagram of Closed-Loop Response from Eq (16). | 27 |
| 10 Log-Magnitude Diagram of the Closed-Loop with Feedback Compensation | 28 |
| 11 Block Diagram of the Self-Adaptive Pitch-Rate Control System. | 29 |
| 12 Exploded Root Locus Diagram Near Origin | 33 |
| 13 Closed-Loop Pole-Zero Plot for Disturbance Input. | 34 |
| 14 Response of the Self-Adaptive System for Flight- Condition One | 37 |
| 15 Response of the Self-Adaptive System for Flight- Condition Two | 39 |
| 16 Response of the Self-Adaptive System for Flight- Condition Three | 40 |
| 17 Response of the Self-Adaptive System for Flight- Condition Four. | 41 |
| 18 Response of the Self-Adaptive System for Flight- Condition Five. | 43 |

| Figure | Page |
|--|------|
| 19 Response of the Self-Adaptive System for Flight-Condition Six | 44 |
| 20 Feedback Control Loop | 49 |
| 21 Single-Degree-of-Freedom Configuration. | 52 |
| 22 General Location of the Compensator Poles | 58 |
| 23 Open-Loop Pole and Zero Locations Near the Origin for Flight-Conditions One, Two, and Three | 60 |
| 24 Locus of Complex-Compensator-Pole Positions | 64 |
| 25 High-Gain System Design by Root-Locus Analysis. | 66 |
| 26 Loci from the Compensator Poles | 68 |
| 27 Dominant Roots of the Fixed-Gain System | 69 |
| 28 Variation in the Asymtotic Closed-Loop Bandwidth. | 70 |
| 29 Log-Magnitude Curves for Equation (32). | 73 |
| 30 Phase-Angle Curves for Equation (32). | 74 |
| 31 Log-Magnitude Curves for the Compensated Feedback Loop. | 77 |
| 32 Phase-Angle Curves for the Compensated Feedback Loop. | 78 |
| 33 High-Gain System Design by the Frequency-Response Method. | 79 |
| 34 Response of the High-Gain-Linear System with $K_f=2.52$ | 80 |
| 35 Computer Circuit for the Far-Out Compensator Poles. | 82 |
| 36 Change in the Log-Magnitude of the Compensator with the Final Compensation. | 84 |
| 37 Change in the Phase Angle of the Compensator with the Final Compensation | 85 |
| 38 Response of the High-Gain-Linear System for Flight-Condition One ($K_f = 10$). | 87 |
| 39 Response of the High-Gain-Linear System for Flight-Condition Two ($K_f = 10$). | 88 |
| 40 Response of the High-Gain-Linear System for Flight-Condition Three ($K_f = 10$). | 89 |

| Figure | Page |
|--|------|
| 41 Response of the High-Gain-Linear System for Flight-Condition Four | 90 |
| 42 Response of the High-Gain-Linear System for Flight-Condition Five | 91 |
| 43 Response of the High-Gain-Linear System for Flight-Condition Six. | 92 |
| 44 Open-Loop Bandwidth of the Self-Adaptive Feedback Loop. | 95 |
| A.1 Single Input Feedback Loop. | 104 |
| A.2 Two Input Feedback Loop | 106 |
| B.1 Computer Circuit for Vehicle Simulation | 108 |
| B.2 Computer Diagram of the Vehicle for Flight-Condition One. | 109 |
| B.3 Computer Diagram of the Vehicle for Flight-Condition Two. | 109 |
| B.4 Computer Diagram of the Vehicle for Flight-Condition Three. | 110 |
| B.5 Computer Diagram of the Vehicle for Flight-Condition Four | 110 |
| B.6 Computer Diagram of the Vehicle for Flight-Condition Five | 111 |
| B.7 Computer Diagram of the Vehicle for Flight-Condition Six. | 111 |
| C.1 Computer Diagram for the Self-Adaptive System | 113 |
| D.1 Intersection Points of the Root Loci Crossing into the Unit Circle. | 116 |
| E.1 Computer Diagram for the Root Locus Design. | 119 |
| F.1 Computer Diagram of the High-Gain-Linear System Designed by the Frequency Response Method | 121 |

Abstract

The primary advantages of feedback control systems have been sacrificed to some extent in the design of self-adaptive flight control systems. To establish the differences between self-adaptive and normal linear designs, both systems are applied to the problem of controlling the short-period dynamics of the X-15 research vehicle in the altitude range of sea level to 140,000 feet at speeds from Mach 0.2 to Mach 6. The self-adaptive system studied is an early design of the MH-96 Autopilot built by the Minneapolis Honeywell Regulator Company, Aeronautical Division, and the system components, other than compensation, are also used in the high-gain-linear system. The significant features of the self-adaptive system are: (1) the gain changer which varies the forward-branch gain to maintain neutral stability and senses the change in the amplitude of the oscillations as the response of the system changes to control the gain, (2) a prefilter used to establish the response of the system, (3) the rate-gyro and servo characteristics provide necessary compensation, and (4) a piecewise linear analysis of the system is valid. The high-gain-linear system is designed on the basis of selecting the forward-branch compensation so that the system is insensitive to vehicle-parameter variations over the bandwidth of the desired response and a prefilter or feedback-branch compensation is used to obtain the desired command response. The root-locus method is used in the initial design of the system; but, although the design appeared to

be satisfactory, the system could not be simulated on the analog computer. The frequency-response method was used for the design of a second system. The technique was to use fixed compensation to obtain a 10 decibel gain margin for all flight conditions and, with the system simulated on an analog computer, the gain of the system was established so that the response matched the output of the model prefilter very closely. The gain adjustments necessitated changes in the fixed compensation so that, with a fixed gain of 20 decibels, the lowest gain margin is 15 decibels. Computer response data shows that both systems will meet the criteria for command and disturbance inputs. From this linear analysis of design procedures and response data, it is concluded that the high-gain-linear system is preferred to a self-adaptive system; however, an analysis of the effects of system non-linearities and component noise must be made before a fixed-gain system can be applied to the physical problem of widely varying vehicle parameters.

COMPARISON OF HIGH-GAIN-LINEAR AND SELF-ADAPTIVE
FLIGHT CONTROL SYSTEMS FOR A TYPICAL WINGED RE-ENTRY VEHICLE

I. Introduction

Self-adaptive systems have exerted a major influence on the thinking of the flight-control industry since the Flight Control Laboratory at Wright-Patterson Air Force Base initiated an applied research program in 1955. The evaluation of flight-control systems prior to 1955 points out how control engineers progressed from simple fixed-gain-linear designs to the more complex self-adaptive techniques adopted from the research study. Advocates of fixed-gain-linear design are now challenging the change in design philosophy by asserting that no justification was given for adopting the more complex techniques. The motivation behind each argument can best be understood after a brief look at flight-control development.

In the late 1940's and early 1950's aircraft were developed with increased ranges of speed and altitude. The range of dynamic pressures which these aircraft encountered during normal operation caused the aircraft dynamics to change considerably. Control engineers found that the inherent damping of the aircraft's short-period characteristics was insufficient. Stability-augmentation systems were introduced to artificially provide increased damping of the short-period mode. Because of their concern for stable

systems, control engineers designed for maximum gain margin consistent with the desired short-period damping. The large gain margin was provided to maintain system stability and reasonable damping regardless of the variations of the vehicle parameters over the flight profile. With the advent of supersonic aircraft, the range of parameter variations increased tremendously. Designers claimed that if the previous gain margins were to be obtained, the fixed-gain level of the system would have to be set so low that any further unpredicted decrease by the vehicle dynamics would seriously degrade the system response. This is assuming that a limit on the allowable closed-loop bandwidth was to be sustained. Engineers also believed that if system stability was maintained with a high-gain-linear design, the gain of the system would be so high that noise or disturbance would cause saturation.

This was the turning point in design philosophy. The state of the art was such that fixed-gain systems could no longer absorb the vehicle-parameter variations and maintain a satisfactory gain-stability margin and system response. One obvious solution would be to offset the vehicle gain with an inversely varying system gain. This concept led to the air-data gain-scheduled system. This system varied the gain at several points in the system as a function of Mach number, altitude, or dynamic pressure to maintain a desired damping of the short-period mode and an adequate gain margin. With some semblance of control over the vehicle-gain variations, designers began to investigate the advantages of high-gain feedback systems (rejection of disturbance signals and

insensitivity to parameter changes) enjoyed by designers in the telecommunications industry. If maximum gain consistent with stability was to be used in gain-scheduled systems, it would reduce the required number of scheduled-gain changes. Still, the primary considerations were to improve the short-period damping and to preserve a suitable gain margin.

The merits of the gain-scheduled system were soon overcome by its inherent disadvantages. The gain adjustment in this system is an open-loop adjustment. This means that the only change the system senses is the measured air-data supplied by the sensors. Once a gain change is made there is no way for the system to detect whether the closed-loop response was actually improved or not. The system is therefore vulnerable to errors in sensed data, flight data, or those caused by changes in system components. Since the system is only aware of measured air-data and the corresponding programmed-gain adjustment, the above errors could seriously affect the flight characteristics of the vehicle. The second major disadvantage of the gain-scheduled system was the requirement for an accurate gain-adjustment program. To obtain an accurate program required: (1) complete and accurate knowledge of the aircraft's dynamics at all flight conditions, (2) reliable sensors for measuring the air-data for all conditions, (3) calculation of the proper gain settings for sensed air-data, and (4) extensive flight testing to verify the program. As a result the flight-control systems for advanced aircraft were not ready for operation until well after the aircraft was first flown. As the flight domain of

aircraft increased and aerospace planning began, it was apparent that flight-control systems would have to be ready for operation during the first flights and that some vehicles would be operating in environments where air-data measurements are unreliable or in some instances unobtainable. Engineers realized that the disadvantages of gain-scheduled systems were becoming insurmountable.

To avoid the problems of open-loop adjustment and measured air-data, the research program of 1955 initiated the search for a closed-loop method of gain adjustment to provide a more reliable and adaptable flight-control system. As methods of mechanization were recognized, they were called self-adaptive flight-control systems and were classified by definition as systems which change parameters through an internal process to maintain system performance in a changing environment both internal and external to the vehicle under control. In other words, a closed-loop adaptive technique keeps adjusting its parameters until the desired response is reached. At the same time that self-adaptive systems were being investigated, the model pre-filter system came into favor. These two principles were complementary and were soon mated to provide a flight-control system whose dynamics were primarily those of the model while the self-adaptive mechanism maintained a high feedback-loop gain to decrease the sensitivity of the system to changes in vehicle dynamics. One such system which has been successful is described in Reference 11 and will be used for the comparison in this paper. A more complete history of self-adaptive flight-control systems can also be found in this reference.

Horowitz, an advocate of linear design with high fixed gain, challenged the emphasis being placed on self-adaptive control systems (Ref 7). He claimed that the complex mechanization required for self-adaptive systems could not be justified until high-gain-linear design was proved to be incapable of providing the desired flight characteristics. Horowitz points out that the limitations of the fixed-gain system, that was replaced by the gain-scheduled system, applied only to the classical single-degree-of-freedom configuration. With proper design techniques and a thorough understanding of the principles of feedback, he claims that a classical two-degree-of-freedom structure will cope with the problems of sensitivity to parameter variations and disturbances and still have design freedom to meet the response criteria.

The purpose of this thesis is to show by comparison whether the self-adaptive or the high-gain-linear approach is more promising for the design of future flight-control systems. The initial design of the pitch-rate loop (stability-augmentation system) of the MH-96 self-adaptive flight-control system will be compared to a high-gain-linear design to be based on Horowitz' principles. Each system will have the same basic components: vehicle dynamics, servo, actuator, and rate gyro. The compensation and gains to be used will be chosen to suit the particular design.

Chapter II describes the system components and establishes the design criteria. Chapter III contains the design of the self-adaptive system and shows the response obtained from computer simulation. Chapter IV contains the design procedures used to develop

GGC/EE/63-2

the high-gain system and displays the results of the computer simulation. Chapter V discusses the conclusions drawn from the comparison of the design techniques and their associated computer simulations.

II. Vehicle Dynamics and System Hardware

The vehicle dynamics are from preliminary data obtained for the X-15. The associated hardware is that proposed by the Minneapolis-Honeywell Regulator Company, Aeronautical Division, in an early design of the MH-96 self-adaptive flight-control system. The source of this information is Reference 11.

Vehicle Dynamics

The dynamics of the vehicle will be represented by the short-period-mode transfer function (Eq 1).

$$\frac{\dot{\theta}(s)}{\delta_e(s)} = -M_\delta \frac{s + 1/T_a}{s^2 + 2\zeta\omega_a s + \omega_a^2} \quad (1)$$

Data will be taken for six different flight conditions which represent the extremes of the flight envelope in which only the aerodynamic controls of the self-adaptive system operate. Since the objective of the pitch-rate loop is to damp out short-period oscillations, the design and response data obtained will represent the pitch response characteristics of the vehicle satisfactorily. Such a design neglects the possibility of resonance with body-bending modes and control-surface oscillations. These factors are always considered sometime after the preliminary design has been proven to meet the response criteria.

Table I shows the range of values of M_δ , $1/T_a$, $2\zeta\omega_a$, and ω_a^2 for various flight conditions. As can be seen from the table the

Table I

Vehicle Dynamic Data

| Flight Condition | Altitude (feet) | Mach No. | M_δ | $1/T_a$ | $2\zeta\omega_a$ | ω_a^2 |
|------------------|-----------------|----------|------------|---------|------------------|--------------|
| 1 | 0 | 0.2 | 0.22 | 0.0356 | 0.302 | 2.28 |
| 2 | 5,000 | 0.6 | 16.29 | 1.163 | 2.226 | 6.51 |
| 3 | 10,000 | 1.2 | 52.95 | 2.070 | 4.980 | 56.10 |
| 4 | 60,000 | 6.0 | 20.86 | 0.325 | 0.652 | 18.71 |
| 5 | 100,000 | 4.0 | 2.24 | 0.0366 | 0.0792 | 3.68 |
| 6 | 140,000 | 6.0 | 0.70 | 0.00794 | 0.0165 | 0.65 |

vehicle characteristics vary considerably over the flight regime. The natural frequency (ω_a) of the vehicle changes in the ratio of 9.3 : 1 and the damping ratio varies as 42.7 : 1, but the largest change occurs in the control-surface effectiveness (M_δ) which changes in the ratio of 240 : 1. The change in frequency and damping ratio can be seen more easily in the pole-zero plot of Figure 1.

Hardware

The first component required to complete the pitch-rate loop is a control-surface actuator. The actuator must provide the necessary power to overcome the high hinge moments to be expected in such a system and still have a reasonably fast response. The actuator selected by the aircraft designers to meet these criteria has the transfer function of Equation (2).

$$\frac{\delta_e(s)}{X_a(s)} = \frac{6.67}{s+6.67} \quad (2)$$

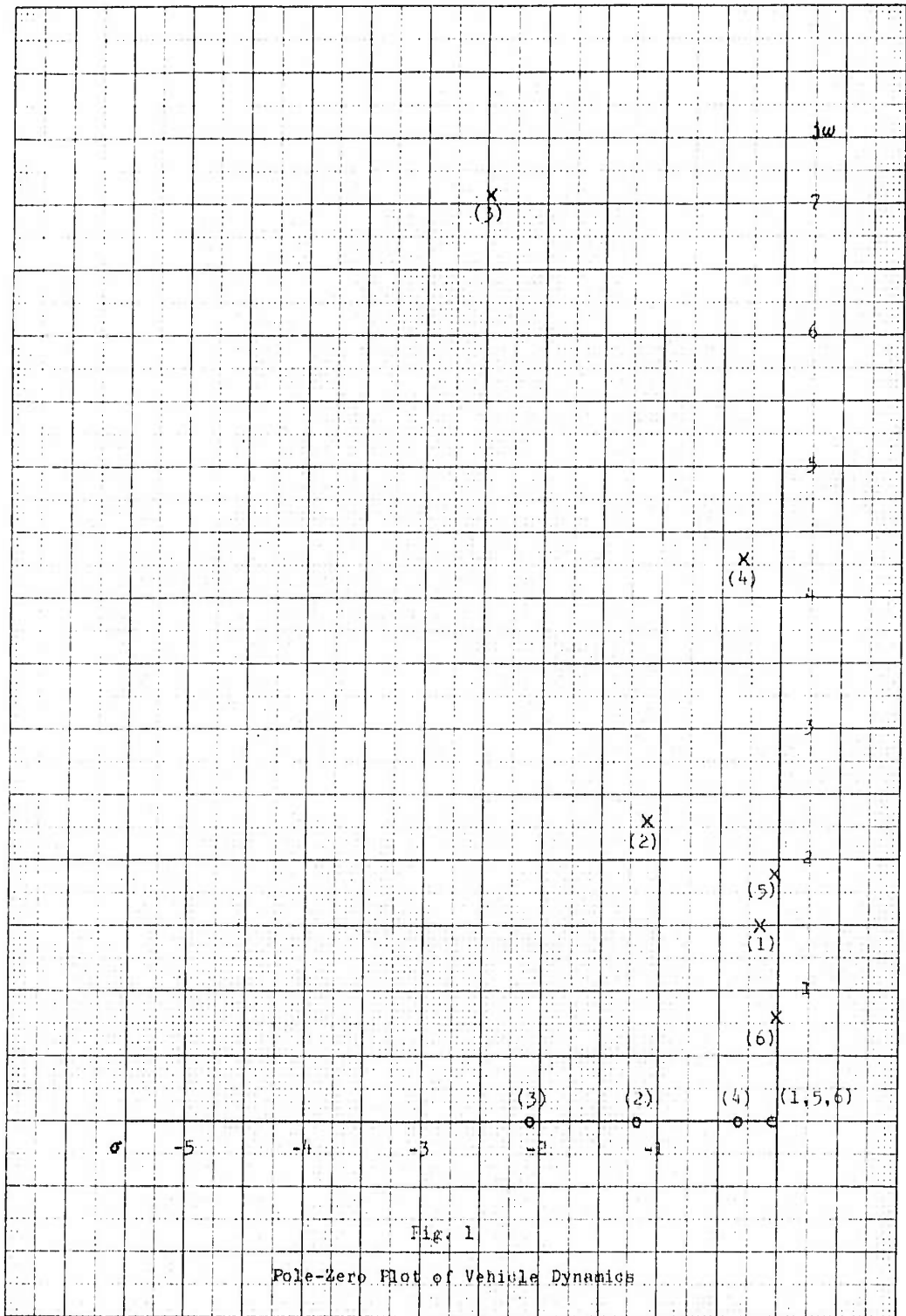


Fig. 1

Pole-Zero Plot of Vehicle Dynamics

This shows the relationship between control-valve position and commanded elevator angle.

The next item required is a control servo which will position the actuator control valve. The selection of this servo is based upon the requirements of the self-adaptive system. The servo must have a high natural frequency compared to the vehicle dynamics and must have reasonably high damping. These characteristics are necessary so that the gain controller will operate at maximum effectiveness. This point will be discussed further in Chapter III. The second order characteristics selected are a natural frequency of 60 radians and a damping ratio of 0.5. Although these characteristics are selected to meet the requirements of the self-adaptive system, they should not pose a problem in the design of the high-gain-linear system.

In addition to the second-order poles a proportional-plus-integral function is included in the servo. This feature makes the system a type one system (ref 4:126) and results in zero steady-state error in the response to a step command input. The other effect is to cause the steady-state response to a step disturbance input to be zero. This can be shown by analyzing the simple block diagram in Figure 2 with an integrator in the forward branch. With R equal to

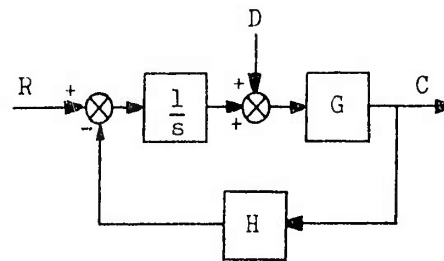


Fig. 2

Block Diagram Showing
Disturbance Input

zero, the closed-loop transfer function for disturbance input (D) is

$$\frac{C}{D} = \frac{G}{1+GH} = \frac{Gs}{s+GH} \quad (3)$$

The final-value theorem with D equal to a unit step shows the steady-state response to be

$$C(t)_{ss} = \lim_{s \rightarrow 0} s \left[\frac{1}{s} \cdot \frac{Gs}{s+GH} \right] = 0 \quad (4)$$

Thus, if the feedback element is not a differential device, the steady-state response to a step disturbance input will be zero provided the forward branch, excluding the controlled element, has at least one pure integrator.

The complete transfer function of the servo for commanded actuator-control-valve position with respect to the servo input voltage is

$$\frac{X_a(s)}{e_s(s)} = \frac{3600 (s+K_i)}{s(s^2+60s+3600)} \quad (5)$$

where K_i is the gain of the integrator of the proportional-plus-integral function. The value of K_i will be established to provide the desired compensation in both the self-adaptive and high-gain-linear systems (Chapters III and IV).

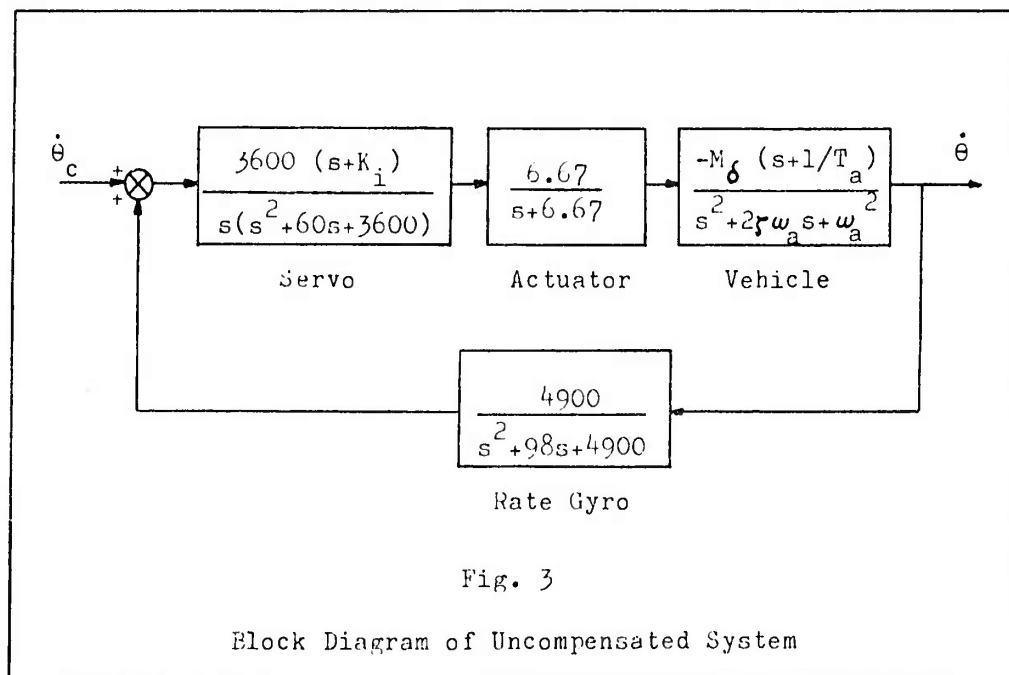
The last piece of hardware required to complete the pitch-rate loop is a sensor that will sense pitch rate and feed back a proportional voltage. For this purpose a rate gyro with the following transfer function was selected:

$$\frac{e_r(s)}{\theta(s)} = \frac{4900}{s^2 + 98s + 4900} \quad (6)$$

The reason for the high damping ratio and high natural frequency is again dictated by the self-adaptive system. As with the servo, these characteristics should pose no problem to high-gain-linear design.

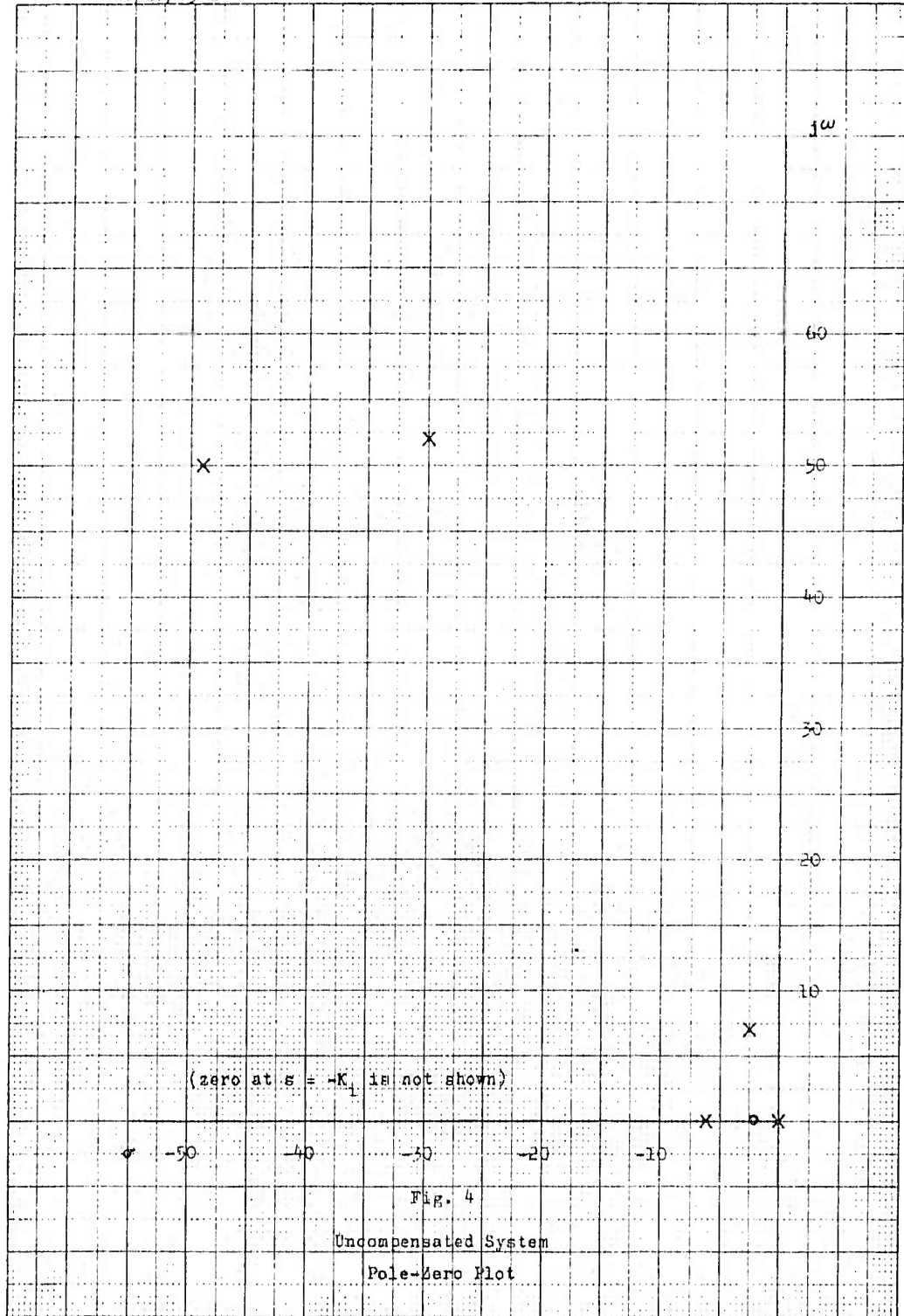
Assembled Components

With the components selected and the vehicle dynamics determined, the system can now be assembled. The job remaining will be to design a compensator to be added to the system to yield the desired flight characteristics. Figure 3 is a block diagram of



the system without compensation. The relationship of the various components can be seen more readily in the pole-zero plot of Figure 4. The vehicle dynamics used for this plot are for

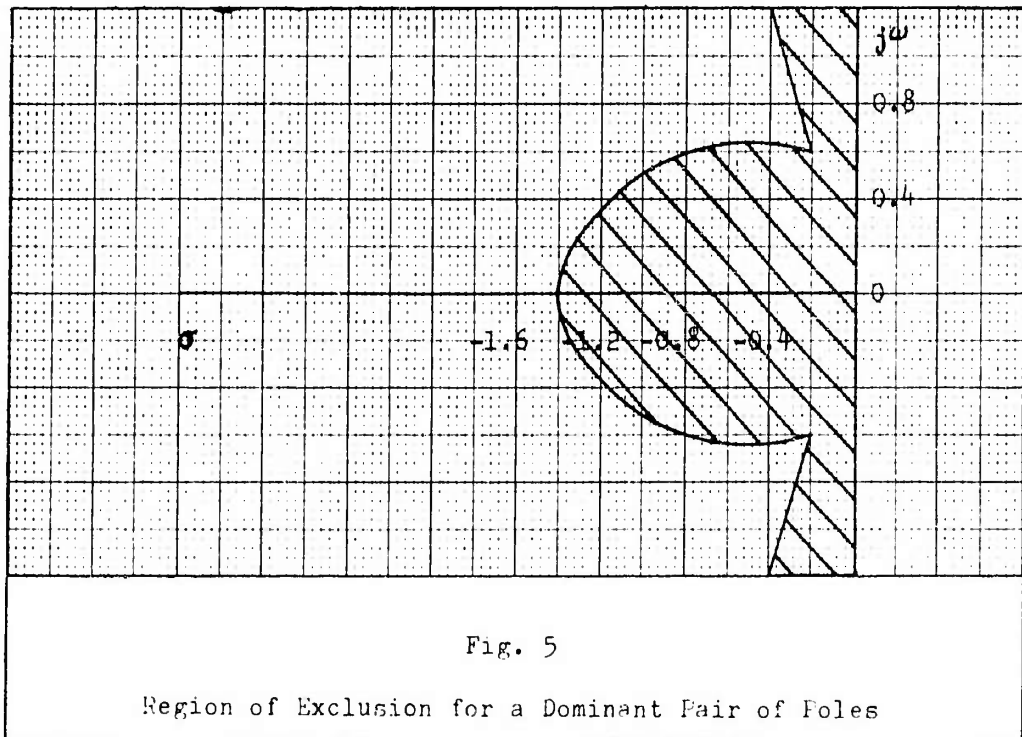
WIC/EF/63-2



condition three and the location of the real zero based on the value of K_i is still to be chosen.

Response Criteria

The response criteria are specified by limitations on the response to command and disturbance inputs. These limitations are based on pilot-preference data such as that presented in Reference 9: Appendix E. First, the response to a step command must have less than 25 percent overshoot and must damp to one-eighth amplitude within one cycle. Additionally, the response must rise to within 90 percent of the commanded value in less than three seconds. Second, gust disturbance response is to be damped to less than one-fourth amplitude in one cycle. From these criteria the minimum damping ratio of the closed loop system for both command and disturbance inputs can be determined by making use of subsidence ratio data (Ref 4:479). The minimum closed-loop-damping ratio for command inputs is about 0.32 and for disturbance inputs is about 0.22. Although these values are based upon a dominant second order approximation for the pitch-rate loop, the specifications do not preclude the possibility of first-order contributions to the total response. The three-second-response criterion also limits the minimum natural frequency that a dominant second-order response may have. The natural frequency which meets the criterion is dependent on the damping ratio. For this reason the envelope of minimum natural frequencies can be shown most clearly in the s plane along with the minimum damping ratio (Fig.5).



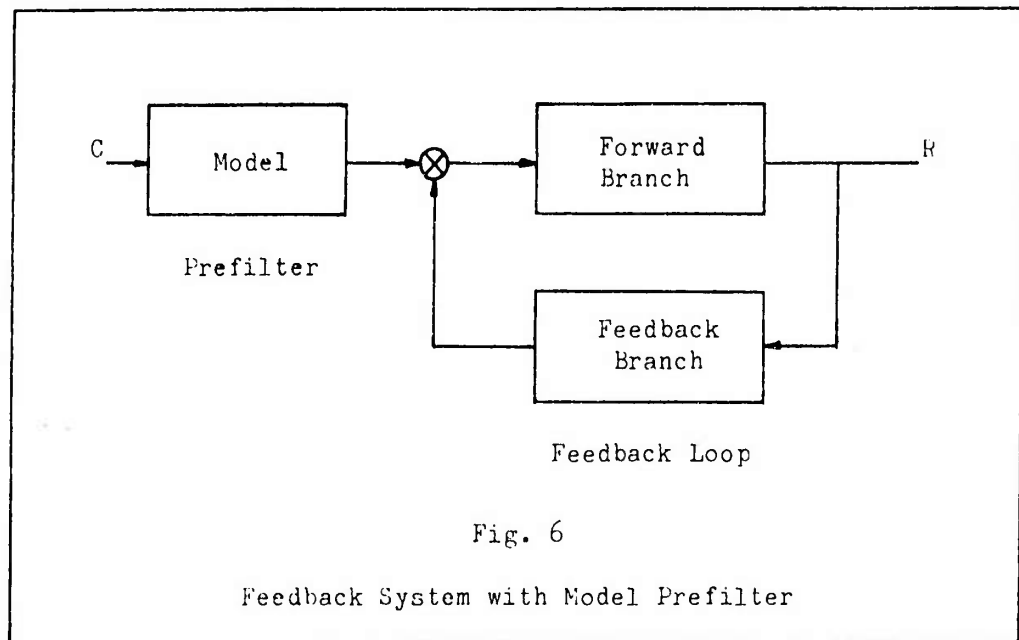
This data is calculated from second-order step-response characteristics in Reference 4:59. Dominant complex-conjugate poles must be outside the shaded portion of the figure to meet the response criteria.

III. The Self-Adaptive System

The self-adaptive pitch-rate control system to be studied is an early design for the MH-96 Autopilot. The principal reason for using the early design is to obtain a more realistic comparison with the high-gain-linear system. This places each design at approximately the same stage of development in designing a complete flight-control system. No attempt will be made to improve the basic design in this thesis because several changes have been made by the manufacturer to cope with problems encountered in the X-15 program. When the changes in the system seem appropriate to the discussion in this thesis, they will be mentioned. More information on these developments can be obtained from References 3 and 12.

Principles of Design

If the response to command inputs is considered, a perfectly designed pitch-rate loop for an autopilot would have the same closed-loop transfer function for every flight condition. This is to say that the closed-loop is completely insensitive to vehicle-parameter variations. Although it is very improbable that such a system could be designed for a vehicle with such wide parameter variations as those of the X-15, the model concept allows a system design which will be very close to optimum. Such a system uses a model or pre-filter (Fig. 6) having the transfer function desired from the system, and the feedback loop is designed to have a closed-loop bandwidth several times greater than the model for all flight



conditions. Thus the dominant response of the system is that of the model.

The model initially selected for use in the MH-96 system had the following transfer function:

$$\frac{4}{s^2 + 4s + 4} \quad (7)$$

However, when piloted simulator studies were made a faster response was desired so the model was changed to

$$\frac{2}{s+2} \quad (8)$$

This is the model which will be used throughout the work which follows. The change in model tends to improve the response of the system by decreasing the rise time.

Several factors influence the design of the feedback loop and since the design analysis of the self-adaptive system will be carried out by the root-locus method, the principles of design for the feedback loop will be expressed in root-locus terminology. First, the vehicle dynamics fall into a region near the model pole. To obtain the dominance of the model, the residues of the closed-loop poles on the loci near the model pole must be negligibly small. This result can be achieved if the compensator and aircraft zeros are near the open-loop poles and a high-gain design is used for the feedback loop. Second, to maintain the stability of the system and to keep the gain as high as possible for all conditions, a gain changer will be placed in the system. The use of the gain changer is based on the premise that the gain can be changed faster than the vehicle parameters change. (This has worked out in practice except under maximum acceleration of the X-15. When this condition exists, the gain changer lags but the system response is still satisfactory.) The gain changer is a linear attenuator that changes gain as a function of the amplitude of the oscillations (limit cycle) which occur when the system begins to go unstable. In the MH-96 system the limit cycle is sensed at the output of the servo and fed through a bandpass filter. The filter attenuates all signals outside the band of limit-cycle frequencies. From the filter the limit cycle goes to an absolute value circuit and on to a comparator where the voltage is compared to a set-point value. The error generated is either positive or negative depending on whether the amplitude of the limit cycle is greater or less than the set point.

The error from the comparator drives the gain controller. For a positive error the gain is decreased. This corresponds to a limit-cycle amplitude greater than the set point. For a negative error the gain is increased. In this manner the gain changer keeps the gain of the feedback loop at the point of neutral stability. If the system parameters change so that the feedback loop becomes less stable, the amplitude of the limit cycle increases beyond the set point and drives the gain down. Conversely, if the amplitude of the limit cycle decreases below the set point, the gain increases. Thus the amplitude of the limit cycle is dependent upon the set-point voltage. The amplitude of the limit cycle is controlled so that the aircraft response to the limit cycle is generally below the pilot's threshold. A more detailed analysis of the operation of the gain changer can be found in Reference 5. Since the gain changer maintains the gain for neutral stability with only slight variations, the design of the self-adaptive feedback loop can be approached with linear techniques.

The use of the gain changer places additional restrictions on the loci which cross the imaginary axis. In order to make the pass band of the filter as small as possible, the loci must cross the axis at approximately the same frequency for all flight conditions. The loci must also cross the axis at a low slope so that as the gain changes, the frequency of the limit cycle will not vary enough to cause the limit cycle to be amplitude modulated by the filter. If this condition exists the gain changer may hunt excessively.

With these principles in mind, the feedback loop of the self-adaptive pitch-rate system can be designed to meet the bandwidth requirements. The principles established so far are based chiefly on obtaining the desired response to command inputs. Disturbance criteria will be investigated after the preliminary design is analyzed.

Design Analysis

To show the effects of the self-adaptive design the flight conditions which represent the extreme excursions of the vehicle dynamics will be used. These are conditions three and six from Table I.

The zeros that shape the loci from the vehicle poles must be placed so that the loci move into a region of high damping where the time constant will be small compared to that of the model. This must be done so that if the residue of the closed-loop poles on these loci becomes large enough to contribute to the closed-loop response, the effect on the total response will be small. The location of these poles is also important when considering disturbance response because the location of the closed-loop poles is the same for both command and disturbance inputs. It was found that the loci could be forced into the real axis to provide maximum damping; therefore, a double zero was placed at $s = -5$ (Fig. 7 and 8). One of these zeros comes from the proportional-plus-integral portion of the servo. The integral gain (K_i) was selected to be five for this system. This makes the servo transfer function (Eq 5)

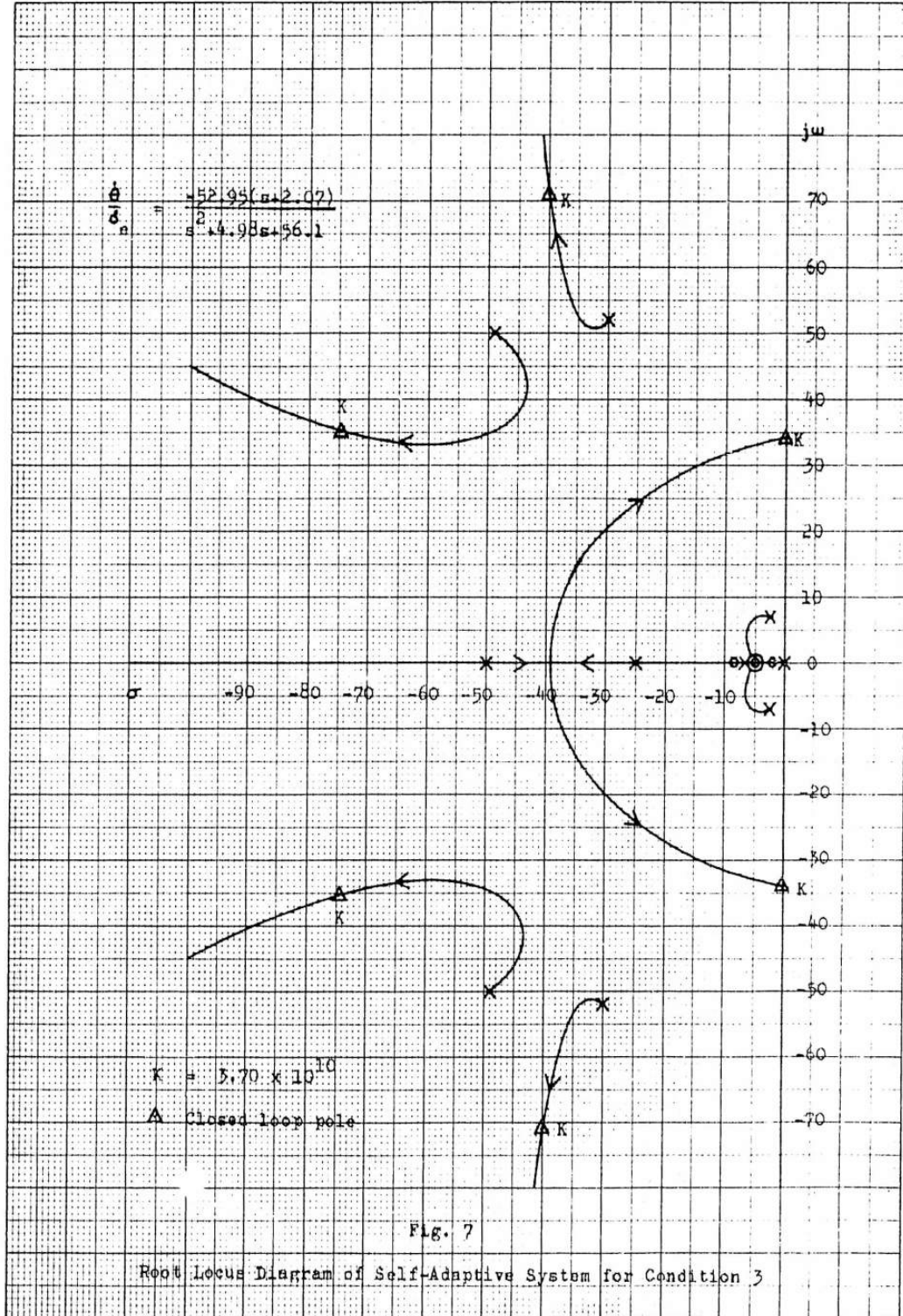
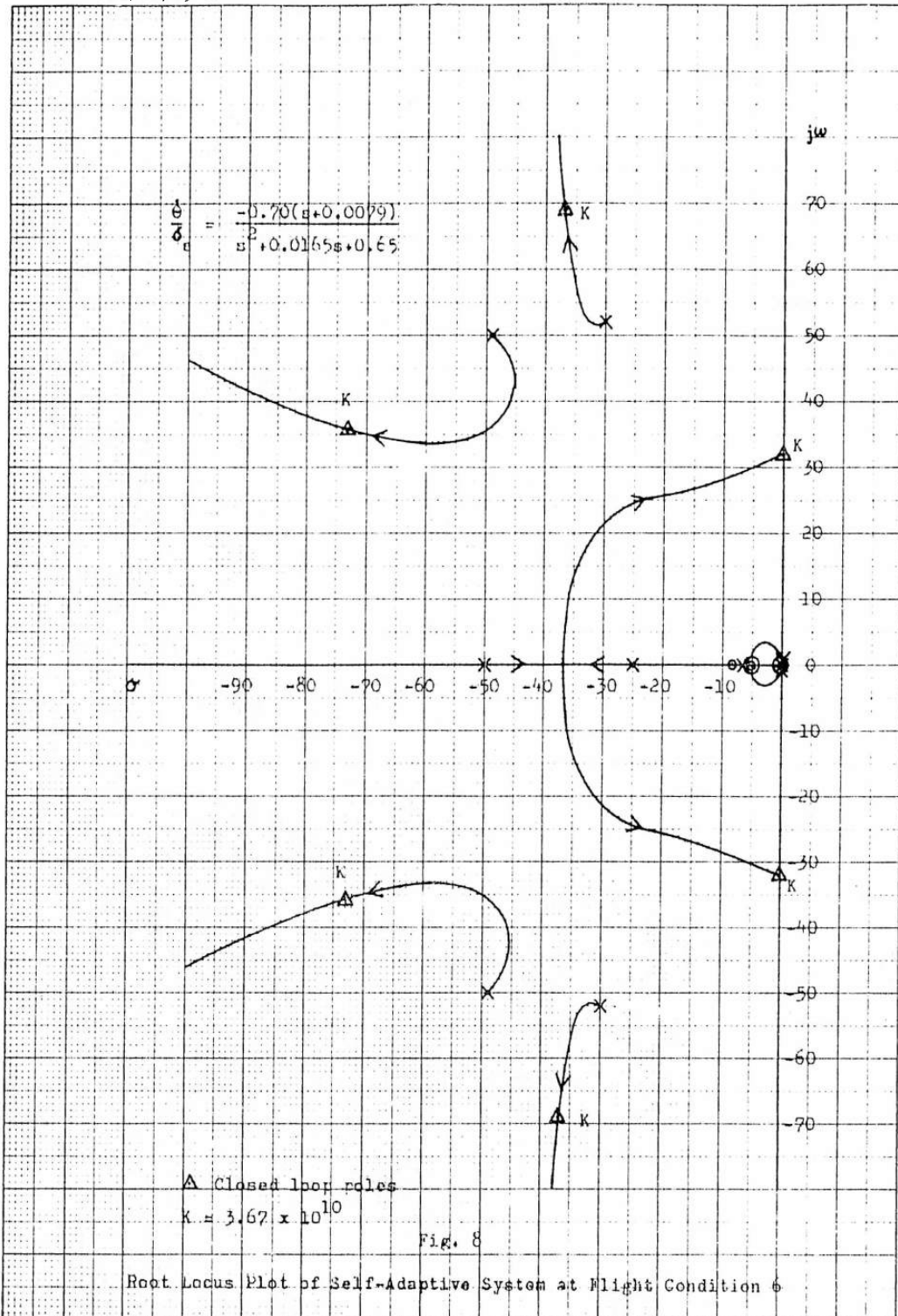


Fig. 7

Root Locus Diagram of Self-Adaptive System for Condition 3



$$\frac{3600 (s+5)}{s(s^2+60s+3600)} \quad (9)$$

The second zero comes from a lead compensator with a pole as far out as the practical limitation of passive lead networks allows. The transfer function of the compensator is

$$\frac{10 (s+5)}{(s+50)} \quad (10)$$

A second lead network is selected so that the breakaway point for the loci which cross the imaginary axis will be as far to the left as possible. The zero of this lead network is placed slightly to the left of the actuator pole. Thus the second lead compensator is

$$\frac{3 (s+8.33)}{(s+25)} \quad (11)$$

The loci of the system is shown in Figures 7 and 8 for flight conditions three and six.

The reason for selecting a servo and rate gyro with high natural frequencies should now be apparent. The frequencies are about 10 times the highest natural frequency of the vehicle. This causes the poles of the servo and rate gyro to be dominant in determining the shape of the root loci that cross the imaginary axis. As a result the shape of these loci for the two extremes of vehicle dynamics is very much the same. The point of neutral stability which determines the limit cycle frequency falls in nearly the same location for both conditions. The values of limit cycle frequencies ($\omega = 32$ and 34 radians per second) will be considered

the bounds of the limit cycle frequency variation because the two cases shown represent the maximum excursion of the vehicle poles and zeros. The choice of damping ratio for the rate gyro and servo is based on a trade off between a low slope at neutral stability and a high static loop sensitivity. The static loop sensitivity is the constant coefficient (K) when the open-loop transfer function is expressed with the coefficients of s equal to unity

$$G(s) H(s) = \frac{K \prod_{m=1}^n (s-z_m)}{s^x \prod_{c=1}^v (s-p_c)} \quad (12)$$

and is the product of the sensitivities (S_1, S_2, \dots, S_k) of the individual components of the system when the transfer functions are as follows:

$$\frac{S_k \prod_{m=1}^n (s-z_m)}{s^x \prod_{c=1}^v (s-p_c)} \quad (13)$$

This design gives slightly more weight to high static loop sensitivity.

The decision to have the loci which break out from the compensator poles cross the imaginary axis is based on more than the low slope principle. The limit-cycle frequency has to be kept below anticipated structural modes of oscillation. At the same time the limit-cycle frequency must be higher than the natural frequency of

the vehicle. Hardware problems were also an influencing factor. The location of the compensator poles can be fixed with more certainty than the servo poles, which may vary significantly under operating conditions.

With this compensation, the operation of the system can now be determined. The first thing to be established is the range of gains over which the gain changer must vary to maintain neutral stability. The static loop sensitivity (K) is the product of the control surface effectiveness (M_δ), the sensitivity of the other components of the system (S), and the gain of the gain changer (K_G). Now S is constant for all conditions and is equal to 3.53×10^9 . Hence,

$$K_G = \frac{K}{3.53 \times 10^9 M_\delta} \quad (14)$$

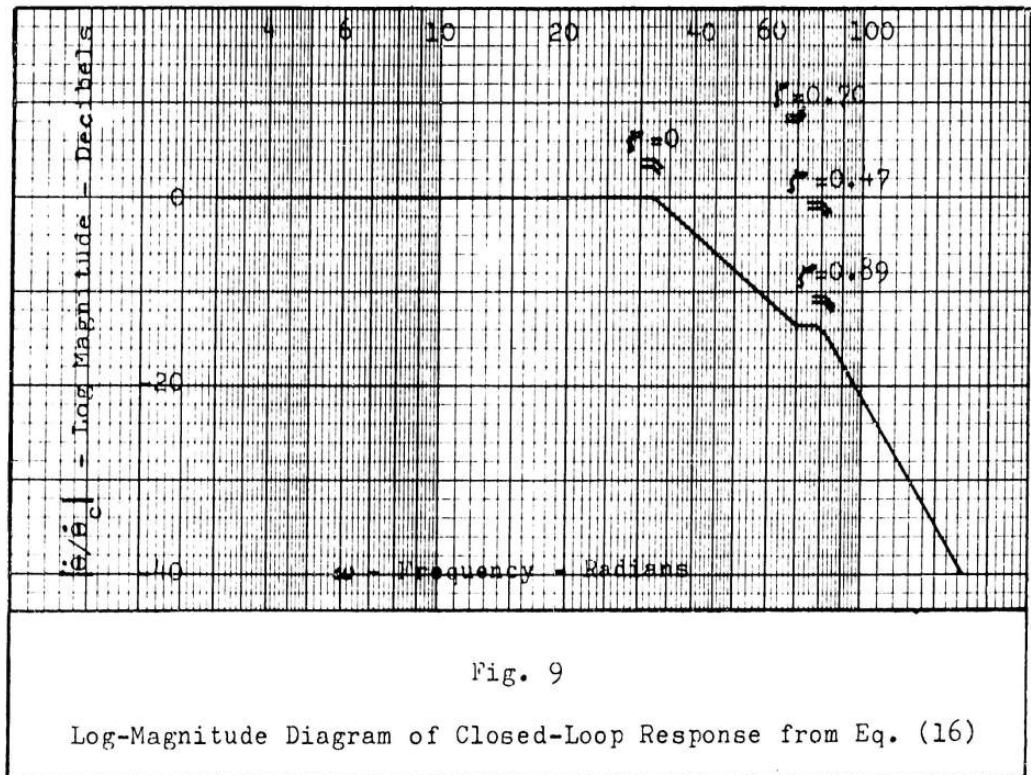
The static loop sensitivity for condition three is 3.70×10^{10} and K_G equals 0.198. For condition six K equals 3.67×10^{10} and K_G equals 14.85. From this data it appears that K_G is inversely proportional to M_δ because the value of K is nearly constant. To check the validity of this assumption K for condition one was calculated to be 3.65×10^{10} . Hence, for the purpose of analysis K_G is considered to be inversely proportional to M_δ . The range of gain to be covered by the gain changer can now be calculated from conditions one and three, which represent the extreme values of M_δ . As a result K_G must vary from approximately 0.2 to 47. The gain changer itself can only attenuate; therefore, a fixed gain of 47 must be placed in the loop. Then the gain changer will establish the value of K_G by attenuation.

With the static loop sensitivity determined, the location of the closed-loop poles can now be found. The location of the six roots with high natural frequencies is shown in Figures 7 and 8. As expected, the location of these roots is nearly the same for the extremes of vehicle dynamics. Some idea of the closed-loop bandwidth can be obtained from the closed-loop transfer function formed from these six roots by assuming that the residues associated with the closed-loop poles near the origin are small. In reality, however, the combination of poles and zeros near the origin causes some attenuation before the first corner frequency of the six roots considered is reached. The transfer functions, assuming the compensation is placed in the forward branch (Fig. 3), are:

$$\text{Condition 3} \quad \frac{\dot{\theta}(s)}{\theta_c(s)} = \frac{-10.4 \times 10^6 (s^2 + 98s + 70^2)}{(s^2 + 34^2)(s^2 + 80s + 80^2)(s^2 + 149s + 83^2)} \quad (15)$$

$$\text{Condition 6} \quad \frac{\dot{\theta}(s)}{\theta_c(s)} = \frac{-8.6 \times 10^6 (s^2 + 98s + 70^2)}{(s^2 + 32^2)(s^2 + 74s + 78.2^2)(s^2 + 146s + 82^2)} \quad (16)$$

Because Equations (15) and (16) are nearly the same, the characteristics of the bandwidth of the system can be determined from an asymptotic log-magnitude diagram of Equation (16). Figure 9 is the diagram with the damping ratio shown at the corner frequencies. From the figure it is readily apparent that the dominant response of the feedback loop will occur at the limit-cycle frequency. This means that noise entering the system will excite limit-cycle oscillations and will cause the gain to decrease until the ampli-



tude of the oscillations is below the set point. If the feedback loop is allowed to operate in this manner, the response to command inputs could be degraded. The feedback loop can be modified to limit the change in gain resulting from noise or high frequency components of the command input appearing at the output of the model by modifying the feedback branch. However, this will not reduce the effect of noise introduced in the feedback branch because all components of the system appear in the forward branch of the feedback loop presented to these inputs. The system is sufficiently modified when the second lead compensator (Eq 11) is placed in the feedback loop. By making this change, the closed-loop pole on the loci between -6.67 and -8.33 becomes more dominant

in the response. Limit-cycle oscillations can still be excited, but as the gain decreases the damping of the neutrally stable poles increases and their contribution to the total response becomes less dominant because the corner at the limit-cycle frequency occurs with 11 decibels of attenuation. With the change in design the closed-loop transfer function of Equation (16) becomes

$$\frac{\dot{\theta}(s)}{\theta_c(s)} = \frac{-2.88 \times 10^6 (s+25) (s^2+98s+70^2)}{(s+7.2)(s^2+32^2)(s^2+74s+78.2^2)(s^2+146s+82^2)} \quad (17)$$

and the asymptotic closed-loop frequency response is shown in Figure 10. The block diagram of the system as it will be analyzed

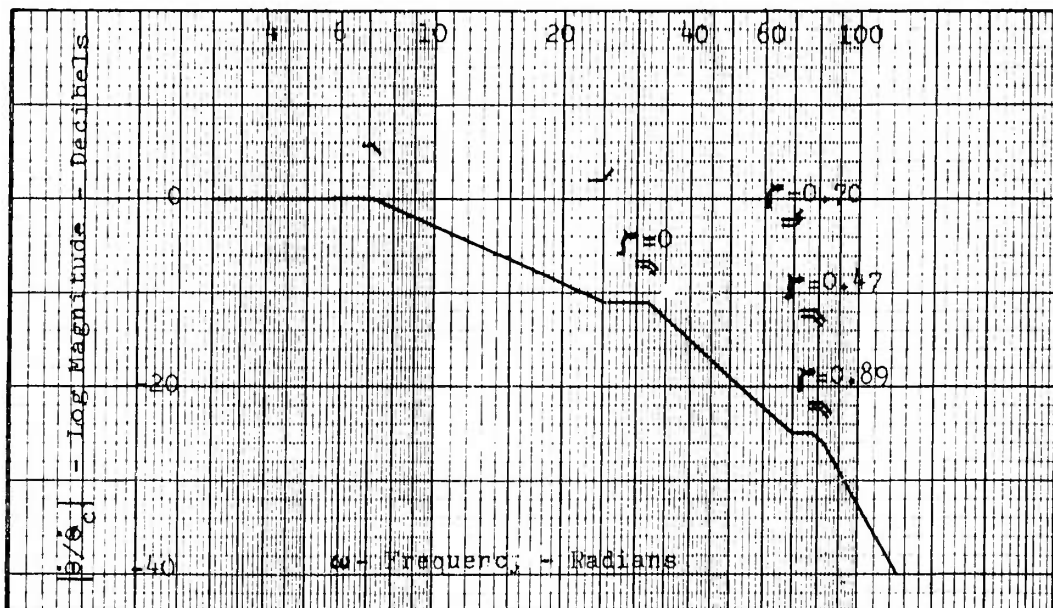


Fig. 10

Log-Magnitude Diagram of the Closed Loop with Feedback Compensation

can now be drawn (Fig. 11).

The question arises as to whether the model is dominant with the bandwidth of the feedback loop from this design. Since the

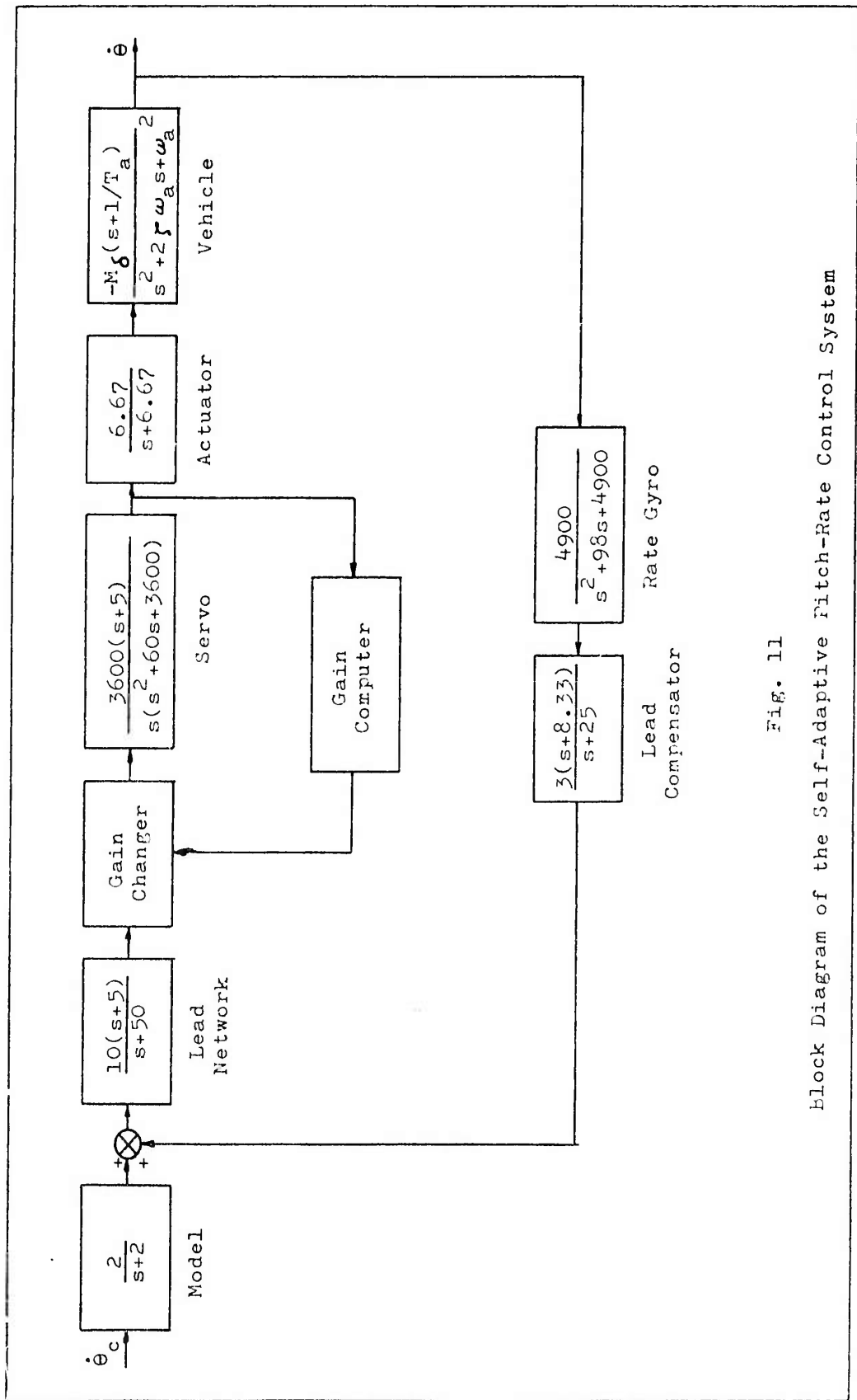


Fig. 11
Block Diagram of the Self-Adaptive Pitch-Rate Control System

question of dominance is essentially based on first order responses, one of which is 3.6 times as fast as the other, the total response will be very nearly that of the model.

The validity of the assumption that the residues of the closed-loop poles near the origin are small must also be checked. By root-locus analysis it is known that the residues associated with a pole will be small if the distances to the closed-loop zeroes are small compared to the distance to the other closed-loop poles. Since the vehicle zero and the compensator zeros at $s = -5$ are also closed-loop zeros, to have small residues associated with the closed-loop poles they must be near these zeros. The complex conjugate closed-loop poles that will appear on the loci between the vehicle poles and the compensator zeros are not a cause of great concern because (1) one half of the loci lies in a region where the damping ratio is greater than 0.7 for all cases and (2) the natural frequency of the closed-loop poles in this region is from 2.5 to 4 times that of the model. The greatest problem, considering the response of the feedback loop to a step input, is the closed-loop pole which lies on the real axis between the servo pole at the origin and the vehicle zero which moves out from the origin as far as $s = -2.07$. The residue associated with this pole has a negative value which means that the term in the time response equation is subtracted from the commanded value. The form of the equation for the time response contributed by this pole is $-Ae^{-t/T}$ where T will be very large when the pole lies near the origin and larger than the time constant of the model for every condition.

If the residue of this pole is significant it will cause the output of the system to be delayed in reaching the commanded value and may even be large enough to keep the system from meeting the response criteria for step command inputs. Since the static loop sensitivity of the system is nearly the same for all flight conditions, the vehicle dynamics which may cause poor performance of the system can be predicted. The residue of the closed-loop pole which moves toward the vehicle zero will be determined largely by the ratio of the distances to the vehicle zero and the pole at the origin (step input) and the ratio of the distance to the compensator zeros at $s = -5$ and the poles on the loci which come into these zeros. The relative locations of the closed-loop poles is dependent upon the location of the vehicle poles and zeros in a way that causes the residue of the pole on the locus to the vehicle zero to be large when the time constants of the vehicle poles ($1/\zeta\omega_a$) and zero are large. On the basis of these considerations Table I indicates that the effect of this pole may be significant at flight conditions one, four, five, and six.

The disturbance response to be expected from the system must now be determined. The response to a step control-surface-angle disturbance is dependent upon the feedback loop alone because the model does not appear in the signal path. In general the transfer function for a disturbance input to the vehicle is

$$\frac{C}{D} = \frac{V}{1+GVH} \quad (18)$$

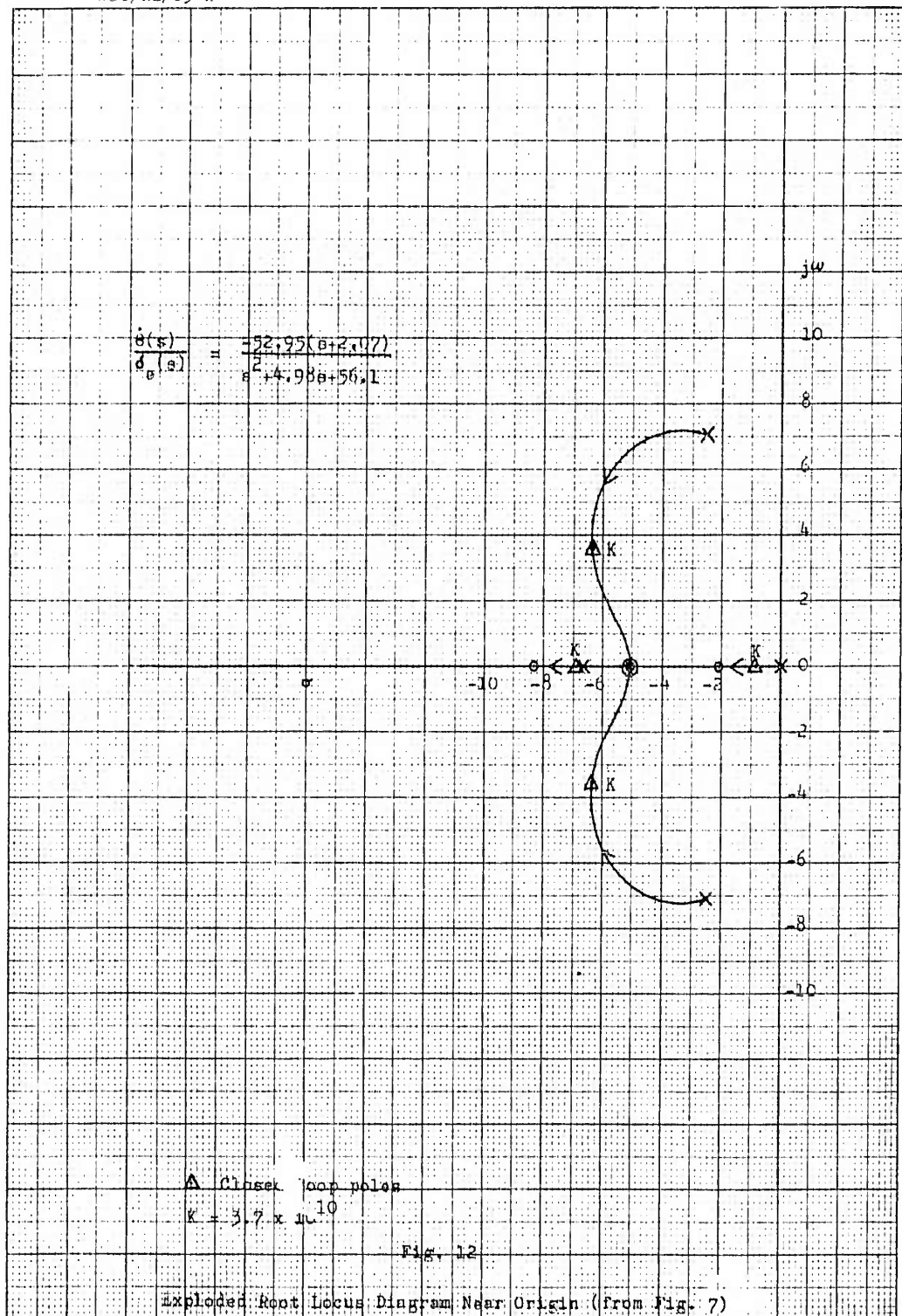
where V is the vehicle and GVH is the open-loop transfer function. Since the vehicle transfer function appears alone in the numerator, the magnitude of the response to the disturbance will be greatest when M_δ is large. Thus, for the purpose of analysis flight condition three will be investigated even though no magnitude limitations are placed on disturbance response in Chapter II. (The largest response to disturbance inputs is generally the most undesirable condition.) The closed-loop poles are the same as those for command inputs; therefore, with information from Figures 7, 11, and 12 the closed-loop transfer function for disturbance inputs (a step δ command) is

$$\frac{\dot{\theta}(s)}{\delta_e(s)} = \frac{-52.95s (s+2.07) (s+6.67) (s+25) (s+50)}{(s+0.85) (s+6.9) (s^2+34^2) (s^2+12.85s+7.3^2)} \quad (19)$$

$$\frac{(s^2+60s+60^2) (s^2+98s+70^2)}{(s^2+80s+80^2) (s^2+149s+83^2)}$$

The location of the poles and zeros in the s plane is shown in Figure 13. The damping of all but the neutrally stable poles is sufficient to meet the disturbance criteria of Chapter II. The relative magnitude of the residue of these poles will determine the way in which the system meets the criteria. The poles at $s = -6.3 \pm j3.6$ have the largest residue (0.032) when the response to a unit step input is considered. However, the neutrally stable poles also have a significant residue (0.011). As a result the small oscillations at the limit-cycle frequency may cause the gain changer to decrease. This in turn causes the poles to shift in

$$\frac{\dot{\theta}(s)}{\theta(s)} = \frac{-92.95(s+2.07)}{s^2 + 4.98s + 56.1}$$



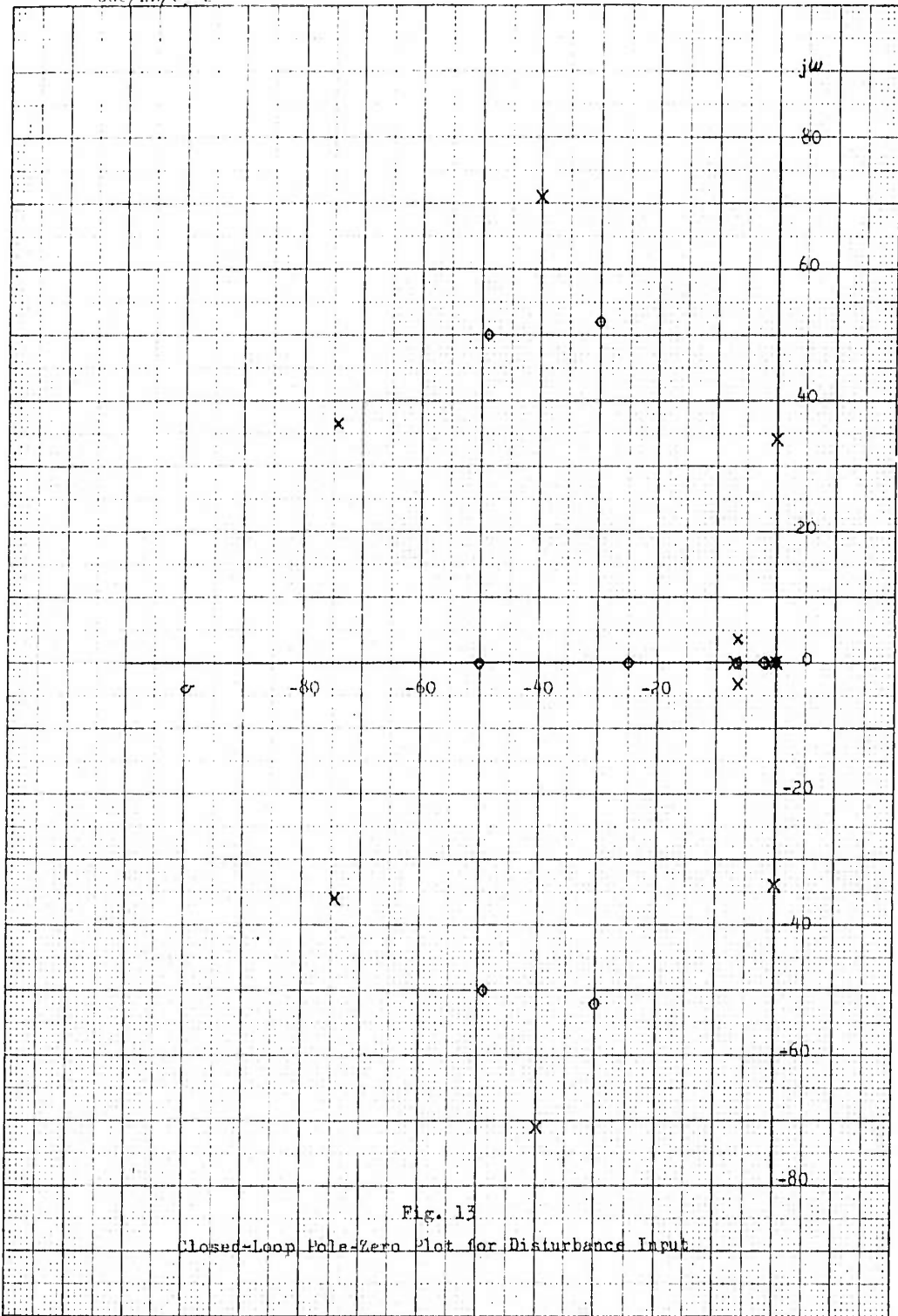


Fig. 13
Closed-Loop Pole-Zero Plot for Disturbance Input

such a way that the difference between the residues of these two pairs of conjugate poles remains nearly constant as the damping of the neutrally stable poles increases. In this manner the effect of the neutrally stable poles on the time response is decreased so that the system meets the criteria. The gain changer influences the disturbance response to a lesser or greater degree depending on the difference between the residues of these two pairs of conjugate poles for each flight condition. The conclusion to be drawn from this analysis is that the disturbance response of the system is partially dependent on the rate at which the gain is decreased. The gain changer for the MH-96 system is designed to decrease system gain faster than it increases gain. This is not only to maintain satisfactory disturbance response but also to insure a conservative search for the neutral-stability gain. The gain computer also includes a limiter to prevent the system gain from going so low that the response to commands is degraded.

Computer Simulation

The self-adaptive pitch-rate control loop was simulated on an analog computer to obtain time response data. The circuit diagrams for the simulation are shown in the appendices. Appendix B contains the diagrams used to simulate the vehicle at the selected flight conditions and Appendix C contains the diagram for the entire pitch-rate loop. For each flight condition the time response of the system is shown above the time response of the model for a step pitch-rate command to the system. Since the model response rises to 90 percent

of the commanded value in 1.15 seconds, the system meets the command response criteria if the output is the same as the model response. The disturbance response is shown above the step disturbance of the control-surface angle (δ).

The response of the system for flight-condition one is shown in Figure 14. Comparison of the model and the system responses indicates that the response of the system takes a long time to rise to final value. However, the initial rise meets the command response criteria of 90 percent of the commanded value within three seconds. The long delay in reaching the commanded value is caused by the closed-loop pole which lies on the real axis between the origin and $s = -0.0356$. This response from the system is not surprising since the possibility of an error of this nature was predicted in the analysis. The long delay in reaching the commanded value caused an error signal to persist for such a long time that the command input had to be kept small to prevent the integrator of the proportional-plus-integral section of the servo simulation circuit from saturating. The saturation of the system is very rapid for command inputs greater than one degree per second because the gain of the gain changer (K_G) is highest for this flight condition. This amplifies the error signal greatly before it is passed to the servo and since the time constant of the error is large, saturation occurs. For a larger command input, the error becomes larger and the integrator reaches the saturation point faster.

The disturbance response is an oscillation at the limit-cycle frequency riding on a decaying signal. The oscillation, which is

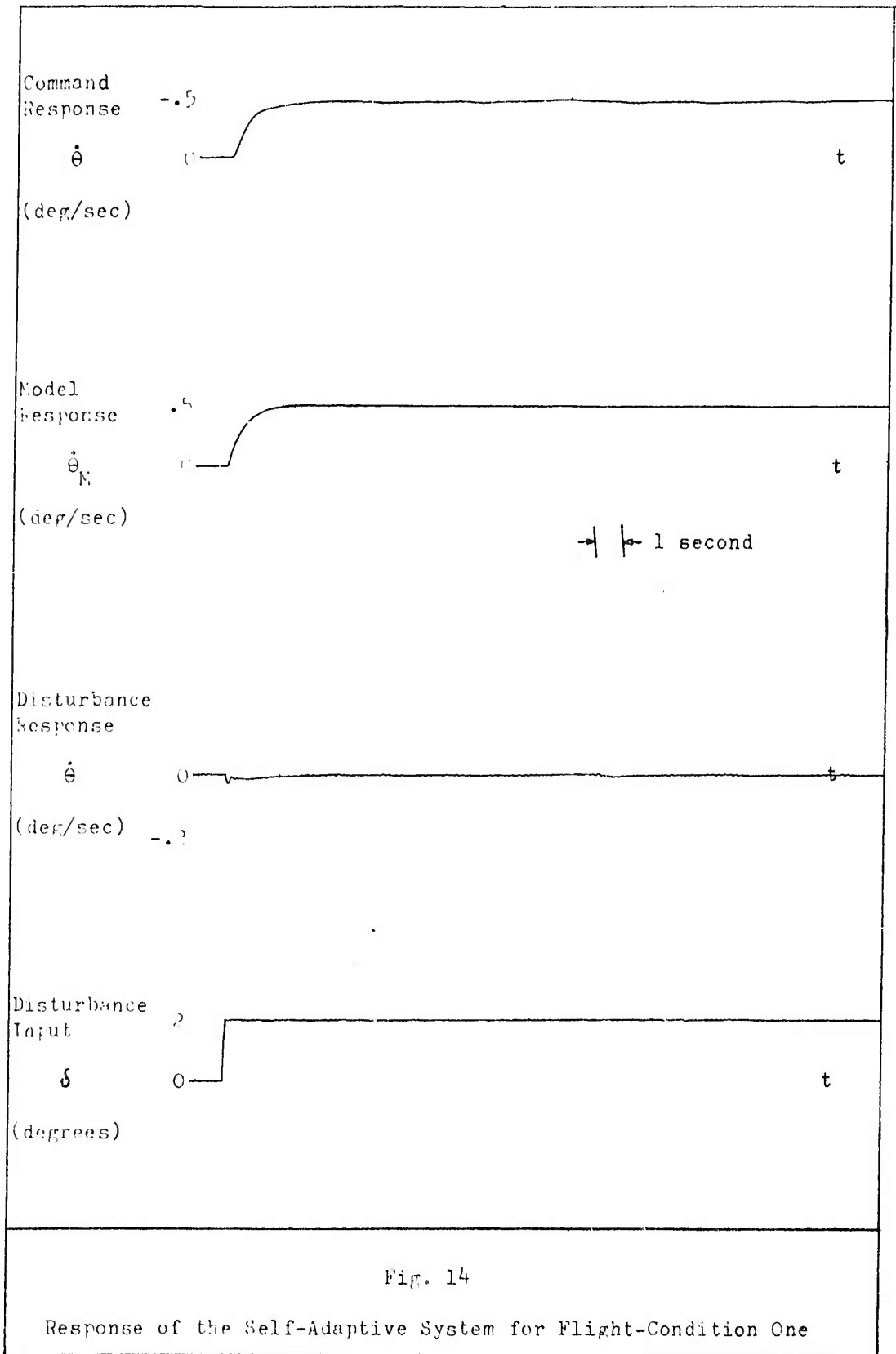


Fig. 14

Response of the Self-Adaptive System for Flight-Condition One

much greater in magnitude than the nominal limit cycle, is damped to meet the disturbance criteria within one cycle. A reduction in the system gain was noted for this flight condition because the magnitude of the response oscillations are greater than the nominal oscillations. At this flight condition the gain changer aids the system to meet the disturbance criteria.

Figure 15 shows the response of the system at flight-condition two. The amplitude of the limit-cycle oscillation has increased and the modulation effect is more pronounced when compared to data for flight-condition one. These two effects will be dealt with in more detail after all of the response data is presented. The system output follows the model without any detectable error to meet the command response criteria. The disturbance response decays within one second without any oscillation other than the normal limit cycle. For this flight condition the gain changer has little to do with meeting the disturbance response criteria because the oscillations do not exceed the limit cycle amplitude. The system, therefore, meets the response criteria for flight-condition two.

The response of the system at flight-condition three as shown in Figure 16 meets the criteria. The results are nearly the same as for flight-condition two except that the limit-cycle amplitude and the disturbance amplitude are larger.

The response of the system at flight-condition four is shown in Figure 17. The command response is affected by the closed-loop pole near the origin. The time constant associated with this pole is not very large so that the delay in reaching the commanded value

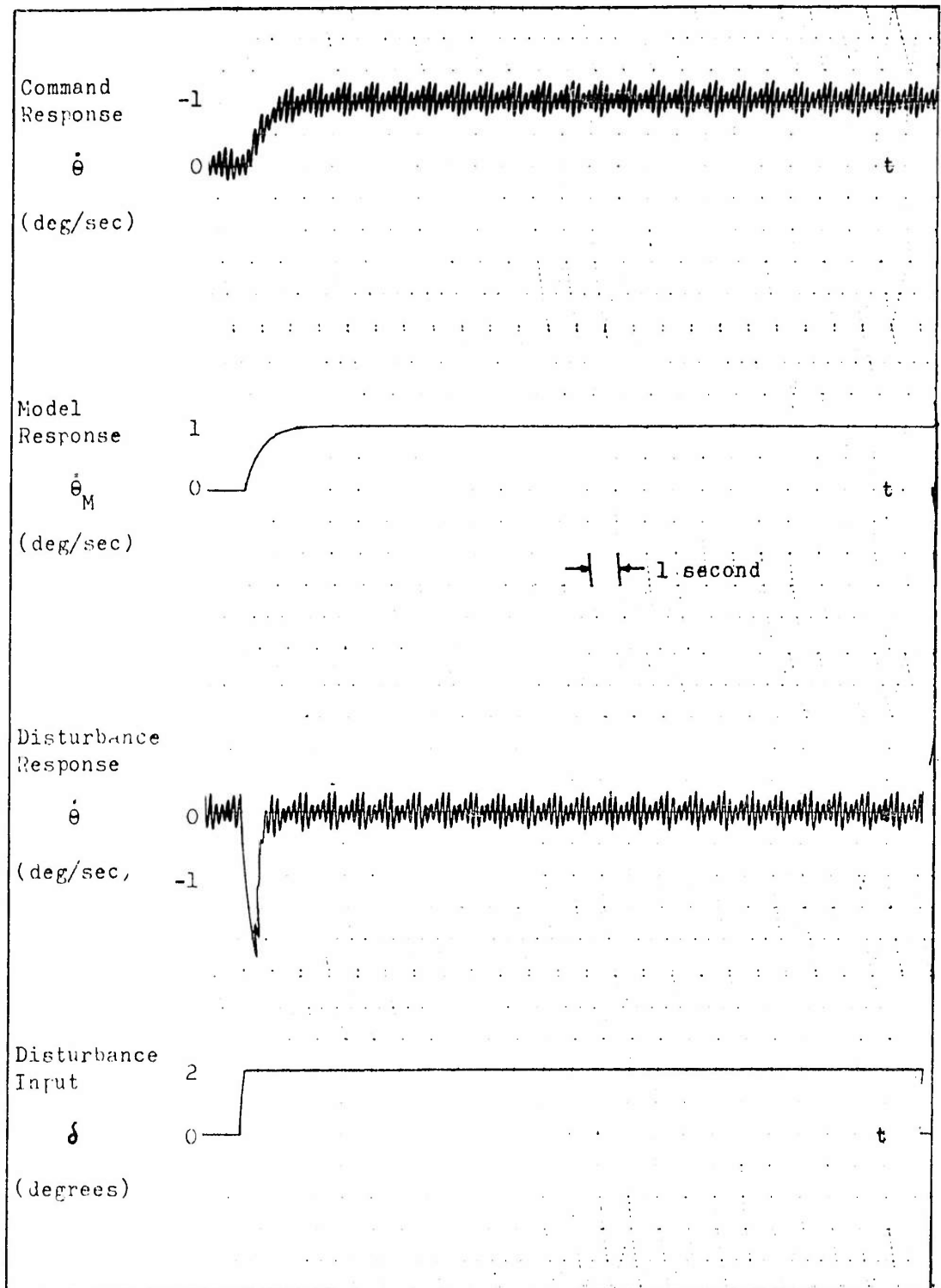


Fig. 15

Response of the Self-Adaptive System for Flight-Condition Two

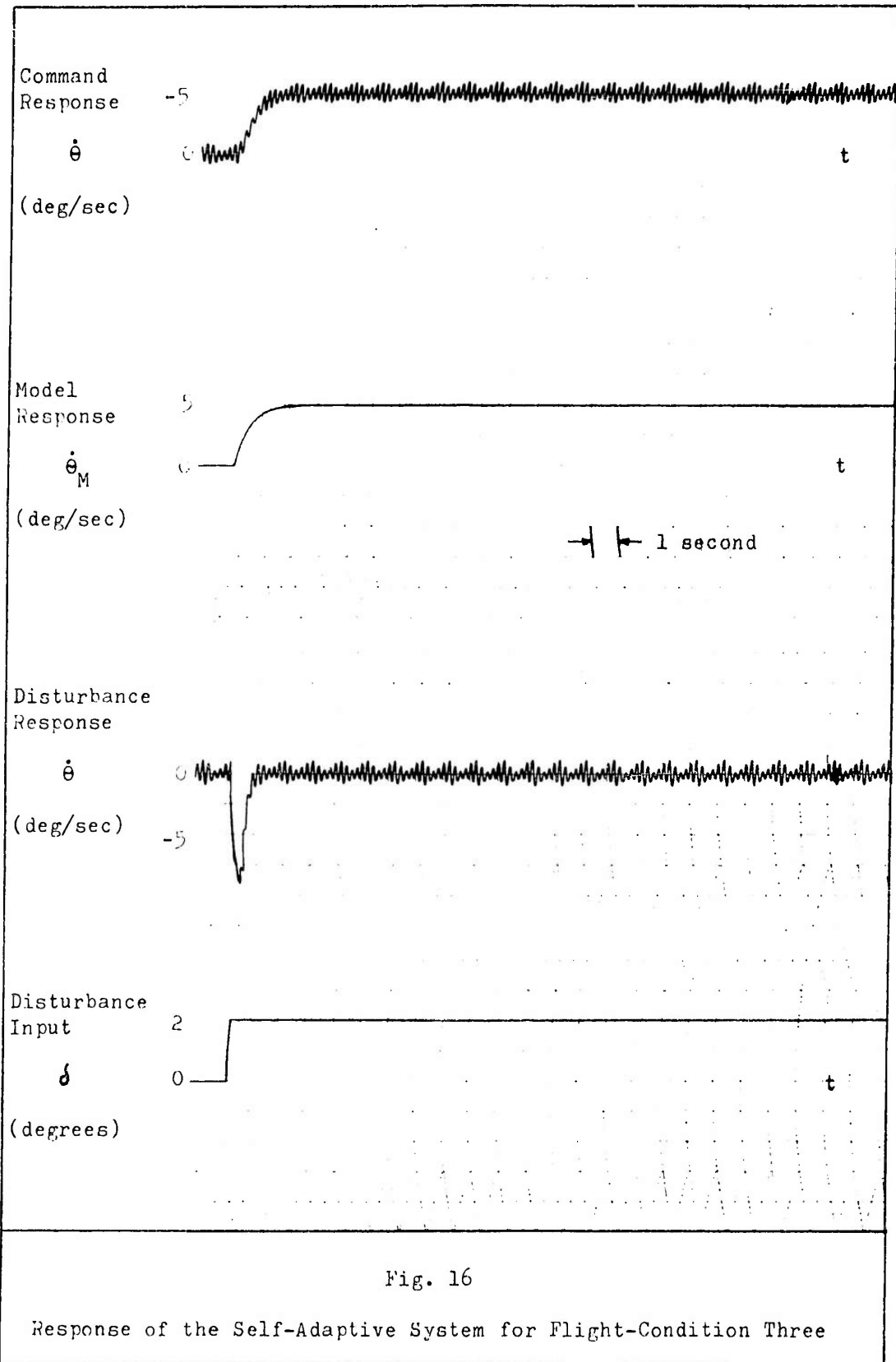


Fig. 16

Response of the Self-Adaptive System for Flight-Condition Three

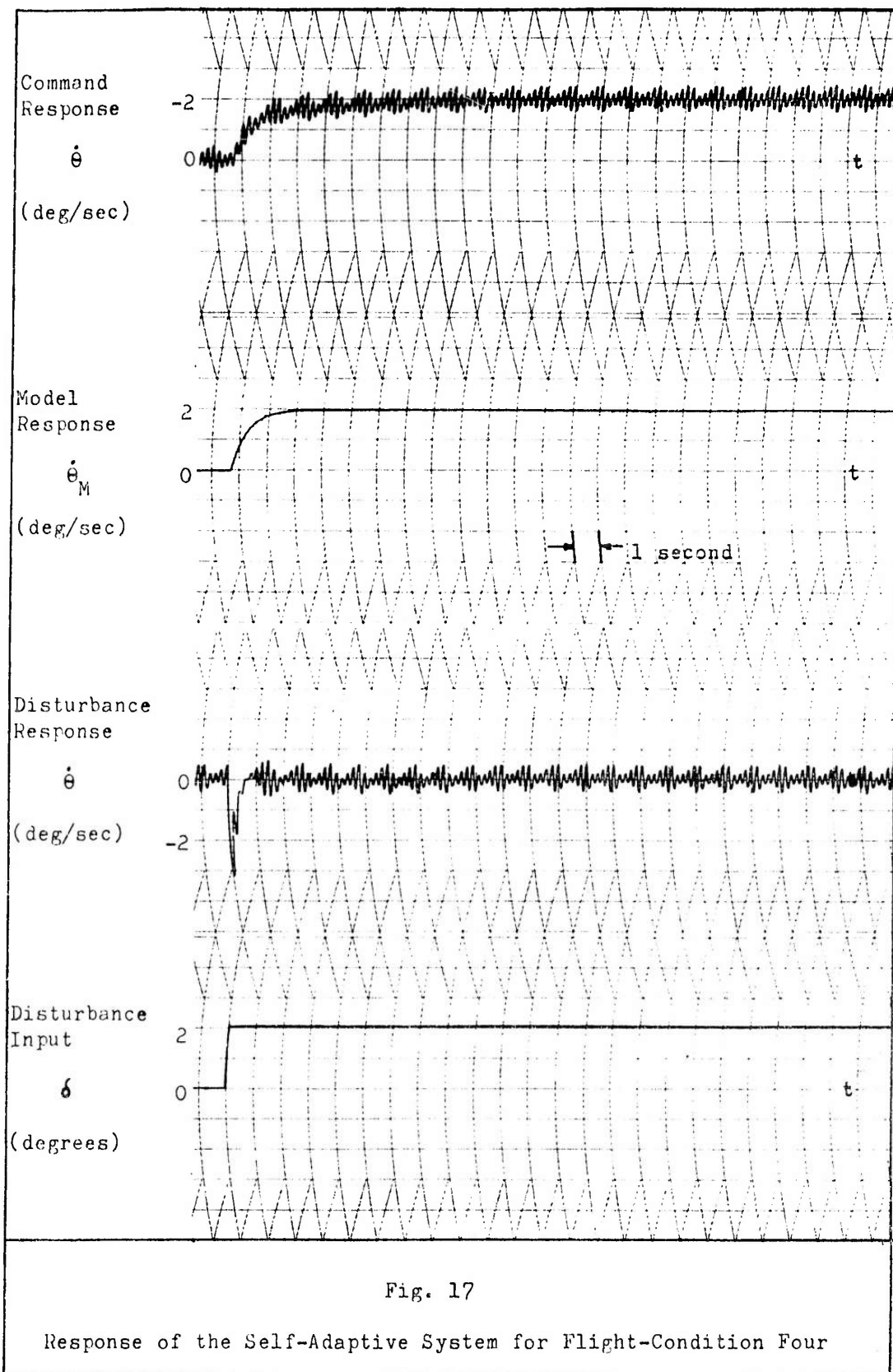


Fig. 17

Response of the Self-Adaptive System for Flight-Condition Four

GGC/EE/63-2

is not as great as for flight-condition one (Fig. 14). However, the residue is large enough to keep the system from meeting the response criteria for this flight condition. The output has reached only 85 percent of the commanded value after three seconds. The disturbance response meets the criteria in the same manner as for flight-conditions two and three.

Figure 18 shows the response of the system at flight-condition five. Once again the effect of the pole near the origin is apparent, but the system meets the response criteria. The disturbance response shows the limit-cycle oscillation on a decaying signal. At this flight condition the gain did not change any more than required to control the nominal limit-cycle oscillation.

The response at flight-condition six appears in Figure 19. The command response at this flight condition follows the model with no noticeable error. The disturbance response is an oscillation at the limit-cycle frequency on a decaying signal. Since the oscillation is slightly larger than the nominal limit-cycle amplitude, the gain of the system is decreased a little lower than for control of the limit cycle. The amplitude is decreased within one cycle to the nominal limit-cycle amplitude. As a result, the system meets the response criteria for condition six.

Some general conclusions can now be drawn from the composite results. The range of limit-cycle frequencies from the computer data is 29.5 to 31.5 radians per second. The values are somewhat less than predicted from the root locus (32 to 34 radians per second). The discrepancy results largely from the inaccuracies in

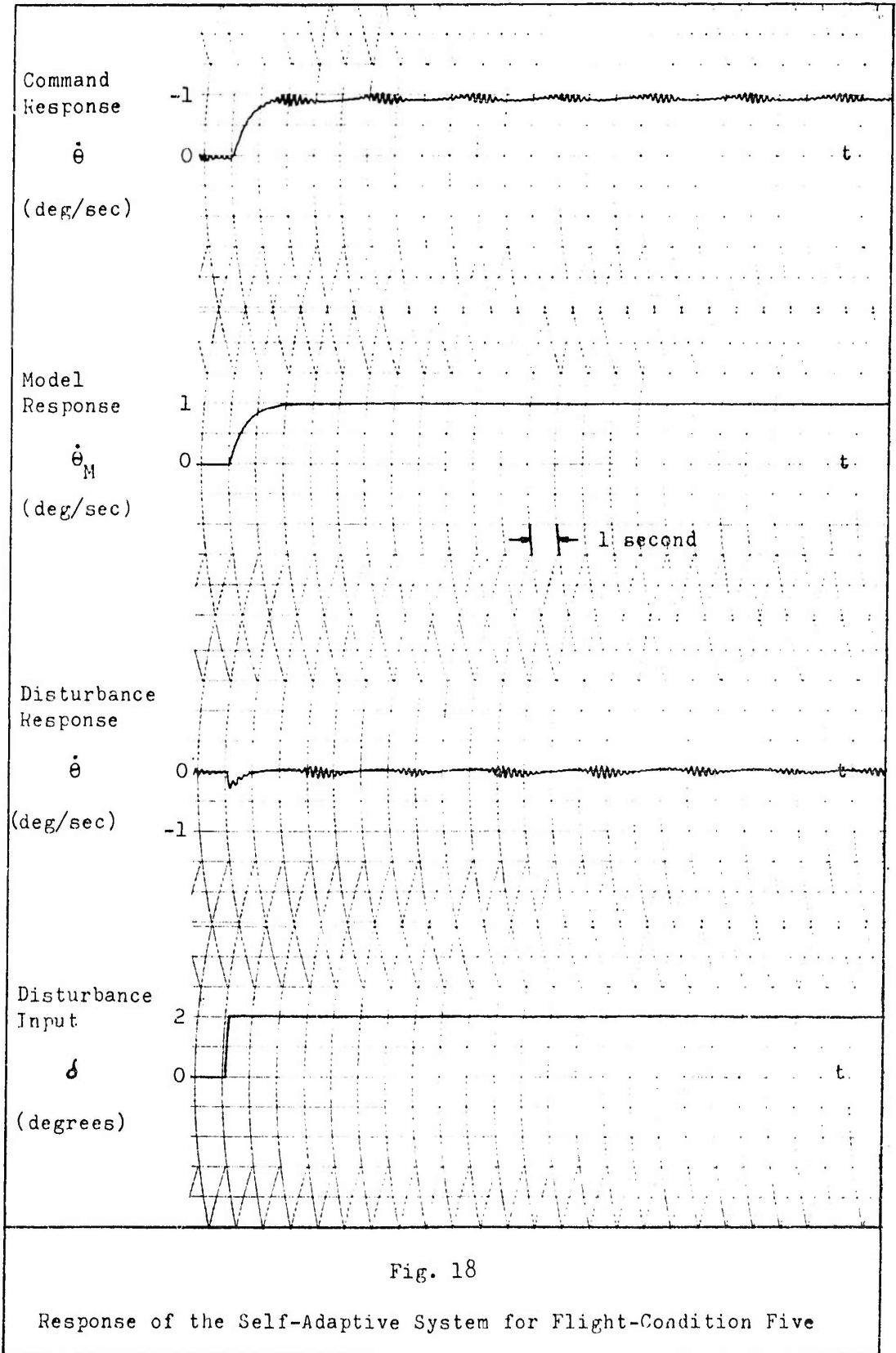


Fig. 18

Response of the Self-Adaptive System for Flight-Condition Five

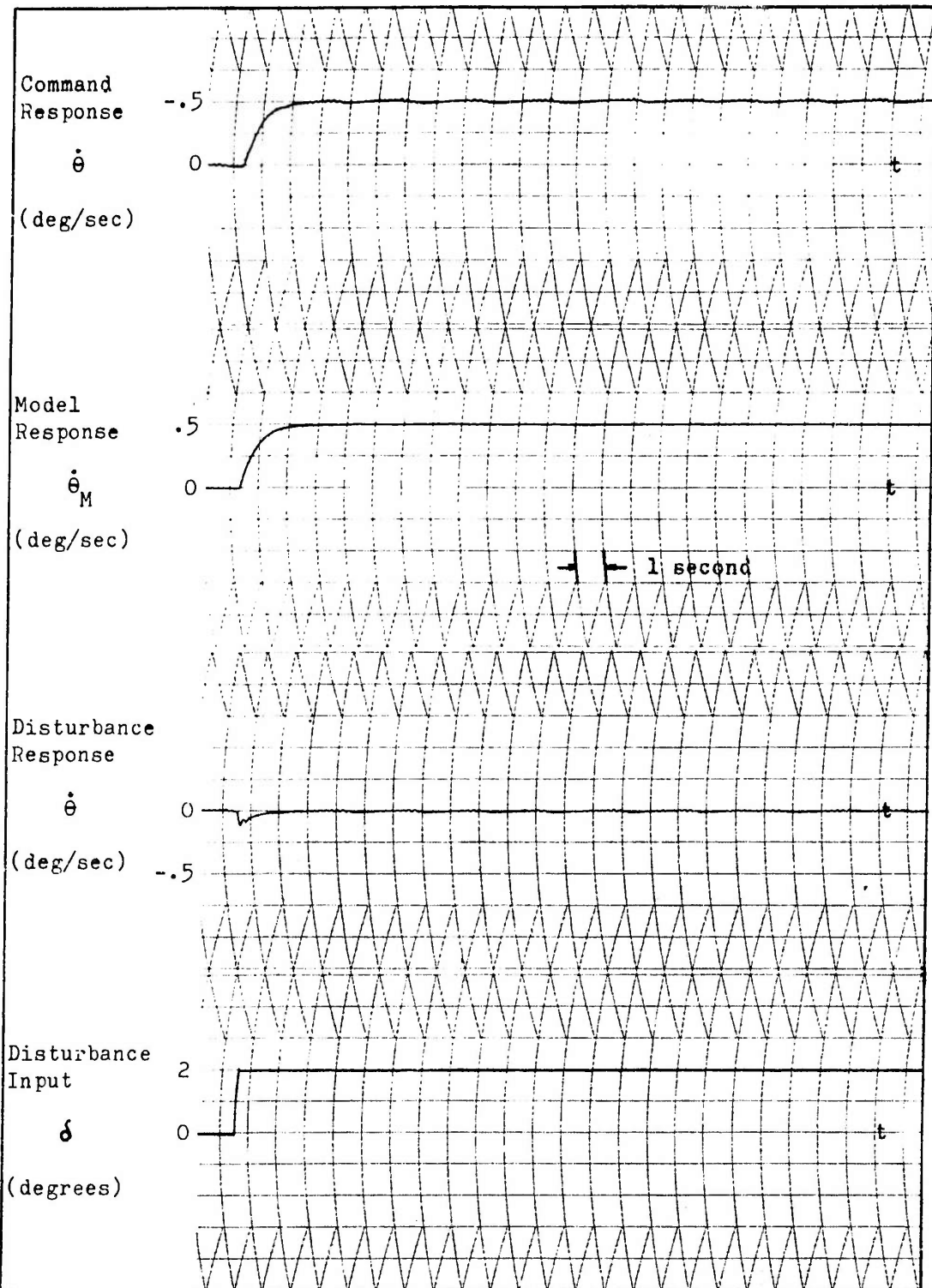


Fig. 19

Response of the Self-Adaptive System for Flight-Condition Six

the capacitors required to simulate the complex poles of the servo and rate gyro. The values of the components used in the simulation reduced the natural frequency and damping ratio of the servo and rate gyro poles slightly. The gain (K_G) of the system was also somewhat less than the predicted values for all flight conditions. For flight-condition one K_G was 45.4 and for flight-condition three K_G was 0.192 compared to the predicted values of 47 and 0.198. The reduction in K_G also indicates that the servo and rate-gyro poles are not located accurately. However, these parameters are close enough to the calculated values that the response data obtained represents the system adequately.

In all of the response data the pitch-rate output of the system shows the limit-cycle oscillation to be amplitude modulated. The nature of this modulation is dependent upon the range of attenuation over which the gain changer is operating because the attenuation is changed in a non-linear manner. This effect is even more pronounced in a linear analysis because the system operation passes from convergent oscillation to divergent oscillation with only a slight change in gain. The limit-cycle amplitude also changes for each flight condition. By comparing the amplitude of the limit cycle in Figures 15 and 16, the limit-cycle amplitude for condition three is about 3.2 times that for condition two. This ratio corresponds very closely to the increase in M_d for these flight conditions (Table I). This is to be expected from this self-adaptive design because of the construction. In Figure 11 the limit-cycle-sensing point is shown to be at the output of the servo.

The gain controller attempts to maintain a constant limit-cycle amplitude at this point. Since this point lies between the gain changer and the vehicle and K_G varies inversely as the value of M_δ , the increase in the amplitude of the limit cycle at the output of the system must be proportional to the increase in M_δ . The limit-cycle amplitude at the output must be controlled by the reference set point of the gain changer to preclude objectionable oscillations. This simulation does not attempt to minimize these oscillations in the output because the main interest is to obtain response data.

The amplitude of the disturbance response is also dependent upon the value of M_δ for each flight condition. For flight-condition two the magnitude of the peak is 2.3 degrees per second and for condition three the magnitude is nine degrees per second. The ratio of the peak value for these two conditions is 3.9 and the ratio of M_δ is 3.25. Thus, the increase in the amplitude of the disturbance response is somewhat greater than the increase in M_δ . The difference is caused by the increase in amplitude of the limit cycle. The settling time of the disturbance response indicates that the response is dependent upon the pair of complex poles on the loci that go into the compensator poles at $s = -5$. This verifies the analysis of the system made in the previous section.

It was noted during the computer simulation that the magnitude of variation in K_G was much greater at the flight conditions where M_δ is low. This in turn caused the output of the system to vary as K_G fluctuated. Figures 14, 18, and 19 show this effect. For

GGC/LE/63-2

flight-condition five (Fig. 18) this output variation can almost be described by a sine wave with an amplitude of 0.04 degrees per second and a frequency of 0.3 cycles per second. This corresponds to the amplitude modulation of the limit-cycle oscillations.

The computer response data shows that the system meets the response criteria except at flight-condition four. The response to command inputs is also less than desirable for flight-conditions one and five. The response at these flight conditions can be improved if the static loop sensitivity of the system can be raised. In the more advanced design (Ref 12:4) the servo and rate gyro characteristics have been improved to yield a higher static loop sensitivity with a resultant improvement in the response of the system.

IV. The High Fixed-Gain Linear System

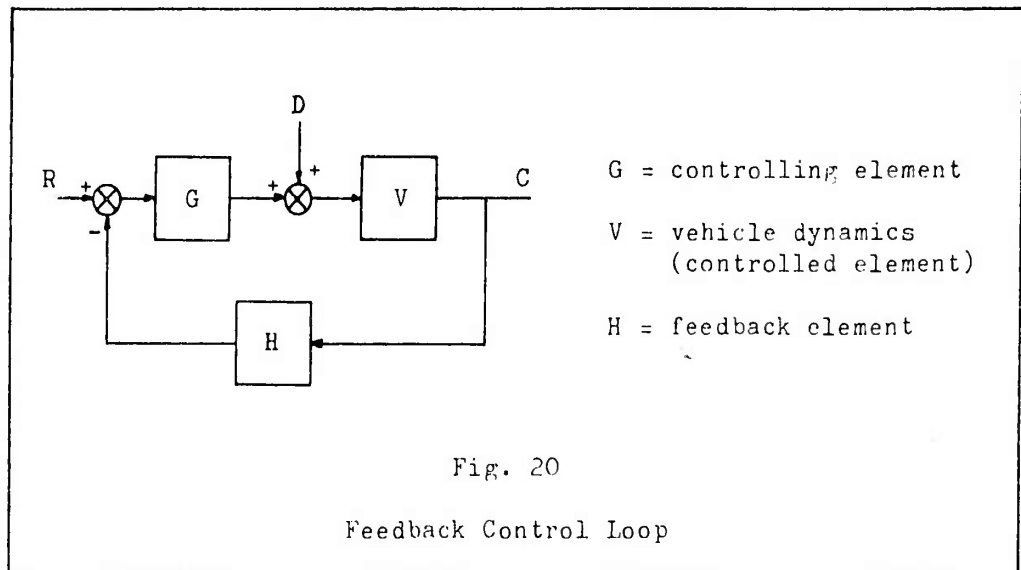
In this chapter a high-gain-linear design will be applied to the X-15 flight-control problem. A pitch-rate control system will be designed for the vehicle and control components described in Chapter II.

The theory of the high-gain-linear design originates from the fundamental properties of feedback derived by Black (Ref 1). Bode established these properties in theorems which show the effects of feedback on electronic amplifier circuits. The theorems are developed in terms of control-system terminology in Appendix A. The properties are reviewed so that the intent of each design principle can easily be understood. Both the root-locus method and the frequency-response method (log-magnitude and phase diagrams) were used to resolve the problem. The reason for the change in method is described later in the chapter. The design techniques used were devised by Horowitz in recent publications (Refs 6, 7, and 8); however in the frequency-response method, the approach was changed somewhat due to the difficulties encountered in translating the time-domain specifications into frequency-response criteria for a non-dominant system. Before proceeding to the design, the principles to be used will be related to the control problem.

Design Principles

The control problem is this: to make the system insensitive to the variation of vehicle parameters so that the response to command and disturbance inputs can be controlled.

The design principle applied to the problem of vehicle-parameter variations is shown in Theorem 2 of Appendix A. The theorem shows that variations in the output, caused by variations of the controlled element, are reduced by feedback in the ratio $(1+GH) : 1$. From the block diagram of Figure 20, the closed-loop



transfer function to a command input (R) is

$$\frac{C}{R} = \frac{GV}{1+GVH} \quad (20)$$

Differentiating Equation (20), keeping G and H constant gives

$$d(C/R) = \frac{1}{1+GVH} \cdot \frac{GdV}{1+GVH} \quad (21)$$

Replacing $\frac{1}{1+GVH}$ by $\frac{C/R}{GV}$ gives

$$d(C/R) = \frac{C/R}{GV} \frac{GdV}{1+GVH} \quad \text{or} \quad \frac{d(C/R)}{C/R} = \frac{1}{1+GVH} \frac{dV}{V} \quad (22)$$

This equation shows that the feedback should be large to reduce the effects of the relative variations of V on the closed-loop response. To make the feedback large, the open-loop gain (GVH) must be large. Since R is independent of the variation of V , the output C is almost independent of vehicle-parameter changes when $GVH \gg 1$. Equation (22) leads to the conventional definition of sensitivity of C/R to V (Ref 8:94-96) which is

$$S_V^{C/R} \triangleq \frac{\frac{d(C/R)}{C/R}}{\frac{dV}{V}} = \frac{1}{1+GVH} = \frac{1}{1+L} \quad (23)$$

where L is the open-loop transmission (GVH). The sensitivity function is a measure of the amount of feedback necessary to suppress the effect on the output of variations in the forward branch. A serious limitation of Equation (23) is that it can only be applied for infinitesimally small variations of V . To consider finite changes in V , let $(C/R)_0$ be the value of the closed-loop transfer function when V is some nominal value V_0 . Let finite changes in C/R and V be represented by

$$\begin{aligned} \Delta V &= V - V_0 \\ \Delta(C/R) &= C/R - (C/R)_0 \end{aligned} \quad (24)$$

With the above equations, the definition of the sensitivity function for finite changes of V can be written as

$$S_V^{C/R} \triangleq \frac{\frac{\Delta(C/R)}{C/R}}{\frac{\Delta V}{V}} = \frac{1}{1+L_0} \quad (25)$$

Where L_o is the nominal open-loop transmission GV_oH . Equation (25) points out that any desired degree of insensitivity can be obtained for any amount of ΔV provided L_o can be made large enough.

In Figure 20 the closed-loop transfer function of the disturbance input D is

$$\frac{C}{D} = \frac{V}{1+GVH} = \frac{V}{1+L} \quad (26)$$

As discussed in Theorem 3 of Appendix A, the effect of disturbance on the output is reduced by feedback in the ratio $(1+GVH): 1$. Equation (26) again shows that the feedback should be large. Comparing Equations (23) and (26) shows that the sensitivity function is also a measure of the amount of feedback necessary to minimize the effects of disturbances. Considering finite changes in V , let $(C/D)_o$ be the value of the closed-loop disturbance transfer function when V is some nominal value V_o . Let finite changes in C/D and V be represented by

$$\begin{aligned} \Delta V &= V - V_o \\ \Delta(C/D) &= C/D - (C/D)_o \end{aligned} \quad (27)$$

With the above equations, Equation (26) can be rewritten as

$$\frac{\Delta(C/D)}{C/D} = \frac{1}{1+GV_oH} \frac{\Delta V}{V} = \frac{1}{1+L_o} \frac{\Delta V}{V} \quad (28)$$

This form shows that unless the magnitudes of G and H are large, relative changes in V can affect relative changes in the closed-loop disturbance transfer function and, therefore, the disturbance response.

The design principle used to meet the response criteria to a command input can be seen from Equation (20). With large feedback, $GVH \gg 1$, Equation (20) can be approximated by

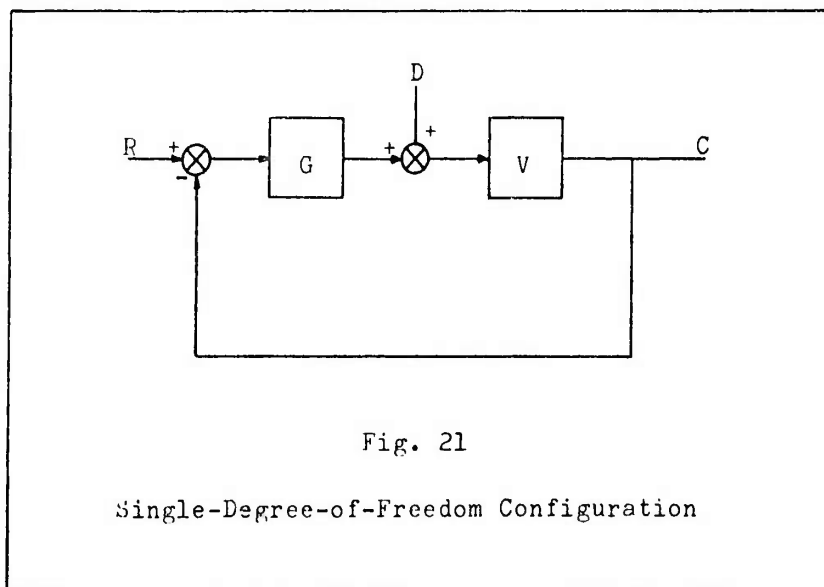
$$\frac{C}{R} \approx \frac{1}{H} \quad (29)$$

This implies that within the open-loop bandwidth the feedback element H provides the design freedom to establish the response and bandwidth of the closed loop.

Horowitz discussed the concept of design freedom by comparing the single- and two-degree-of-freedom configurations (Ref 7:49-50). A single-degree-of-freedom structure, as shown in Figure (21), has the following closed loop transfer functions:

$$\frac{C}{R} = \frac{GV}{1+GV} \quad (30)$$

$$\frac{C}{D} = \frac{V}{1+GV} \quad (31)$$



Equations (30) and (31) show that once G is selected to handle the disturbance and parameter variation problems, there is no freedom left to design the system response to a command input. The configuration of Figure 20 is a two-degree-of-freedom structure since G and H can both be varied to satisfy the independent response criteria of the disturbance input and the command input.

It should be understood that in the preceding discussions, the following qualifications were assumed: (1) there is no leakage transmission between the input and output of the system; (2) there is no interaction or coupling between blocks, except as shown by the connecting lines; (3) the feedback structure is confined to a single loop; and (4) the term "feedback" is expressly meant as the quantity $1 + L$.

In summary, the design principles are: (1) L is designed to obtain the desired system insensitivity to vehicle-parameter variations and to minimize the effects of disturbances; and (2) a two-degree-of-freedom configuration must be used to satisfy the independent response criteria of the disturbance and command inputs so that, with L determined, the compensation can be divided between G (to control disturbance response) and H (to control command response). The design principles were first applied to the problem employing the root-locus method.

Root-Locus Method

It has been shown that the sensitivity function is a measure of the ability of the system to cope with the problems of parameter

variations and disturbances. In terms of a root-locus plot, the sensitivity of the system transfer function is directly related to the maximum permissible drift of the dominant closed-loop poles and zeros (Ref 8:249-250). If this movement is very small, the system is highly insensitive to forward-branch-parameter variations and the variation of the system response in the time domain will be small. In terms of a dominant system design, the above implies that the dominant closed-loop poles should be near open-loop zeros. To have closed-loop poles near open-loop zeros requires a high static loop sensitivity, which implies a large DC gain level and low sensitivity to parameter variations. As in any dominant design, all additional closed-loop poles must have small time constants and residues so that they do not interfere with the dominant system response. This is especially important if the dominant closed-loop poles have small residues. To make the residues associated with the non-dominant closed-loop poles small, the open-loop zeros can be placed in the feedback branch so that they are not zeros of the closed-loop transfer function. This also keeps the residues of the dominant closed-loop poles very near the zeros from becoming too small. Since a detailed description of the design technique is given by Horowitz in References 8:249-267 and 6:9-11, only the important aspects of the technique will be related to the design of the flight-control system.

The first step in the design was to cancel the servo and rate gyro poles with complex compensators. This allows freedom of move-

ment of the poles of the compensators to meet the design requirements. The integral gain (K_i from Chapter II) of the proportional-plus-integral circuit was assigned the value of 6.67 to cancel the effect of the actuator pole which is load dependent. Even though the actuator pole is given at $s = -6.67$, the pole position will shift due to changes in load on the control surface. However, with high gain in the system, any closed-loop pole associated with this loci should be close to the proportional-plus-integral zero, thereby cancelling its effect. The reason for this cancellation is to simplify placement of the compensator poles. After cancellation, the open-loop transfer function of the system hardware and vehicle dynamics is (see Fig. 3)

$$\frac{6.67}{s} \frac{-M_d (s + 1/T_a)}{s^2 + 2\zeta\omega_a s + \omega_a^2} \quad (32)$$

The compensators used to cancel the servo and rate gyro poles yield a minimum of four poles. A compensator to supply the necessary two open-loop zeros to control the loci from the vehicle poles will have a minimum of two poles. Including the poles and zeros of Equation (32), this gives a total of nine poles and three zeros or an excess of six poles. This combination of poles and zeros gives the following angle conditions for the root loci asymptotes:

$$\gamma = \frac{(1+2M) 180^\circ}{9-3} = \pm 30^\circ, \pm 90^\circ, \pm 150^\circ \quad (33)$$

Since the desired location of the dominant closed-loop poles dictates the location of the open-loop zeros, the choice of the

closed-loop pole location was considered first. As shown in Figure 5, the location of the poles must be outside the given region to meet the system performance specifications for all flight conditions. Since the natural frequency ω_n of the poles dictates the system bandwidth, the value of ω_n should be kept reasonably low. This is important since, as will be shown later, the lower the value of ω_n , the lower the gain-bandwidth product required to maintain the desired insensitivity of a dominant system. The selection of ω_n and damping ratio (ζ) for the poles was further based on pilot preference data (Ref 9: Appendix E).

The next consideration was to select the flight condition on which the design for the dominant response is to be based. The vehicle parameter that contributes the largest variation is M_δ , which varies by a factor of 240 : 1. It was found that, in the region of interest, the movement of the dominant closed-loop poles about their corresponding open-loop zeros is primarily influenced by the value of M_δ for each condition. In other words, if the closed-loop poles are originally located using the low M_δ condition, the pole locations for all other conditions will be closer to the open-loop zeros. The above statement is verified in Appendix D. The pole location of the low M_δ condition (flight-condition one) dictates the amount of system insensitivity since it establishes the boundary of the region of pole movement about the open-loop zeros.

The final consideration was to investigate the effect of the maximum value of M_δ on the loci of the compensator poles. As mentioned previously, the minimum number of excess poles is six.

These six poles are the compensator poles and, as shown in Equation (33), they determine the angle conditions for the asymptotes. Equation (33) shows that one pair of loci from these poles will cross the imaginary axis. For dominance, the compensator poles must be located far enough away from the imaginary axis so that for maximum M_δ , which corresponds to the maximum static loop sensitivity, the roots on the crossing loci do not interfere with the dominant roots. To ensure that the above condition is met, a constant σ line is chosen so that if these roots lie on or to the left of the σ line, the time constant will be small enough to make the contribution to the time response negligible (assuming reasonably small residues).

Because of the variation of M_δ , the maximum static loop sensitivity (flight-condition three) will be 240 times the value of the static loop sensitivity at the dominant closed-loop pole location for flight-condition one. The location of the compensator poles is an important factor in obtaining the maximum value of static loop sensitivity (K_m) at the closed-loop poles on the crossing loci (i. e. those which cross the σ line boundary). In Figure 22 five of the compensator poles are located far out and one close to the origin. R_1 is the closed-loop pole on the crossing loci for flight-condition three (maximum M_δ). R_2 is the dominant pole for flight-condition one (minimum M_δ). If the contribution of the open-loop poles and zeros near the origin is neglected, the static loop sensitivity at R_1 is

$$K_{e_1} = ca^5 \quad (34)$$

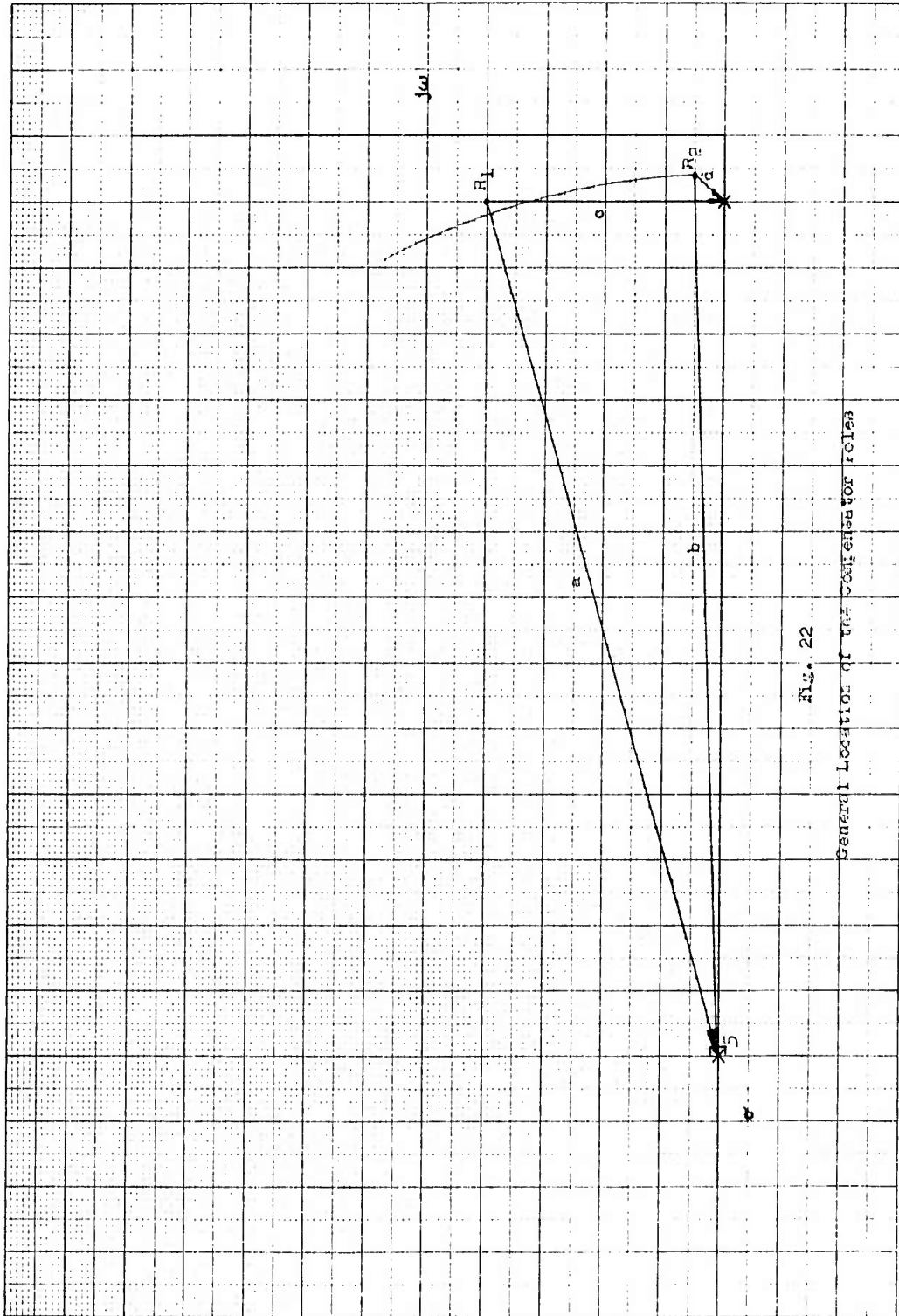


Fig. 22
General Location of the Competitor Roles

GGC/EE/63-2

and at R_2 is

$$K_{e_2} = db^5 \quad (35)$$

Since K_{e_1} must be 240 times K_{e_2} , then from Equation (35)

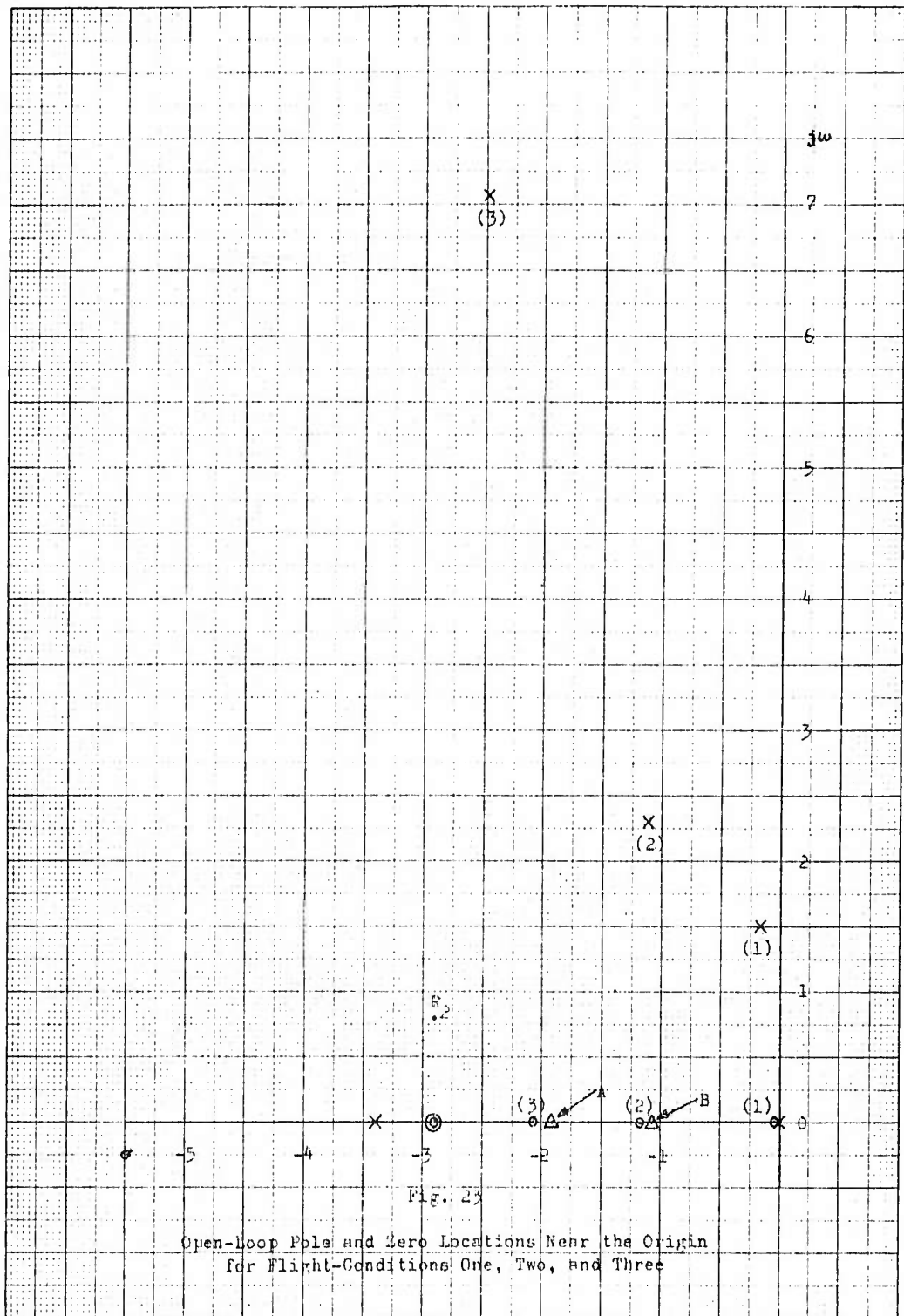
$$K_{e_1} = 240 db^5 \quad (36)$$

For a rough approximation, Figure 22 shows $a \approx b$. Using this approximation in conjunction with Equations (34) and (36),

$$c \approx 240 d \quad (37)$$

Equation (37) shows how the range of static loop sensitivity can be obtained by moving one compensator pole toward the origin; otherwise, with all six poles far out the difference would have to be made up by the two distances a and b , which is impractical as can be seen geometrically. This development also shows that to minimize the static loop sensitivity (and, therefore, the system gain) the distance d should be small. This implies that the dominant closed-loop poles should be close to the compensator pole. If the contribution of the open-loop poles and zeros near the origin is considered at R_2 , K_m would be increased; therefore, that contribution should also be held to a minimum.

Numerous trials were made to determine the best combination of closed-loop pole and compensator-pole locations for flight-condition one. The final result is shown in Figure 23. The closed-loop poles are located at $s = -3.4 \pm j 0.8$ and the compensator pole at



$s = -3.4$. To bound the pole movement, a unit circle was drawn about the closed-loop poles. By applying the 180° root-locus angle condition at the closed-loop pole, trial points were taken along the periphery of the circle to locate the pair of open-loop compensation zeros to be added. The open-loop zeros were both located at $s = -2.9$. This technique assumes that the angle contributions of the far-out poles are negligible.

As discussed in Chapter III (page 30), the effect of the root between the pole at the origin and the aircraft zero at -2.07 (flight-condition three) must be investigated. In Figure 23, the contribution of the poles and zeros to the static loop sensitivity at point A (one-tenth from the aircraft zero) is 1593. In Figure 23, the contribution at the dominant closed-loop poles for flight-condition one is 10.4. Assuming the far-out pole contributions are approximately the same at point A and at the dominant closed-loop poles, the static loop sensitivity at the dominant closed-loop pole is

$$K_{(1)} = 10.4 b^5 \quad (38)$$

and at point A

$$K_A = 1593 b^5 \quad (39)$$

where b is the distance shown in Figure 22. Since the static loop sensitivity for flight-condition three ($K_{(3)}$) is 240 times $K_{(1)}$

$$K_{(3)} = 240 (10.4 b^5) = 2500 b^5 \quad (40)$$

Comparing Equations (39) and (40) shows that the root will lie inside of point A. Since the root is so near the aircraft zero, the magnitude of the transient term due to the root should be very small (Ref 4:265). The only other flight condition where the aircraft zero is far from the pole at the origin is flight-condition two. In Figure 23 the contribution of the poles and zeros to the static loop sensitivity at point B (one-tenth from the aircraft zero for flight-condition two) is 40. By making the same assumption for the contribution from the far-out compensator poles, the static loop sensitivity at B (K_B) is

$$K_B = 40 b^5 \quad (41)$$

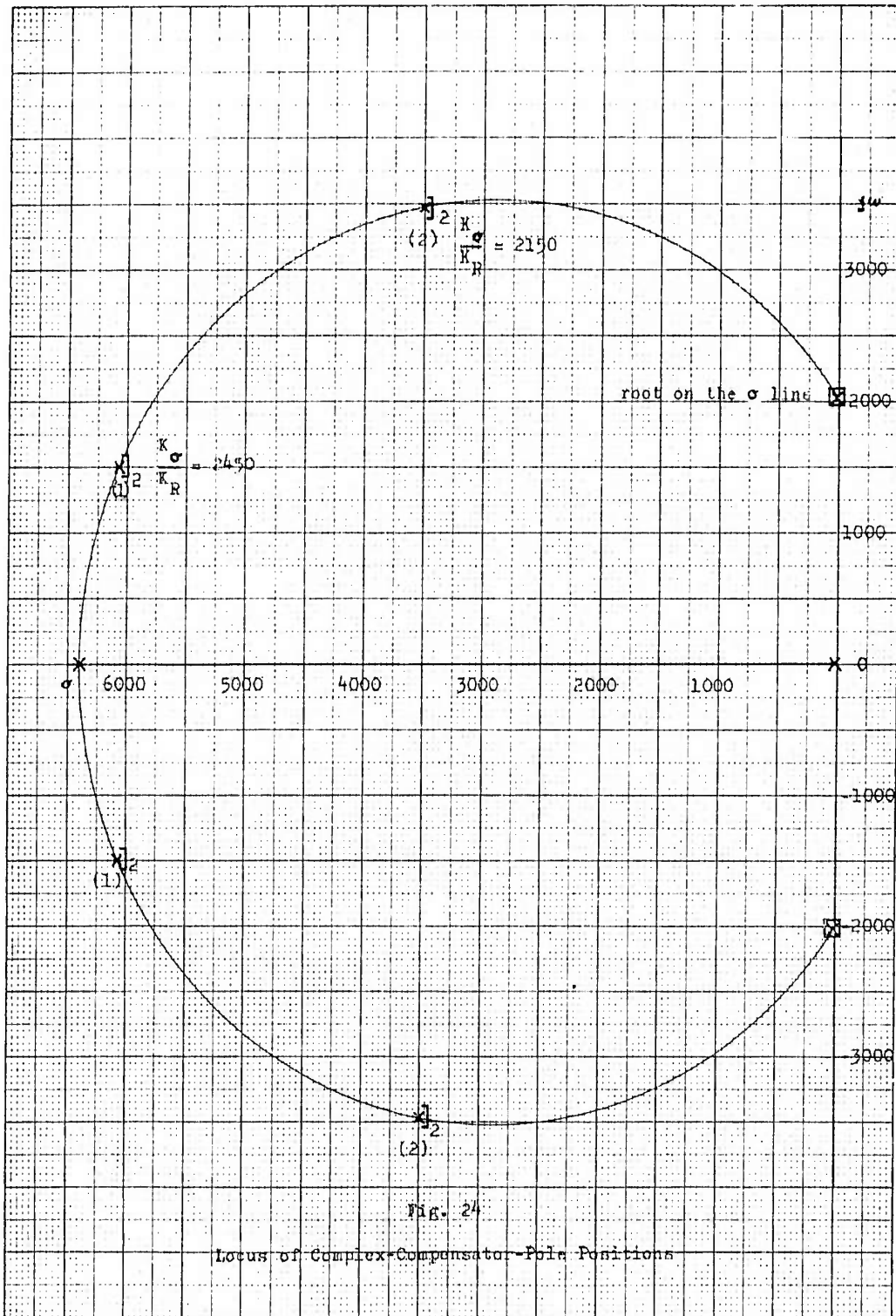
The static loop sensitivity for flight-condition two ($K_{(2)}$) is

$$K_{(2)} = \frac{M_{\delta_1}}{M_{\delta_2}} K_{(1)} = \frac{16.29}{0.22} 10.4 b^5 = 770 b^5 \quad (42)$$

Comparing Equations (41) and (42) shows that the root for flight-condition two will definitely be inside of point B and close to the aircraft zero.

A constant σ line was located at -20 so that the time constant of the dominant roots for flight-condition three would be a least five times the value of the time constant for the non-dominant roots. This is done to insure dominance and also to obtain some gain margin. To establish the remaining compensator pole locations for the minimum value of static loop sensitivity (which will give

the minimum compensator gain-bandwidth product) for flight-condition three, the roots on the crossing loci were assumed to be on the constant σ line. Trial points for the root were made along the constant σ line to find the far-out-compensator-pole locations that would yield a static loop sensitivity at the trial point 240 times the value at the dominant closed-loop pole position for flight-condition one. The location of the compensator poles were found by applying the 180° angle condition at the trial point. To simplify the computation, all five compensator poles were assumed to be at the same point. The root on the constant σ line (root at σ) was found at $s = -20 \pm j2025$ with the five compensator poles located at $s = -6400$. $K_{(1)}$ and $K_{(3)}$ were calculated to be 11.2×10^{19} and 2.684×10^{22} respectively. To see if the value of static loop sensitivity could be further reduced for the initial compensator pole locations, the static loop sensitivity was calculated for the root at σ with the complex-compensator-pole-positions shown in Figure 24. The segment of the circle in Figure 24 represents the locus of pole positions which contribute the same angle to the root at σ (Ref 6:10-11). At the σ -crossing point, the contribution from the poles and zeros near the origin for all flight conditions appears as a single pole located at the origin. The far-out-compensator-pole positions are changed to a pole at $s = -6400$ and two pair of complex poles on the segment of the circle. Since the pairs of complex poles lie on the circle, the 180° angle condition is still met at the root on the σ line. The static loop sensitiv-



ity from the new pole positions are calculated at the root at σ (K_σ). In order that $K_{(3)}$ remains 240 times $K_{(1)}$, the new values at the root on the σ line must be

$$K_\sigma = 240 (10.4 K_R) = 2500 K_R \quad (43)$$

where K_R is the new contribution to the static loop sensitivity (due to the new compensator pole positions) at the dominant closed-loop pole location for flight-condition one. Equation (43) shows that with the new far-out-compensator-pole positions the ratio of K_σ/K_R must be equal to or greater than 2500 for the new values of $K_{(3)}$ to be 240 times $K_{(1)}$. Figure 24 shows that no improvement in the value of static loop sensitivity could be made since the ratio of K_σ/K_R is less than 2500; therefore, the compensator poles were left at $s = -6400$.

The block diagram of the system is shown in Figure 25. If the open-loop zeros at $s = -2.9$ are placed in the forward branch they will appear as zeros of the closed-loop transfer function. Therefore, to preserve the closed-loop bandwidth established by the dominant closed-loop poles, the zeros were combined with two of the far-out compensator poles and placed in the feedback branch. After cancellation, the open-loop transfer function is

$$L = \frac{-2.89 \times 10^{19} K_f M_d (s+1/T_a)(s+2.9)^2}{s (s+6400)^5 (s+3.4)(s^2 + 2\zeta \omega_a s + \omega_a^2)} \quad (44)$$

where K_f is the amount of fixed gain inserted in the forward branch as shown in Figure 25. Considering the vehicle dynamics

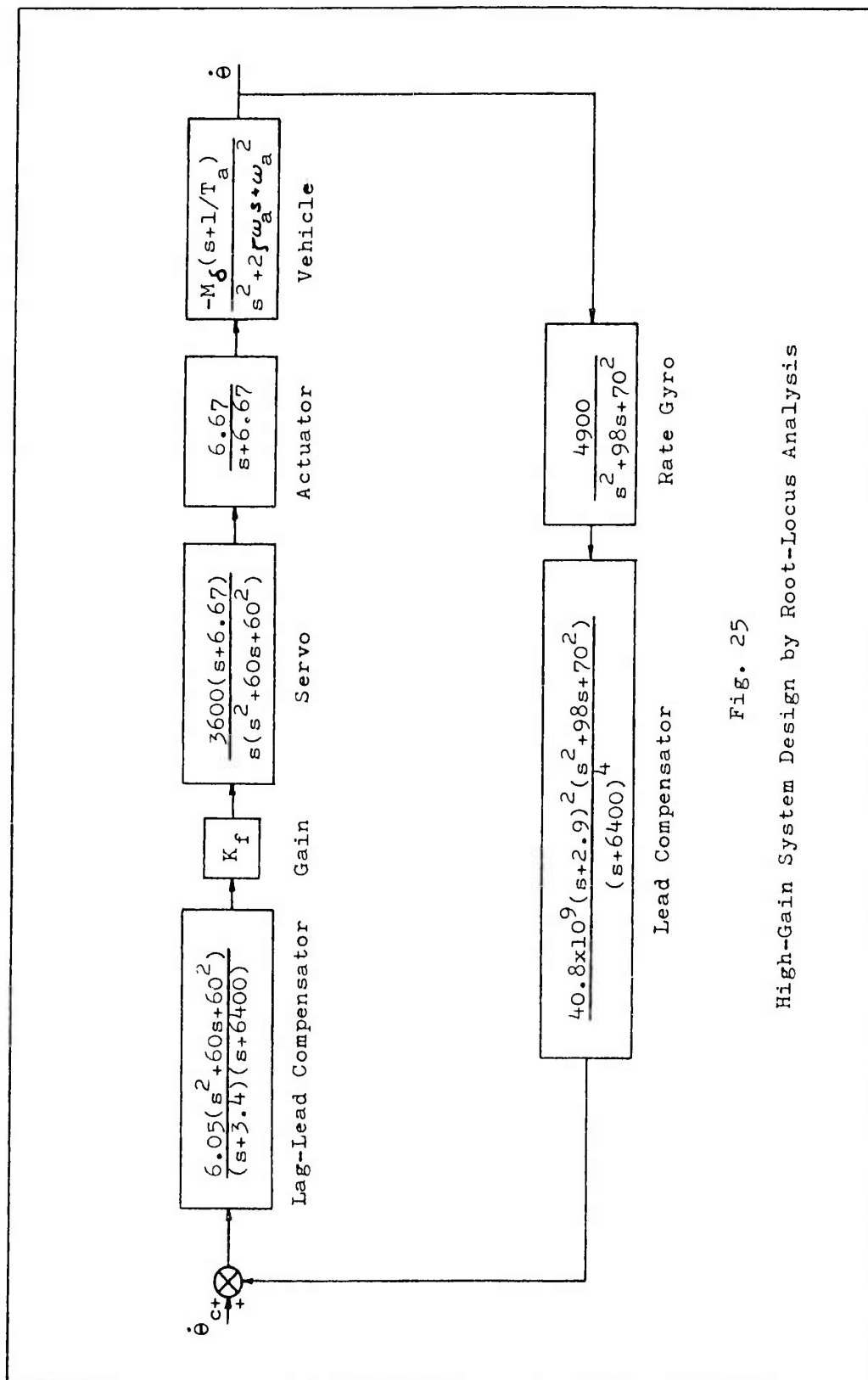


Fig. 25

High-Gain System Design by Root-Locus Analysis

for flight-condition one, K_f can be determined by

$$K_f = \frac{K_{(1)}}{(2.89 \times 10^{19}) M_{\delta(1)}} = \frac{11.2 \times 10^{19}}{(2.89 \times 10^{19})(0.22)} = 17.6 \quad (45)$$

Figure 26 shows the compensation loci. These will be the same for all flight conditions since the contribution of the poles and zeros near the origin appears as a single pole located at the origin for all flight conditions. The loci of the dominant poles for flight-conditions one, three, and six are shown in Figure 27. The dominant pole locations for each condition is shown on the plot. Neglecting the contributions of the far-out non-dominant roots, Figure 28 shows the range of variation of the approximate closed-loop response to command inputs for all flight conditions. The range of variation (shown by the shaded region) indicates that the sensitivity of the closed-loop response to the vehicle-parameter variations is extremely small over a wide range of frequencies.

The analog computer circuitry for the system simulation is shown in Appendix E. Unfortunately, no response data could be obtained because of severe noise problems. The circuits for the compensator transfer functions $\frac{2210(s+2.9)}{(s+6400)}$ (Fig. E-1) caused the greatest difficulty. When the circuits were completely isolated from the computer loop, noise was picked up by the external components causing the circuit to oscillate with peak amplitudes as high as 40 volts. With the circuits connected in the computer loop, the high forward-branch gain would amplify these oscillations causing saturation throughout the system. Because of extremely low pot

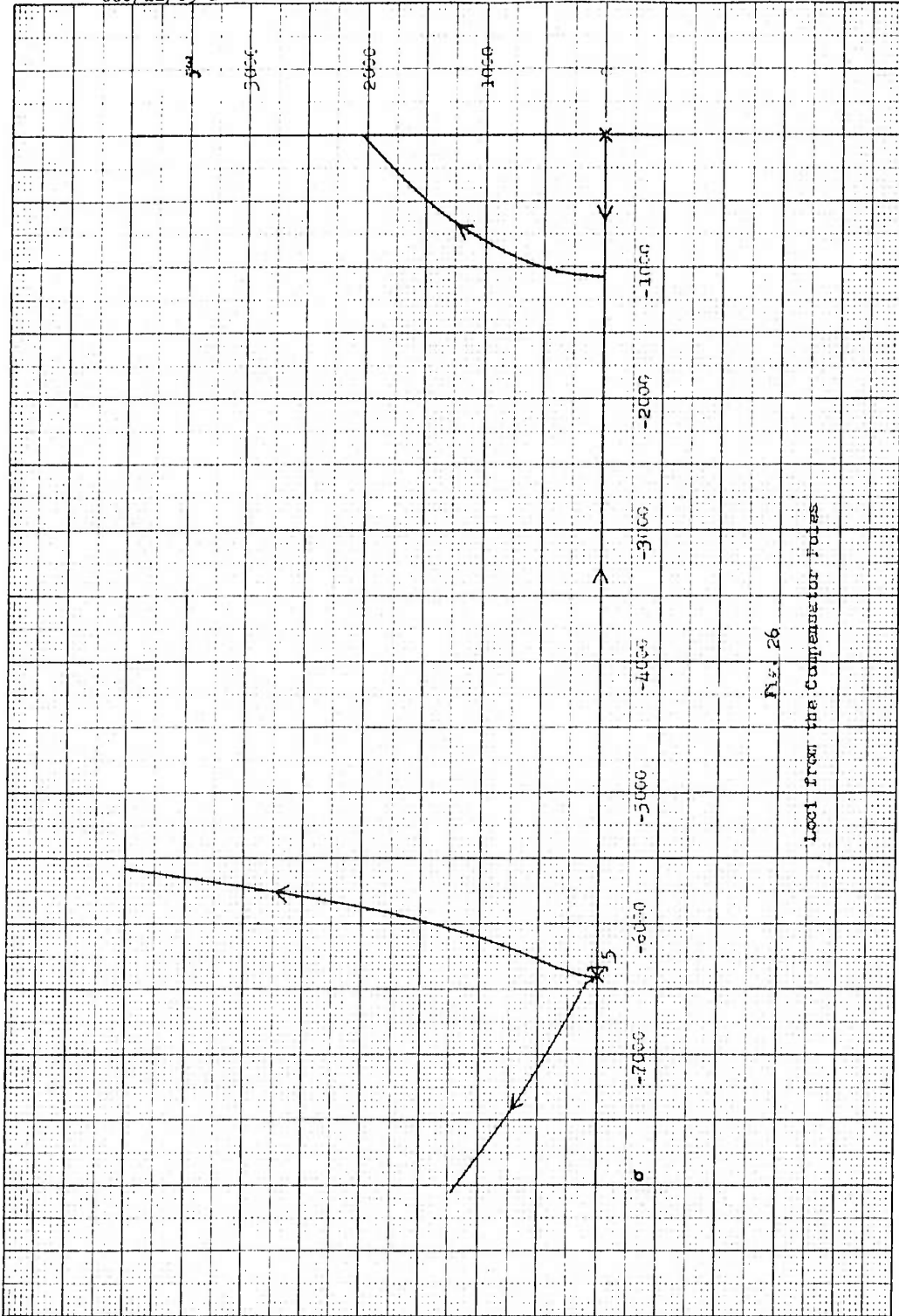


Fig. 26

Loop from the Compensator Poles

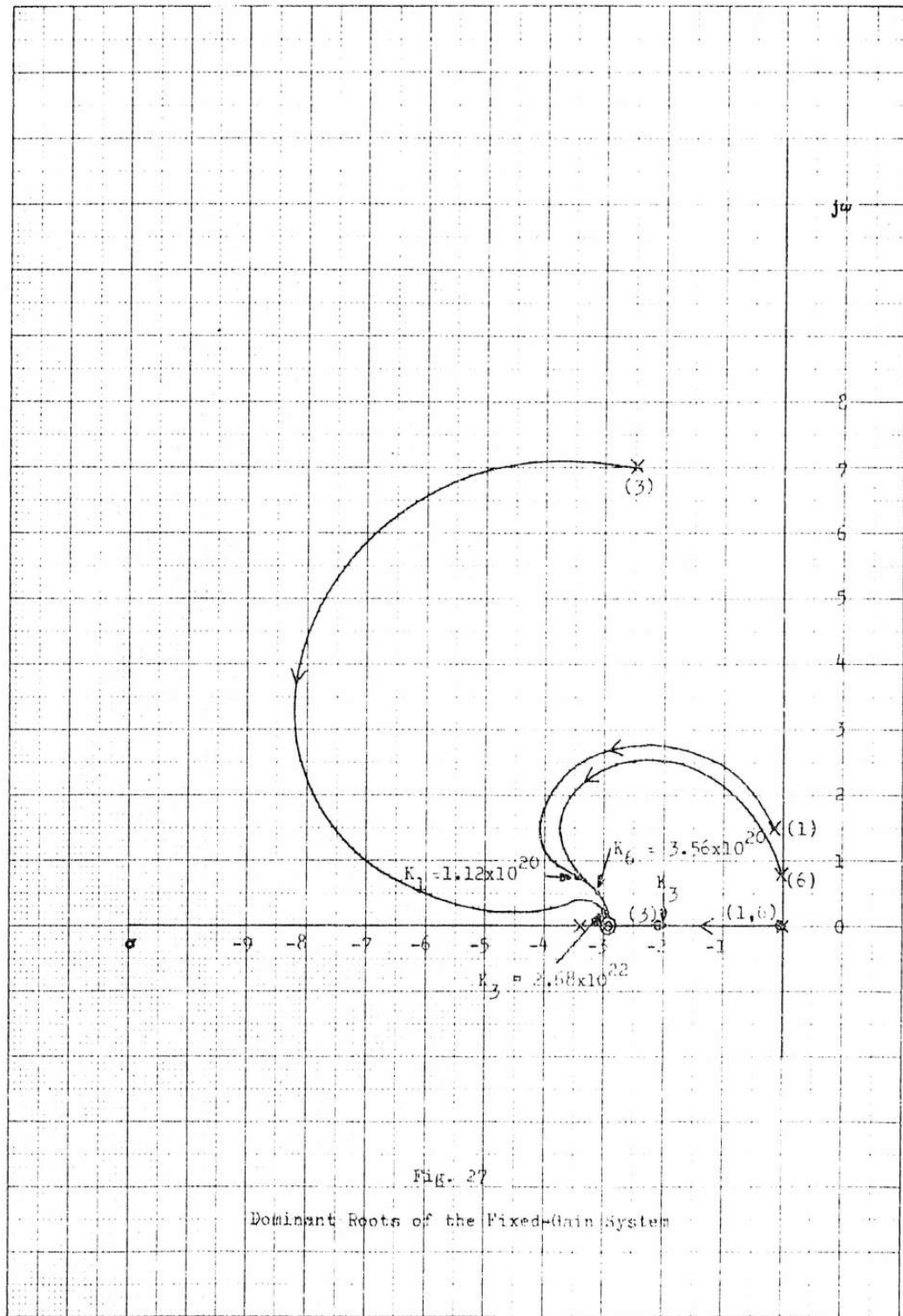
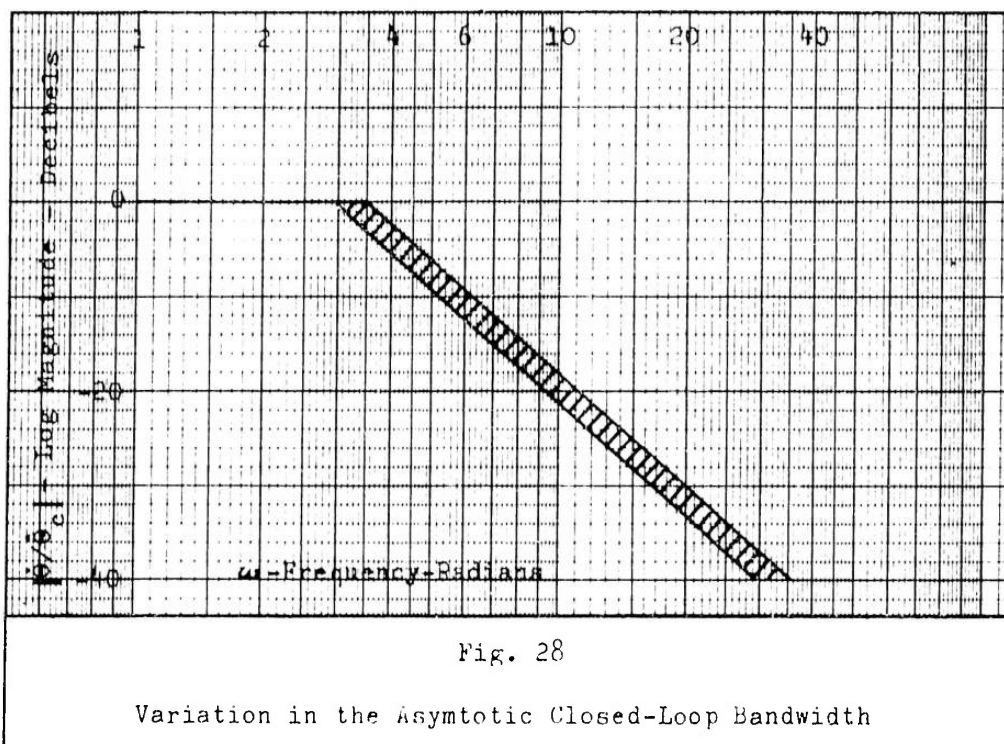


Fig. 27

Dominant Roots of the Fixed-Gain System



settings in the aircraft dynamics circuit, time scaling was limited to a factor of 10. The saturation problem still existed with the circuit time scaled by 10. The compensator circuits were redesigned to give a series, rather than a parallel, input impedance. Within the limited practical range of component values available to simulate the transfer function, no significant improvement could be made in reducing the noise.

The design was re-evaluated to determine if the system gain could be diminished and the large compensator bandwidths reduced. The system insensitivity was decreased by allowing greater movement of the dominant closed-loop poles. The results showed that no significant improvement could be made in reducing the values of static loop sensitivity or the far-out compensator pole locations.

The problem was discussed with Horowitz during a visit to the Flight Control Laboratory. He indicated the gain-bandwidth problems were resulting from the requirements of a dominant system. He had a copy of his recently published text book in which is discussed the costly gain-bandwidth demands on L of a dominant root-locus design (Ref 8:266-267). He states in the text, "...one pays a price in gain-bandwidth for the simpler analytical root locus s -plane design procedure." (Ref 8:363) He recommended that a non-dominant design be attempted using the frequency-response method.

Frequency-Response Method

In the frequency-response approach, the requirement for system sensitivity to vehicle-parameter variations is considered in terms of the system's bandwidth. If the desired system bandwidth is some value ω_b , the system sensitivity can be specified to be extremely low for $0 \leq \omega \leq \omega_b$ and for $\omega > \omega_b$ the requirements can be relaxed in order to economize the gain-bandwidth demands of L . Multiple compensation can be used in conjunction with frequency-response analysis to reduce, by any desired degree, the system insensitivity outside the system bandwidth. In contrast, a dominant root-locus design requires the designer to maintain the system insensitivity far beyond the bandwidth of the system (as was shown in Fig. 28).

To ease some of the feedback-compensation problems experienced in the root-locus design, it was decided to use a model-prefilter system as described in Chapter III and shown in Figure 6. If the

closed-loop bandwidth of the feedback loop is several times the model bandwidth, the system bandwidth is determined by the model. This implies that the system sensitivity requirement can be constrained to a frequency range slightly larger than the model bandwidth.

The transfer function of the model was selected to be the same as the one used in Chapter III ($\frac{2}{s+2}$). The rate gyro and servo poles were again canceled by complex compensation to allow free movement of the four compensator poles. The proportional-plus-integral zero was used to cancel the effect of the actuator pole. Therefore, with the same cancellations, the open-loop transfer function of the system hardware and vehicle dynamics is the same as Equation (32). Figures 29 and 30 show the log-magnitude and phase angle of Equation (32) for all six flight conditions.

The design technique employs log-magnitude and phase diagrams to shape, with compensation networks, the open-loop transfer function of the feedback loop. The requirement for insensitivity over the model bandwidth implies high open-loop gain over this frequency range. With high open-loop gain, the closed-loop transfer function of the feedback loop can be approximated by $\frac{1}{H}$ (Eq 29). This means that the value of H should be unity over a frequency range slightly larger than the model bandwidth so that the feedback loop will transfer the model response directly to the output of the system. Figure 29 shows that the fixed-gain level of the feedback loop must be increased so that flight-condition one can meet the above requirements. It will be shown that the amount the fixed-

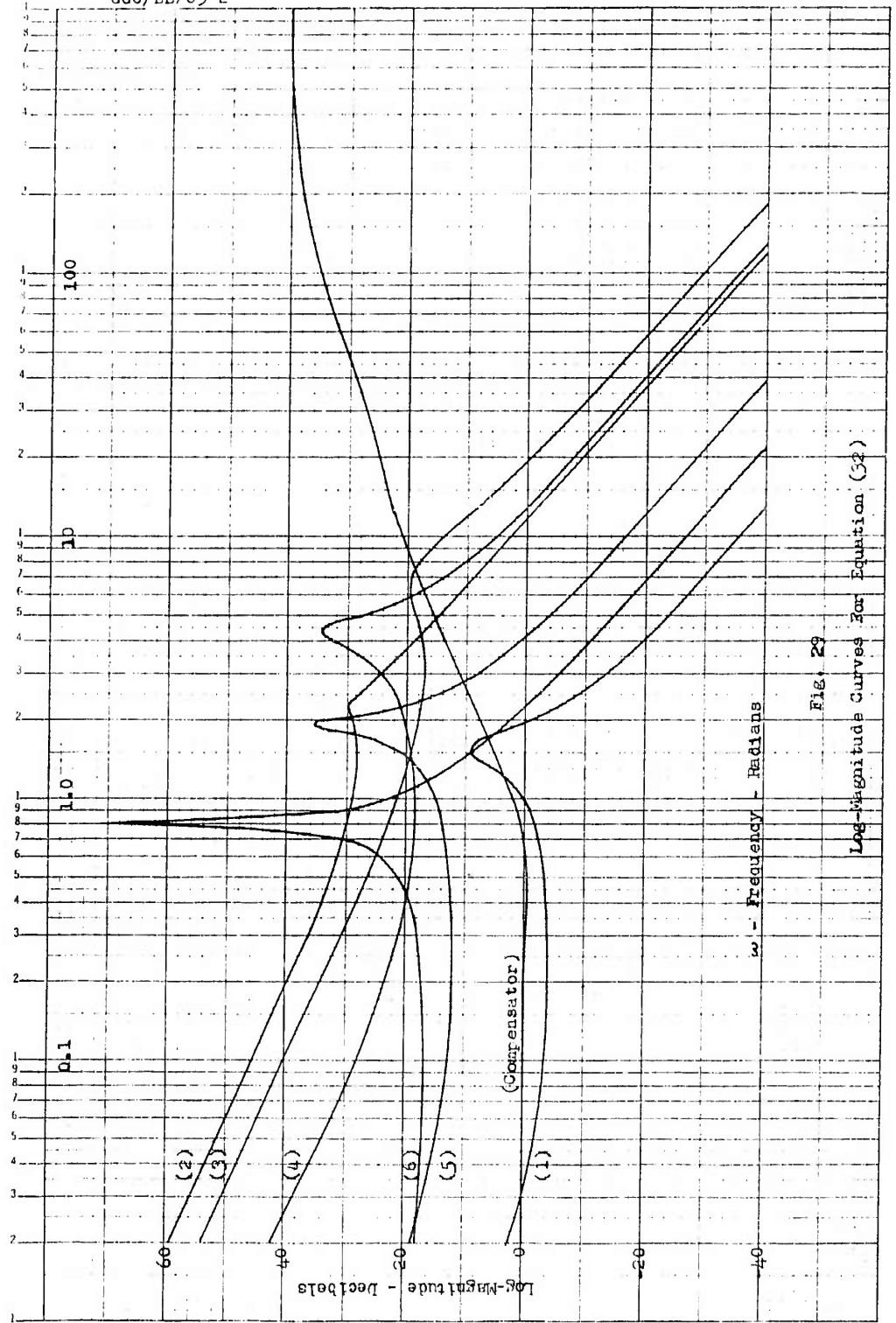


Fig. 29
Log-Magnitude Curves For Equation (32)

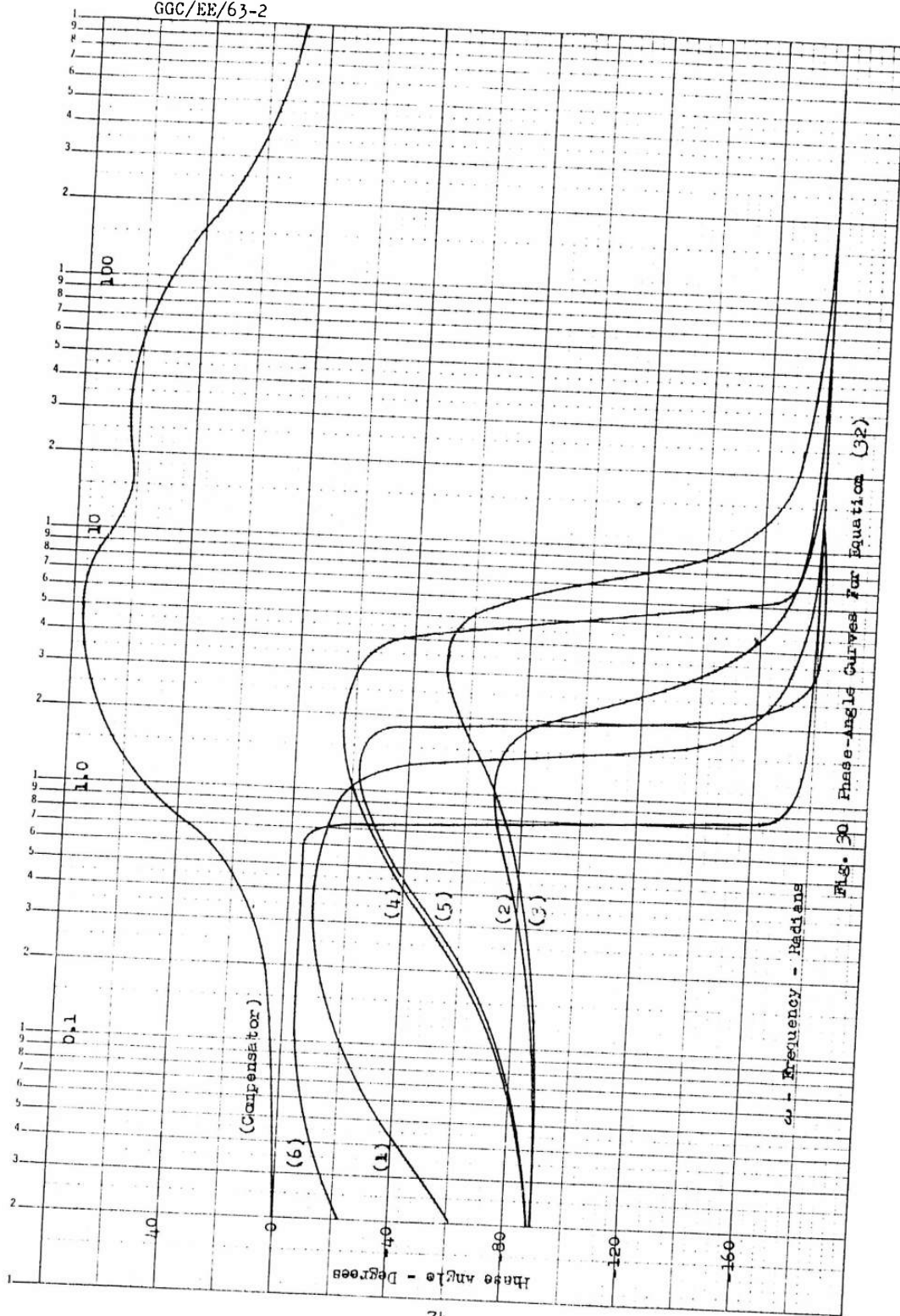


Fig. 30 Phase-angle Curves for Equation (32)

gain level can be increased is dependent on the amount of gain margin that is available for flight-condition three after compensation. Figure 30 shows that the compensation must provide a sufficient amount of positive phase angle (lead) to offset the rapid phase angle descents caused by the lightly damped vehicle poles. The positive phase angle must be provided over a frequency range of 0.8 to 10 radians so that adequate phase margin can be obtained for each flight condition.

The compensator pole and zero locations are shown in Table II.

Table II
Compensator Parameters

| Poles | | | Zeros | | |
|-------|---------|------------|-------|---------|------------|
| Real | Complex | | Real | Complex | |
| 1/T | ζ | ω_n | 1/T | ζ | ω_n |
| 1 | 0.7 | 6.4 | 15 | 0.7 | 0.8 |
| 2.5 | 0.3 | 2500 | | 0.7 | 4.0 |
| 150 | 0.5 | 4400 | | | |

The log-magnitude and phase angle provided by the compensator are shown in Figures 29 and 30. The complex zeros at $\omega_n = 0.8$ were located to offset the phase angle descent of condition six. To limit the log-magnitude and positive phase-angle contributions of the compensator, two real poles were located at 1 and 2.5. The complex zeros at $\omega_n = 4$ were located to serve two purposes: (1) to increase the bandwidth of condition one so that it will be

at least twice the model bandwidth and (2) to maintain the positive phase angle of the compensator out to 10 radians. The complex poles at $\omega_n = 6.4$ were located to reduce the log-magnitude of the compensator and thereby decrease the open-loop bandwidths of conditions two, three, and five. The real zero and pole, located at 15 and 150 respectively, were placed to shape the descent of the compensator phase-angle curve. The four poles associated with the compensators used to cancel the rate gyro and servo poles were located last. The four poles were positioned to give a 20° phase margin and 10 db gain margin for flight-condition three when an additional fixed-gain factor (K_f) of 2.52 (8db) is added to the feedback loop. The pole locations are shown in Table II as $\omega_n = 2500$ and $\omega_n = 4400$.

The compensated curves for all flight conditions are shown in Figures 31 and 32. Figure 33 is the block diagram for the complete system. After cancellation, the open-loop feedback transfer function is

$$L = \frac{-8.06 \times 10^{16} K_f M_d (s+1/T_a) (s^2+1.12s+0.8^2)}{s(s^2+2\zeta\omega_a s+\omega_a^2)(s+1)(s+2.5)(s^2+8.96s+6.4^2)(s+150)} \frac{(s^2+5.6s+4^2)(s+15)}{(s^2+1500s+2500^2)(s^2+4400s+4400^2)} \quad (46)$$

Computer Simulation

The analog computer circuitry for the system simulation is shown in Appendix F. The additional fixed-gain factor (K_f) was set at 2.52 (8db). Figure 34 shows the model and system response to a command input ($\dot{\theta}_c$) for flight-conditions one and three. For flight-

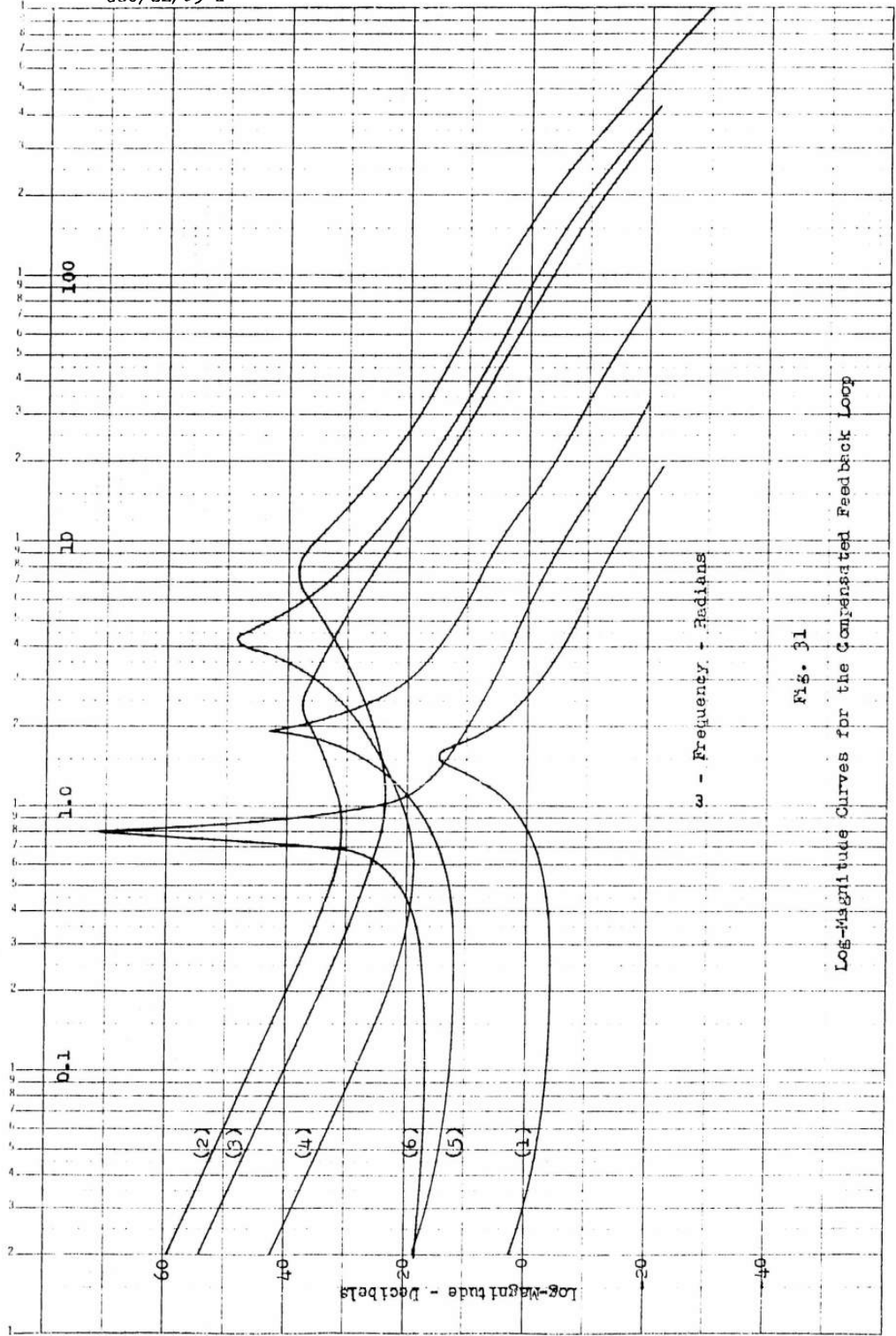
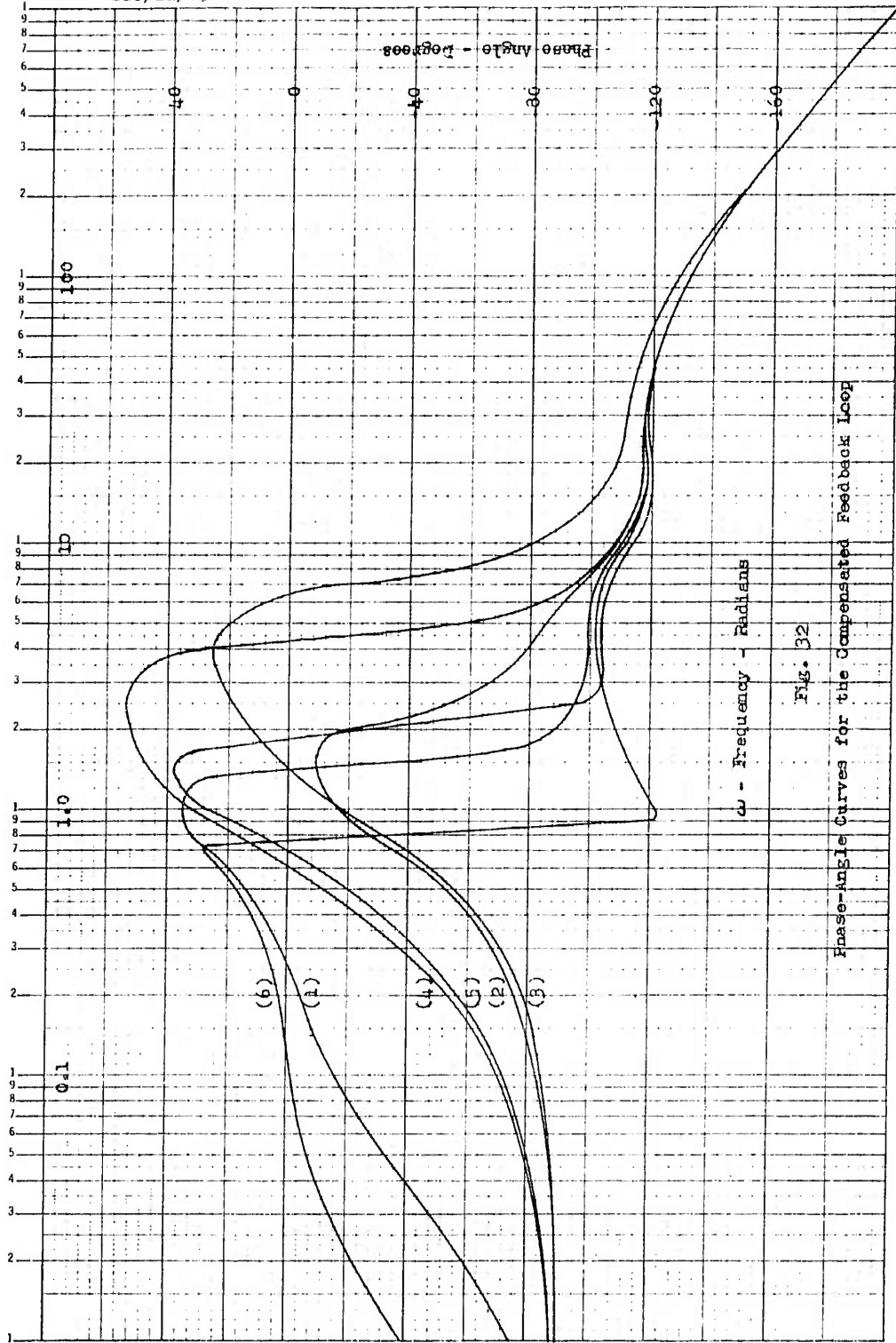


Fig. 31

Log-Magnitude Curves for the Compensated Feedback Loop



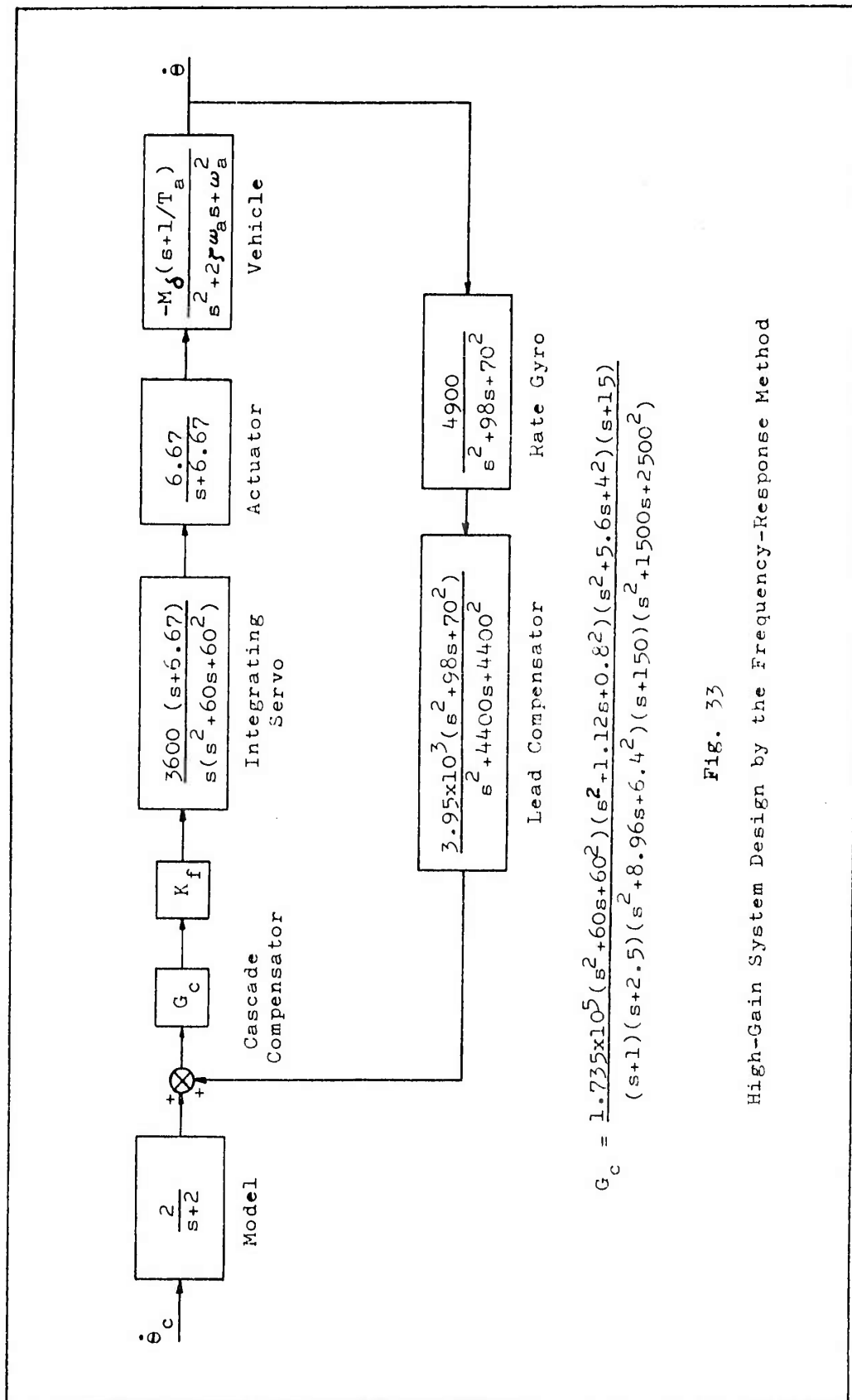


Fig. 33

High-Gain System Design by the Frequency-Response Method

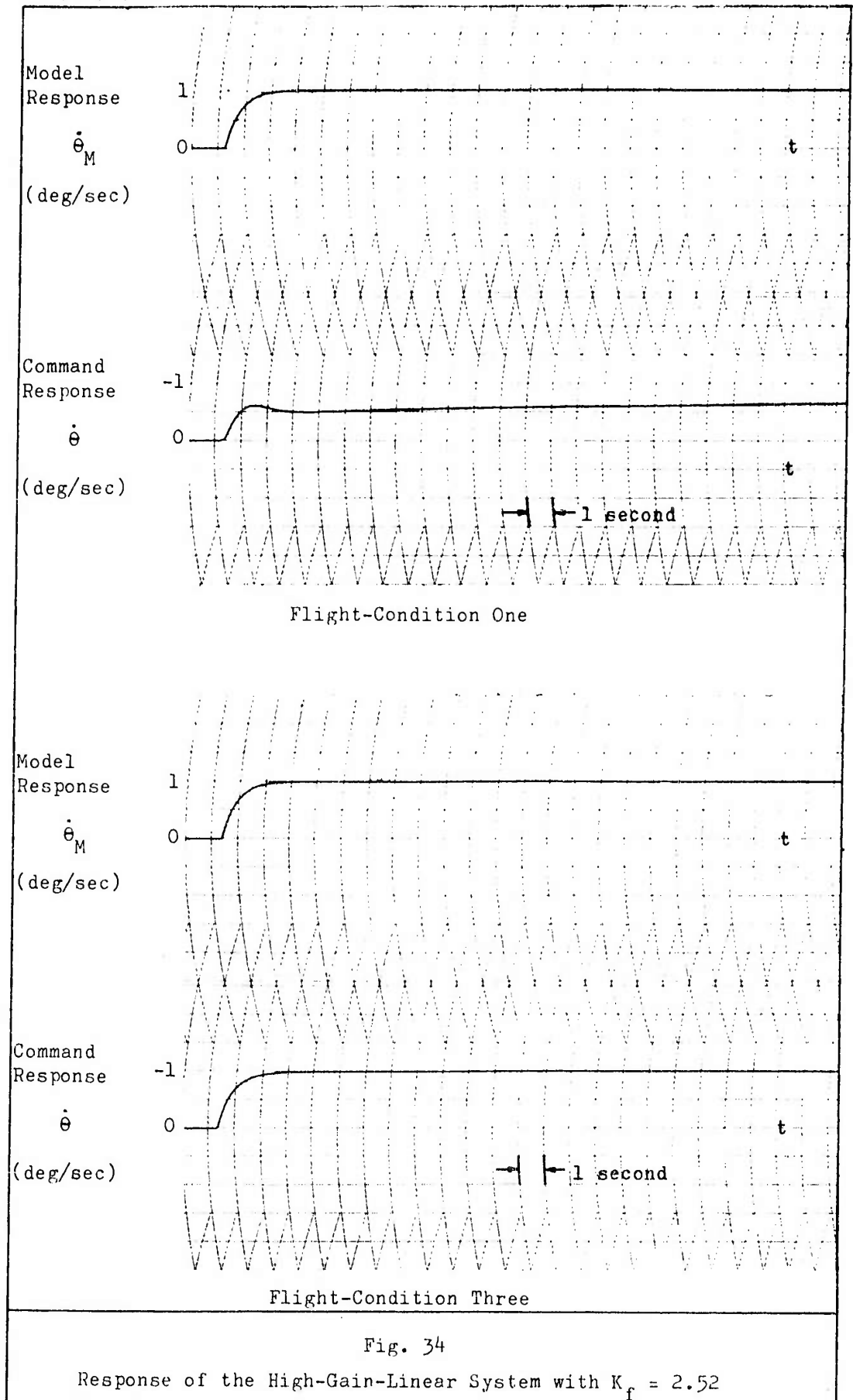
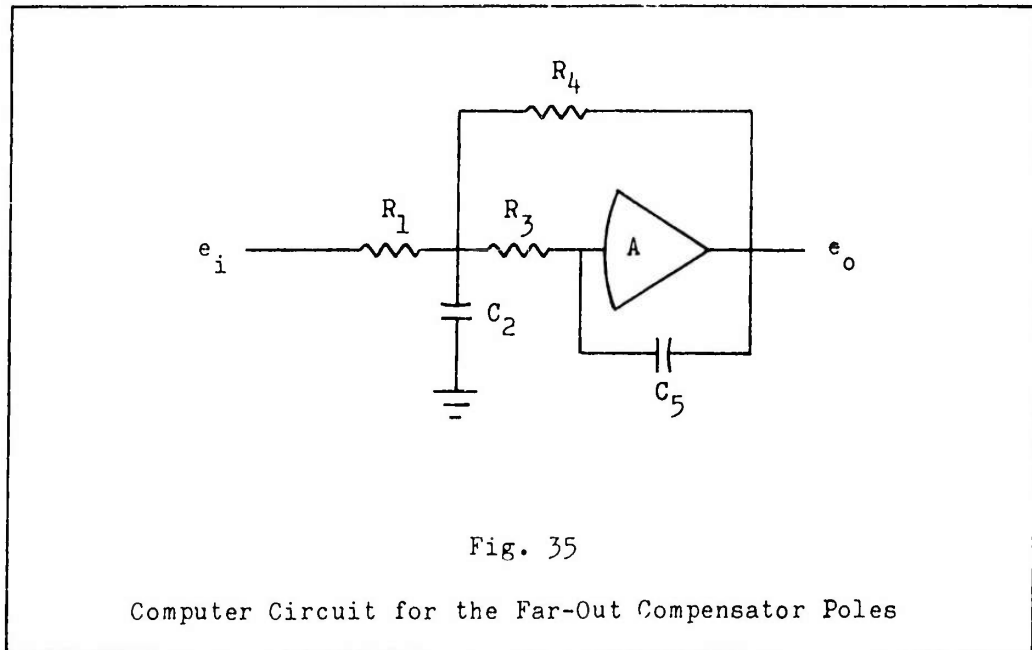


Fig. 34

Response of the High-Gain-Linear System with $K_f = 2.52$

condition three (maximum M_d), the feedback loop follows the model response "exactly". The system response for flight-condition one (minimum M_d) does not meet the command response criteria (90 percent of the commanded value within three seconds) since it is 50 percent of commanded value at three seconds. The slow rise to the commanded pitch rate is due to the closed-loop pole between the integrator pole at the origin and the aircraft zero at $s = -0.0356$. The transient response of this closed-loop pole is of the form $Ae^{-t/T}$. The time constant T is large and the value of the coefficient A is negative since the residue associated with the pole is negative. To offset the effect of the large time constant, the residue must be made very small to reduce the value of A . This is accomplished by having the feedback-loop gain high enough to move the pole very close to the aircraft zero. From the computer analysis, it was determined that if the feedback-loop gain was increased by increasing K_f to 10 (20db) the slow rise was eliminated. The value of K_f that can be used for all flight conditions is dependent upon the gain margin available at flight-condition three. It was found that with $K_f = 2.52$ only 4 db of gain margin was available at flight-condition three instead of the 10 db predicted from the design analysis. The reason for the discrepancy is attributed to the following two factors: (1) the accuracy obtainable from graphical analysis, and (2) the effect of the computer circuits that were used to simulate the complex compensator poles located at $\omega_n = 2500$ and $\omega_n = 4400$. Figure 35 shows the general computer circuit used to simulate these compensator poles. The feedback capacitor C_5



was $800\mu\text{f}$ in the circuit simulating the poles at $\omega_n = 2500$ and $756\mu\text{f}$ in the circuit simulating the poles at $\omega_n = 4400$ (see Fig. F-1). Capacitance values in this range can be greatly affected by increases due to stray or wiring capacitance. The effect of increasing C_5 can be seen from the transfer function of the general computer circuit, which is (Ref 10:445)

$$\frac{e_o}{e_i} = \frac{1/R_1 R_3 C_2 C_5}{s^2 + \frac{(R_3 R_4 + R_1 R_3 + R_1 R_4)}{R_1 R_3 R_4 C_2} s + \frac{1}{R_3 R_4 C_2 C_5}} \quad (47)$$

Equation (47) shows that if C_5 is increased ω_n is decreased. With ω_n decreased, the phase angle associated with these complex poles will shift the phase-angle curve for flight-condition three more negative at the gain-crossover frequency, ω_ϕ . With the phase-angle curve more negative at ω_ϕ , the frequency ω_c at which phase

crossover occurs (i.e. 180° crossover frequency) will be reduced. Since the log-magnitude of the highly-damped far-out poles does not affect the log-magnitude curve near ω_c , reducing ω_c will reduce the gain margin.

To obtain a $K_f = 10$ for all flight conditions, the real zero and pole originally located at 15 and 150 respectively, were increased in value on the computer while monitoring the stability of flight-condition three. With the real zero and pole located at 80 and 800 respectively, a feedback-loop gain level with $K_f = 10$ was obtained for flight-condition three. The gain margin for condition three with $K_f = 10$ was determined by the computer analysis to be 3.2 db.

As mentioned previously, the purpose of the real zero and pole is to shape the descent of the compensator phase-angle curve. Figures 36 and 37 show the change in log-magnitude and phase angle of the compensator due to the relocation of the real zero and pole to 80 and 800. Figure 32 shows that for $\omega > 10$ the phase-angle curves for all flight conditions are essentially the same as the compensator phase-angle curve. Therefore, with the new compensator zero and pole location, the change in the flight-condition phase-angle curves for $\omega > 10$ can be seen from Figure 37. Figure 36 shows that the new compensator has a reduction in log-magnitude for $10 < \omega < 1000$. Referring to Figure 31, with the operating point at -20db ($K_f=10$) the log-magnitude reduction of the compensator will reduce the open-loop bandwidth for all six flight conditions since they lie in the same frequency range. With the new compensator

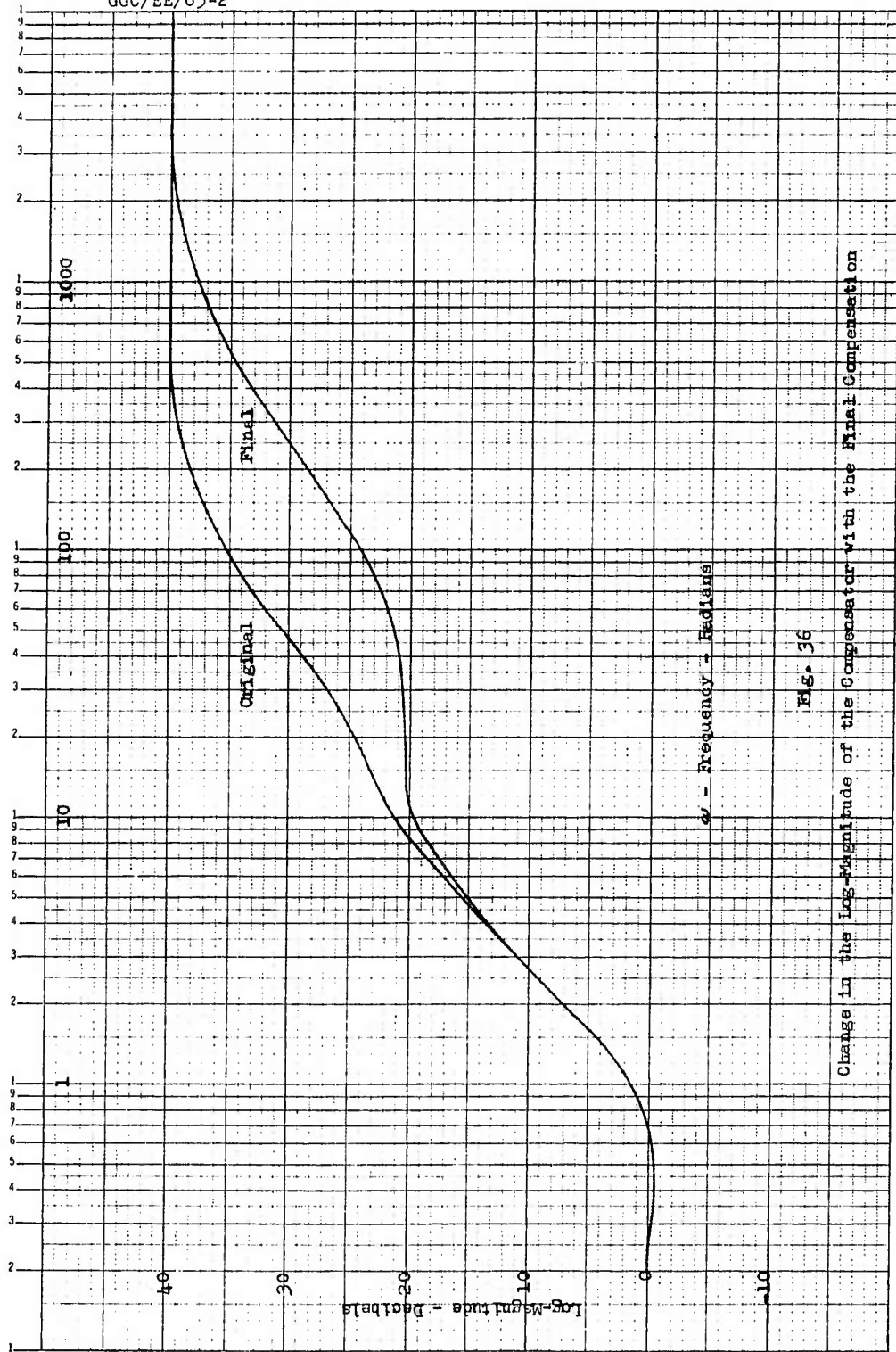


Fig. 36

Change in the Log-Magnitude of the Compensator with the Final Compensation

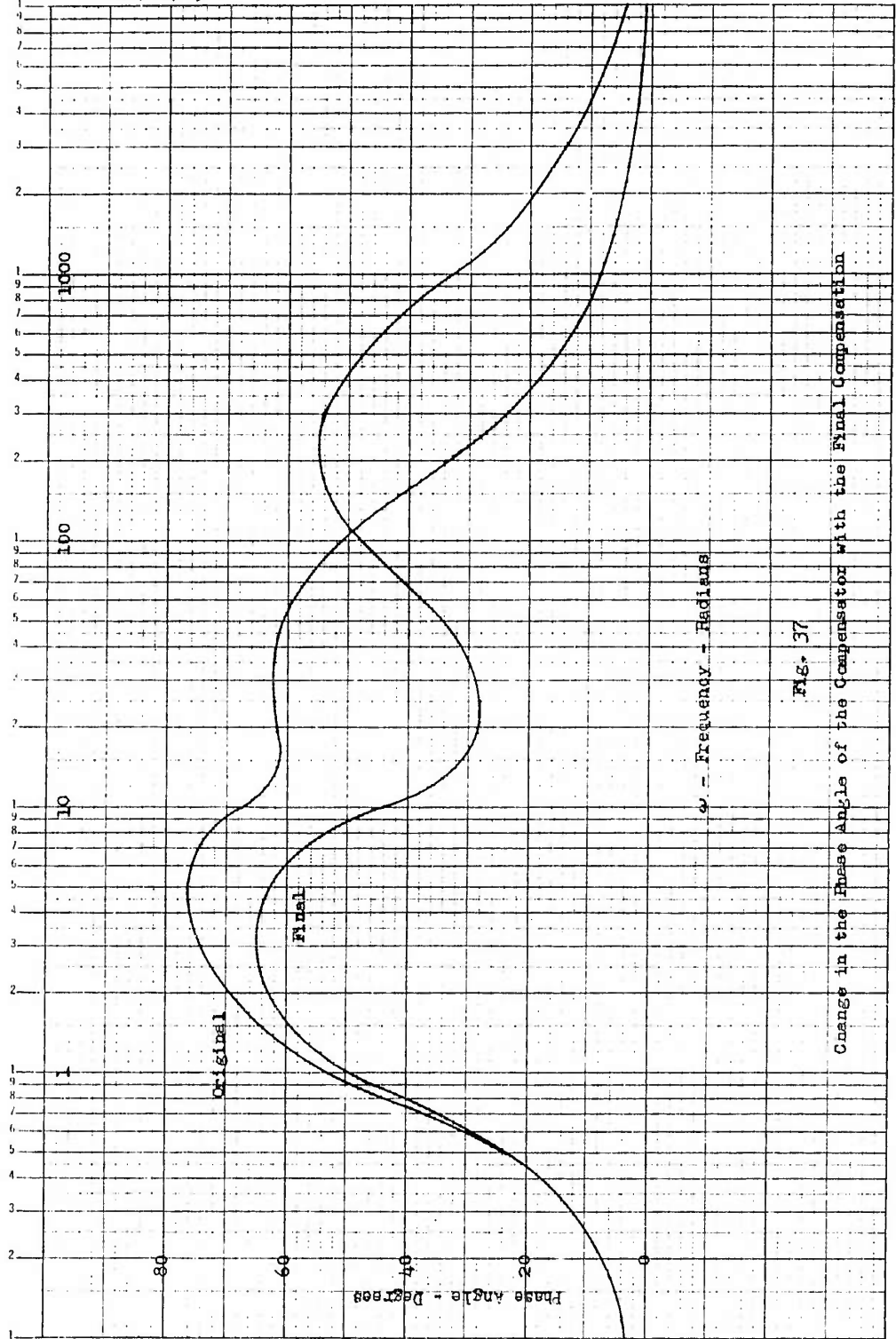


FIG. 37

Change in the Phase Angle of the Compensator with the Final Compensation

frequency-characteristic curves the open-loop bandwidth, the phase margin, and the gain margin were obtained from the graphical analysis for all flight conditions and are shown in Table III.

Table III

Open-Loop Frequency-Response Data for the Linear System

| Flight Condition | Open-Loop Bandwidth (Radians) | Phase Margin (Degrees) | Gain Margin (db) |
|------------------|-------------------------------|------------------------|------------------|
| 1 | 15.2 | 36 | 52.8 |
| 2 | 210.0 | 52 | 24.6 |
| 3 | 520.0 | 46 | 15.2 |
| 4 | 275.0 | 50 | 21.0 |
| 5 | 48.5 | 32 | 30.7 |
| 6 | 26.2 | 28 | 39.5 |

Figures 38 through 43 show the step response of the system to a commanded pitch rate and a disturbance of the control surface angle (δ) for all flight conditions with $K_f = 10$. The command response meets the criteria of 90 percent of the commanded value within three seconds for all flight conditions. The disturbance criteria (disturbances will be damped to less than one-fourth amplitude in one cycle) is met since the response oscillation is damped out within one cycle for all flight conditions. As was predicted from Equation (26), the magnitude of the disturbance response is small for all flight conditions because of the large open-loop gain of L. As shown by Equation (28), the relative change in the disturbance response will be small if G and H are large. By comparing the disturbance response of flight-conditions one and

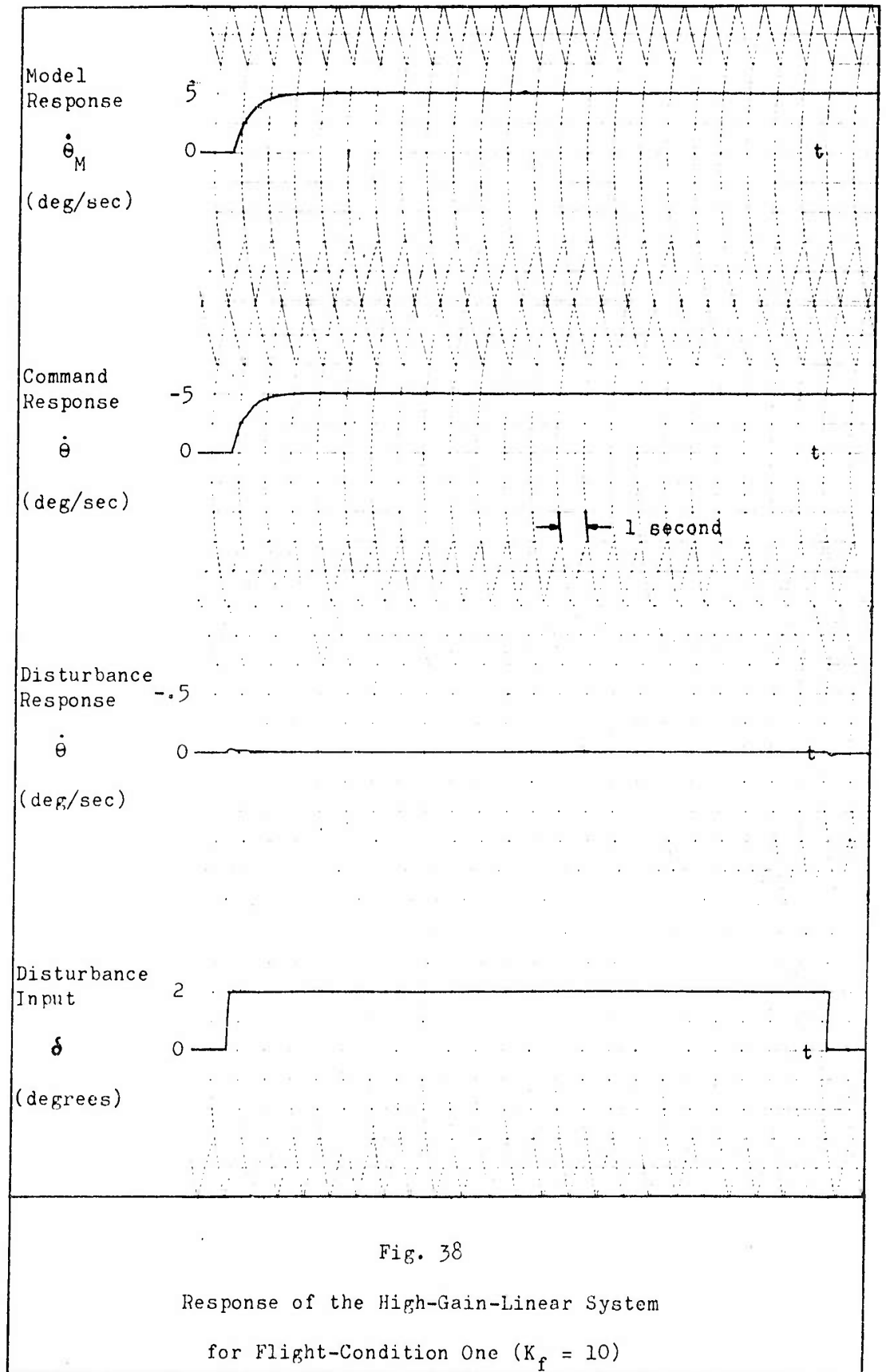


Fig. 38

Response of the High-Gain-Linear System

for Flight-Condition One ($K_f = 10$)

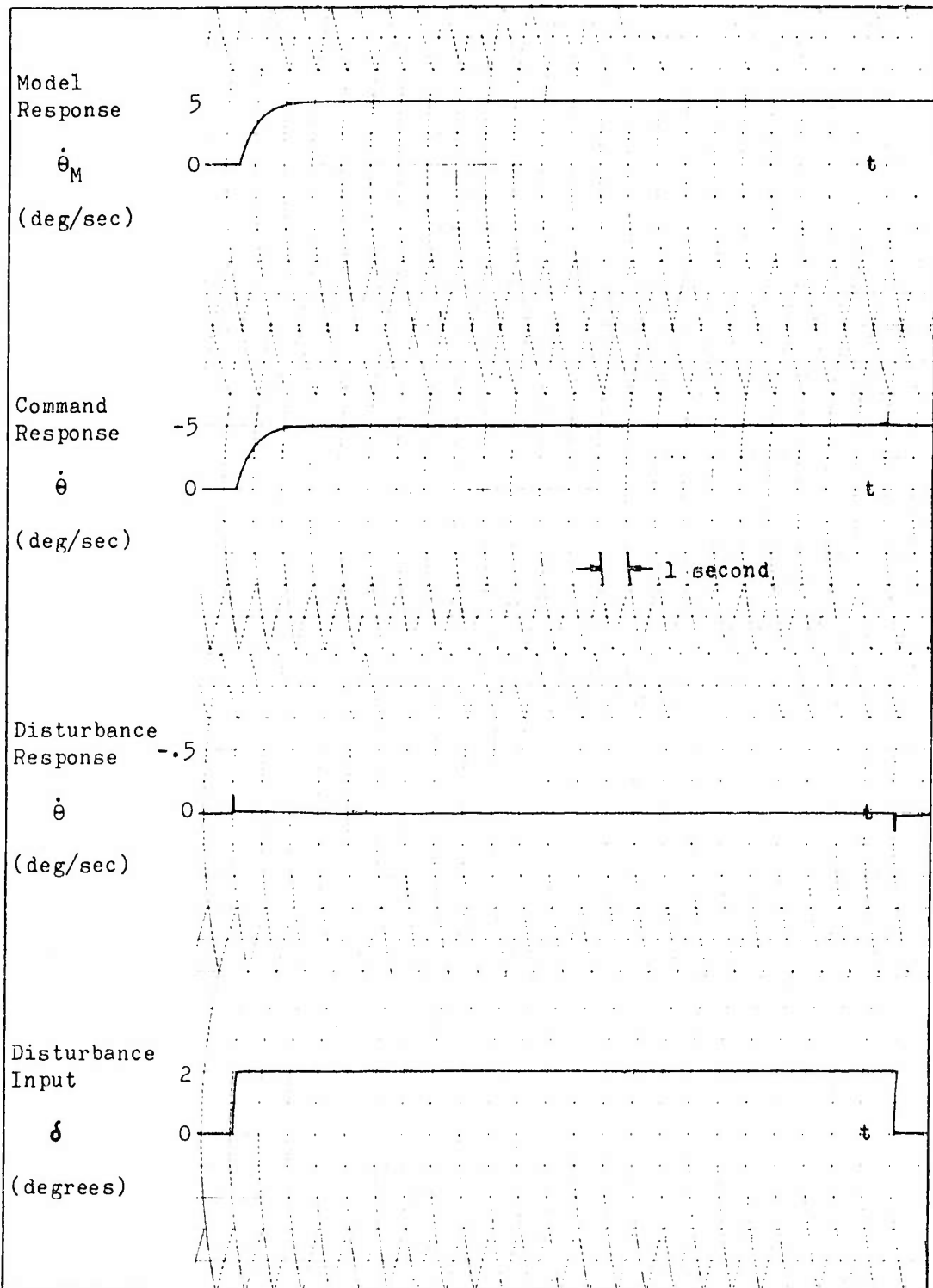


Fig. 39

Response of the High-Gain-Linear System
for Flight-Condition Two ($K_f = 10$)

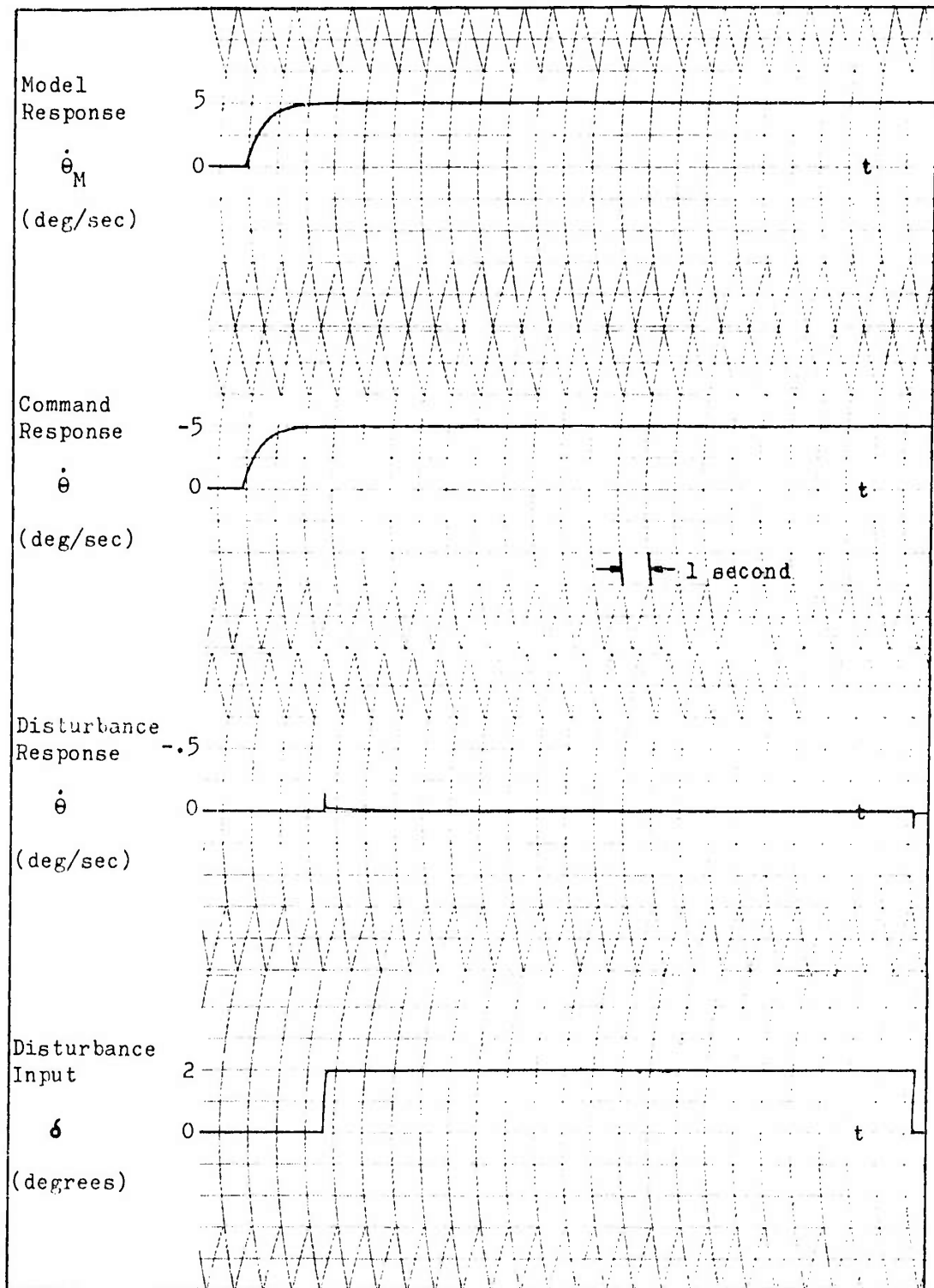
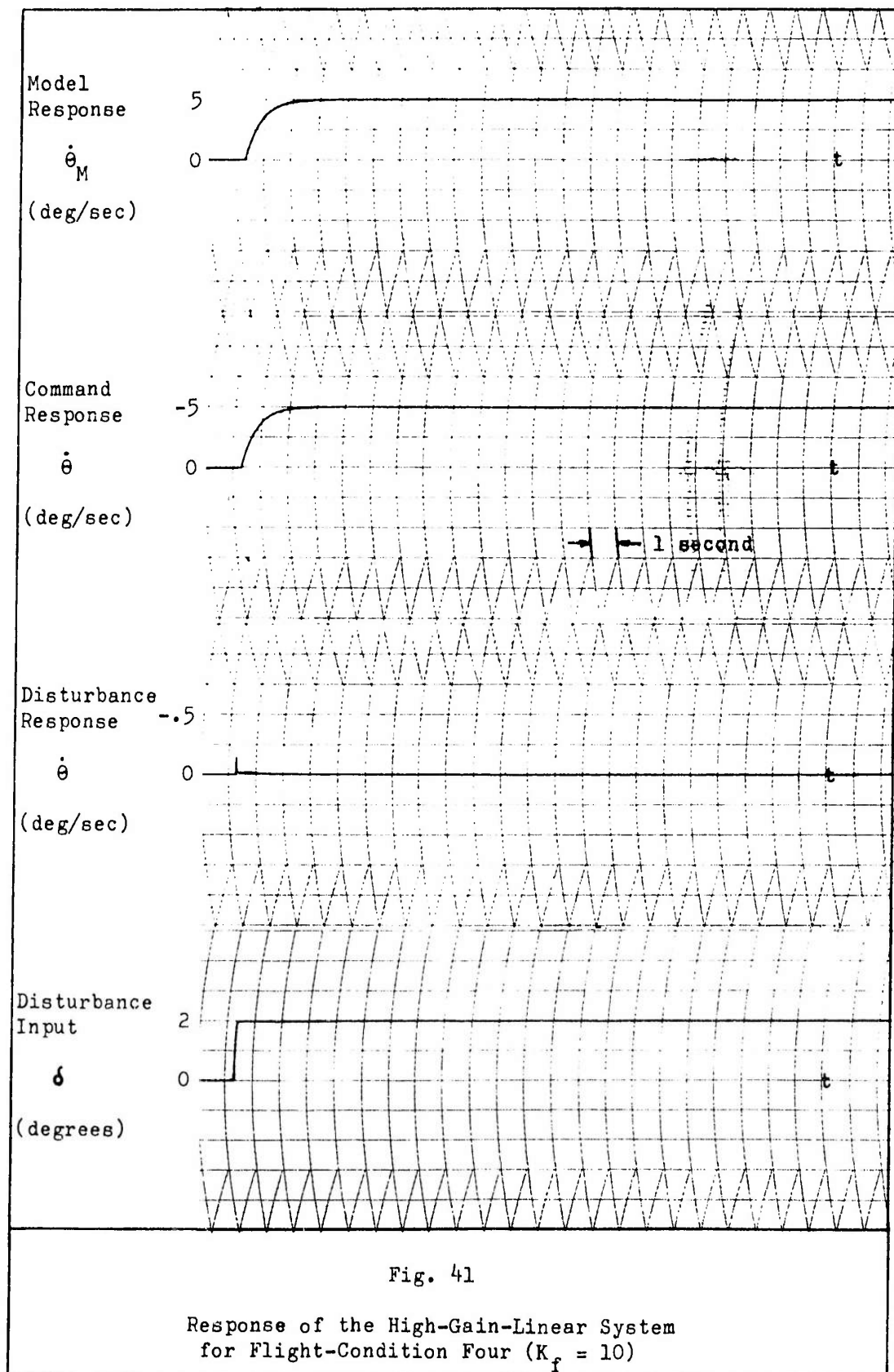


Fig. 40

Response of the High-Gain-Linear System
for Flight-Condition Three ($K_f = 10$)



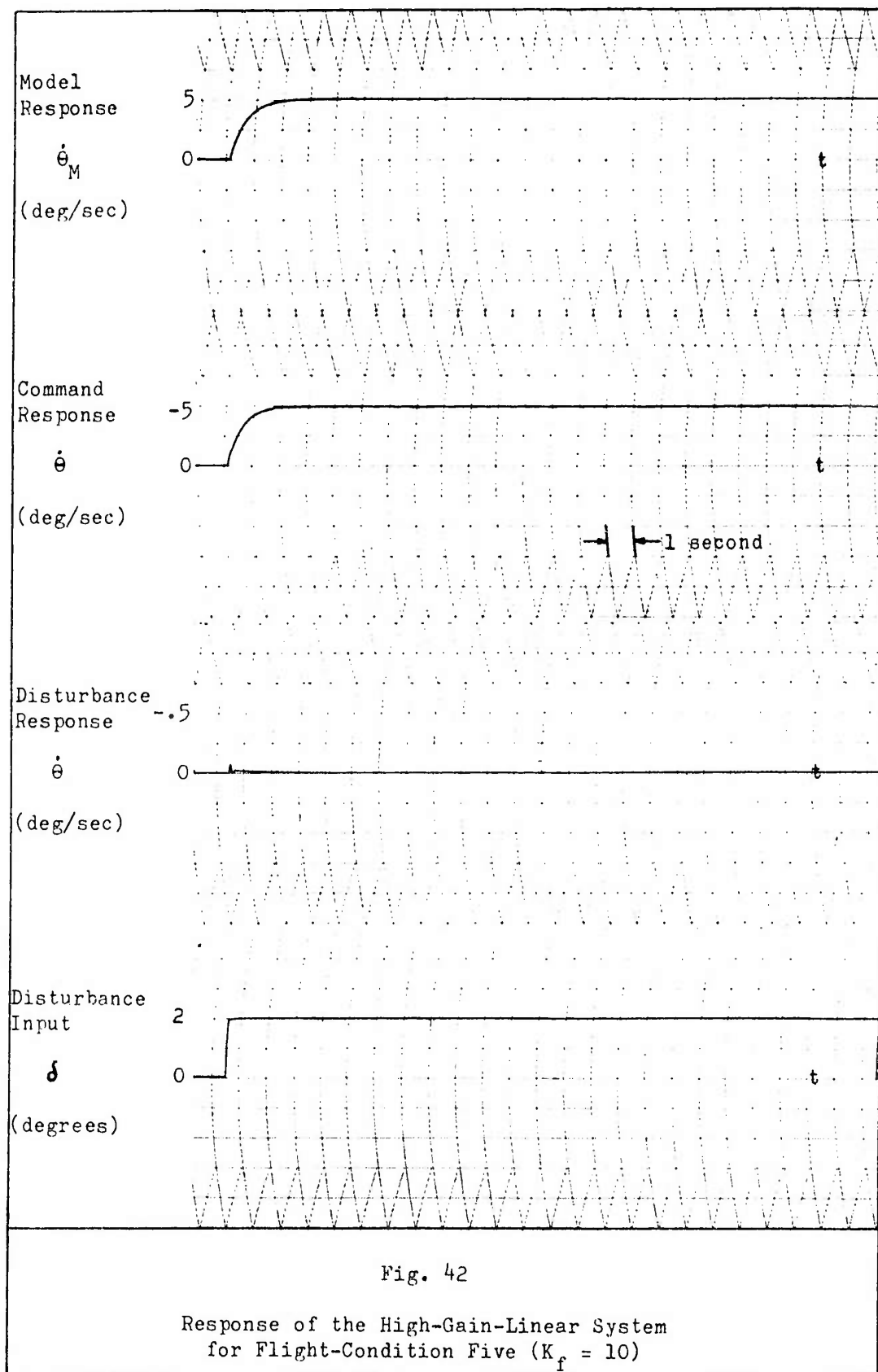


Fig. 42

Response of the High-Gain-Linear System
for Flight-Condition Five ($K_f = 10$)

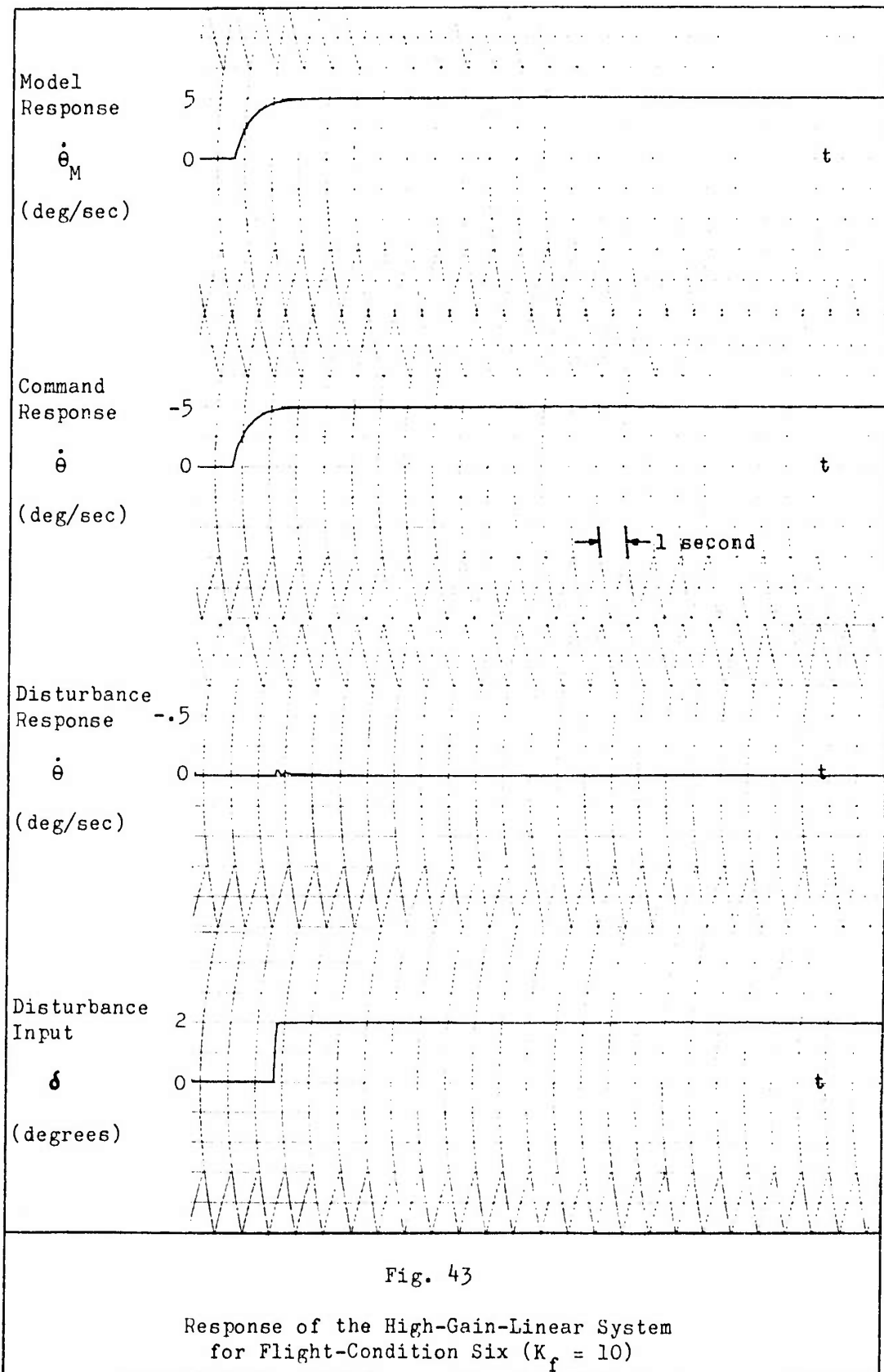


Fig. 43

Response of the High-Gain-Linear System
 for Flight-Condition Six ($K_f = 10$)

three, it is seen that the relative change in the magnitude of C/D is only 3 : 1 while the relative change in V , considering only the change in M_d , is 240 : 1.

With $K_f = 10$ Equation (46) shows that the static loop sensitivity for the feedback loop is $80.6 \times 10^{16} M_d$. By comparing this value with the values obtained from Equations (44) and (45) for the root-locus design, the frequency-response design has resulted in a reduction of the static loop sensitivity by a factor of 6.32×10^2 . This indicates the savings in the gain-bandwidth of L by the frequency-response design as compared to the root-locus design.

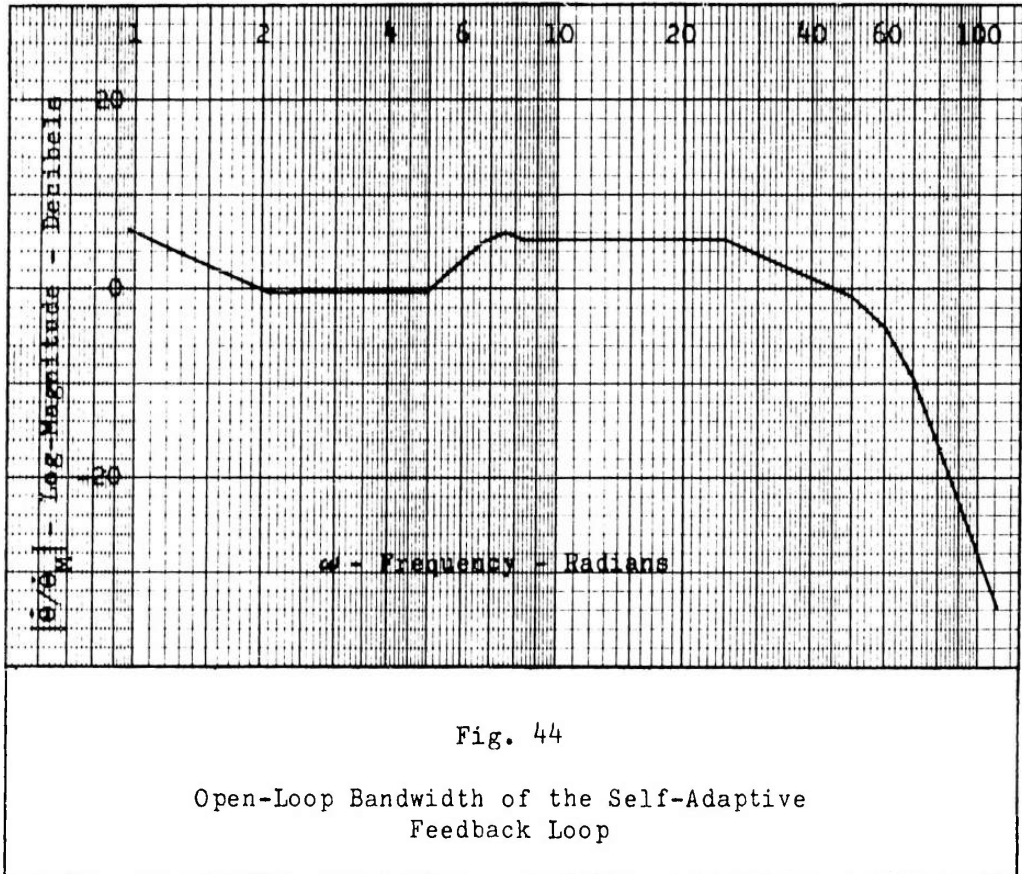
The design analysis revealed that the problem was basically to obtain the desired insensitivity for flight-condition one while maintaining stability for flight-condition three. The shaping of the compensator phase-angle and log-magnitude curves between the two extreme M_d cases was a problem of insuring an unconditionally stable system for all the intermediate flight conditions. The design and computer analysis showed that a high-gain-linear system can be designed to be insensitive to the vehicle-parameter variations and to meet the response criteria for command and disturbance inputs.

V. Comparison of the Systems and Conclusions

The comparison was limited to a linear analysis of the two flight-control systems; therefore, a selection of one system over the other will have to be made with qualifications dependent on further investigation into areas outside the scope of this study. A comparison of the two systems is made in the following areas: (1) the design considerations that are made when applying each design technique to the flight-control problem, (2) the control systems that resulted from the two methods of design, and (3) the response data obtained from the simulation of the systems. Conclusions drawn from the above comparison and recommendations of further areas of investigation are discussed at the end of this chapter.

Comparison of the Systems

Both systems employ lead compensation to increase the phase-margin frequency (ω_ϕ). The difference in the relative complexity of the compensation is attributed to the fact that in the high-gain-linear design the phase-angle curve must be shaped, prior to the 180° phase-crossover point, over a much greater range of frequency. The greater range of frequency is indicated by the difference in the open-loop bandwidth of each feedback loop at the maximum- M_g flight condition. Figure 44 shows that the open-loop bandwidth of the self-adaptive feedback loop is approximately 50 radians compared to 520 radians for the high-gain-linear system (from Table III). This gives an indication of the difference in



ω_ϕ for the two systems at flight-condition three. Although the purpose of the lead compensation is similar (to increase ω_ϕ), the fundamental difference in the gain of the systems leads to the wide separation in ω_ϕ .

As discussed in Chapter III, a gain changer is used in the self-adaptive design to provide a variable gain (K_G) in the forward branch. However, the use of the gain changer involves additional design considerations which relate to the shape of the locus. In order to make the pass band of the filter used in the gain-changer loop as small as possible, the loci must cross the imaginary axis at approximately the same frequency for all flight conditions. The loci must also cross the axis at a low slope so that as the gain

changes, the frequency of the limit cycle will not vary sufficiently to cause the limit cycle to be amplitude modulated by the filter. The above requirements must be taken into account: (1) when applying the lead compensation, (2) when selecting the system components (rate gyro, servo, and actuator) with their associated dynamics, and (3) when considering the effects on the loci caused by the vehicle-parameter variations.

In the high-gain-linear design, the forward-branch gain is fixed. The value of this fixed gain is dependent on the relationship of L to the desired system insensitivity for all flight conditions. Therefore, to obtain a value of fixed gain requires a translation of the response criteria in the time domain into sensitivity criteria in the frequency domain. Sensitivity is formulated by the sensitivity-function which is a measure of the amount of feedback $(1 + L)$ necessary to obtain the desired system insensitivity to vehicle-parameter variations and to minimize the effects of disturbances on the output. The magnitude of L_0 dictates the amount of the relative change in the output signal caused by a relative change of the vehicle dynamics (see Eq 25). The problem is therefore to determine the value of L_0 over the significant frequency range (slightly larger than the system bandwidth) that will maintain the relative changes of the output signal within the limits specified by the response criteria. Unfortunately, there is no empirical formula or direct mathematical relationship to relate the sensitivity requirement, based on the magnitude of L_0 , to the response specifications in the time domain. To avoid this problem of translation, a technique

was used in this study that proved very satisfactory. The system was first compensated to obtain at least a 10 db gain margin for all flight conditions. With the compensated system simulated on the computer, the magnitude of L_0 required to meet the response specifications was obtained by varying the additional gain factor (K_f) until the desired system response was obtained for flight-condition one (where $V = V_0$). This procedure allows the value of fixed gain to be determined so that the time response criteria are met.

The discussion thus far has compared the basic design considerations for the two systems. A comparison of the resulting control systems reveals two significant differences: (1) the value of static loop sensitivity, and (2) the bandwidth of the feedback loop. In the self-adaptive design the static loop sensitivity (K) remains relatively constant, varying from 3.65×10^{10} to 3.70×10^{10} . The reason for this small variation can be shown by changing Equation (14) of Chapter III into the form

$$K = 3.53 \times 10^9 K_G M_\delta \quad (48)$$

Since K_G is inversely proportional to M_δ , the value of K remains relatively constant. In the high-gain-linear design, the static loop sensitivity changes with each flight condition. Equation (46) of Chapter IV shows that the static loop sensitivity for the high-gain-linear system is

$$K = 8.06 \times 10^{16} K_f M_\delta \quad (49)$$

Since K_f is a constant value of 10, K increases proportionately with increases in M_g . The range of static loop sensitivity for the high-gain-linear system is from 17.7×10^{16} to 42.6×10^{18} . By comparing Equations (48) and (49), it is seen that the constant factor multiplying $K_f M_g$ is much larger than the constant factor multiplying $K_G M_g$. In the high-gain-linear design, the rate gyro and servo dynamics were canceled by complex compensation. The portion of the static loop sensitivity associated with this compensation is 6.86×10^6 . This means that the compensation causes a large increase in the gain-bandwidth of L ; however, since the rate gyro and servo dynamics were not in a frequency range where they could aid in the compensation of the system phase angle, cancellation compensation had to be used.

Since the major effect of the vehicle-parameter variations is caused by M_g , the variation of static loop sensitivity gives an indication of the variation in the closed-loop bandwidth of the feedback loop. Hence in the self-adaptive system, since K remained relatively constant, the closed-loop bandwidth of the feedback loop remains nearly constant. The closed-loop bandwidth ranges between seven and eight radians (depending on the flight condition) with the effect of the gain changer considered (ref page 28). In the high-gain-linear design the magnitude of the feedback element (H) is unity out to $\omega = 4400$ radians. This means that the closed-loop bandwidth of the feedback loop will be approximately equal to the open-loop bandwidth, which varied from 15.2 to 520 radians (from Table III). Although there is a large difference in the bandwidths

of the two feedback loops, the bandwidth of each system (model plus feedback loop) is essentially the same. This is so since: (1) both systems used the same model pre-filter, and (2) both systems were designed to have the bandwidth of the feedback loop several times greater than the model so that the dominant response of the system is essentially that of the model.

The comparison of the feedback-loop bandwidths was made to emphasize the need for an investigation of the effects of noise in the high-gain-linear system. The filtering property of the feedback loop is dependent on the closed-loop bandwidth for noise generated between the model and the input to the feedback loop. For feedback-transducer noise, the filtering property is determined by the open-loop bandwidth. With high system gain, which implies a large open-loop bandwidth, there is also the possibility of saturation due to noise or large disturbances. The high-forward-branch gain is in the feedback branch for a disturbance input. If saturation occurs in the feedback branch, the feedback signal could be reduced to the point of degrading the disturbance response. If saturation due to noise occurs in the feedback loop, the system response to a command input could also be degraded. Hence, the possible effects of saturation should be considered for future investigation. Since the effects of nonlinearities (hysteresis and saturation) and a noise analysis were not included in this study, no further attempt was made to refine the high-gain-linear system beyond that which was required to meet the command and disturbance response criteria.

The response of the self-adaptive system to a command input revealed a slow rise to the commanded pitch rate for three flight conditions. As discussed in Chapter III, the delay in reaching the steady-state value is caused by the closed-loop pole which lies on the real axis between the integrator pole at the origin and the aircraft zero. At flight-condition four, the residue of the real pole was large enough to prevent the system from meeting the response criteria. The response at flight-conditions one and five showed the effects of the real pole; however, the residue was small enough to allow the response to reach 90 percent of the commanded value within three seconds. The simplest method to decrease the effect of the real pole is to increase the static loop sensitivity. As mentioned in Chapter III, the advanced design of the self-adaptive system yields a higher static loop sensitivity which results in a system response that meets the criteria for all flight conditions.

In contrast, the high-gain-linear system meets the command response criteria for all flight conditions. The small variation of the system response from that of the model indicates the insensitivity of the system to changes in the vehicle parameters.

The disturbance response of both systems meets the criteria for all flight conditions. The responses differ only in the relative change in magnitude between the low- M_0 and high- M_0 flight conditions. The high-gain-linear response changed in a ratio of 3 : 1, while the self-adaptive response changed essentially in the same ratio as M_0 (240 : 1). The difference in the reduction of the disturbance responses for the two systems is attributed to:

(1) the large difference in the values of the static loop sensitivities at the low- M_δ condition, and (2) the static loop sensitivity of the self-adaptive system remains relatively constant, whereas the static loop sensitivity of the high-gain-linear system increases proportionately with M_δ . The combination of wide bandwidth and high gain in the high-gain-linear system provides a large, fast responding feedback signal to cancel the disturbance on the input.

Conclusions and Recommendations

Based on the comparison of the two pitch-rate control systems, the following conclusions are made.

1. A high-gain-linear system can be designed to be insensitive to the variation of vehicle parameters so that the response to command and disturbance inputs can be controlled.

2. Using the more economical frequency-response method, the high-gain-linear design technique is a more direct design procedure. In addition to designing the system to meet the response criteria, the self-adaptive technique requires the design of the gain-changer loop. This involves the considerations associated with the loci that cross the imaginary axis.

3. Based on the linear analysis and response data obtained, the high-gain-linear system is selected as the preferred system with the qualification that further evaluation be made to determine the effects of noise and nonlinearities on the system performance.

In order to make a final selection without qualifications, the following recommendations are made for further investigation.

1. It is recommended that a study be made of the effects of noise and nonlinearities on the performance of the high-gain-linear system. It is suggested that further refinements of the system design be attempted before conducting this study.

2. It is recommended that the possibility of using other servo and rate gyro components with dynamics that will meet the necessary operational requirements and that are in a range where they can be employed in the phase-angle compensation. This would eliminate the necessity of compensation to cancel these dynamics.

3. It is recommended that a study be made to determine the feasibility of using a simple gain change in the high-gain-linear system. The requirement for a large magnitude of L_0 to obtain the system insensitivity is based on the low- M_0 flight condition. Figure 31 shows that at the high- M_0 flight conditions the magnitude of L is large enough to obtain the system insensitivity without the fixed gain (K_f) in the system. A simple gain change could be made as a function of dynamic pressure to remove the fixed gain at the high- M_0 flight conditions. The purpose of the gain change is to reduce the bandwidth of the system at the high- M_0 flight conditions.

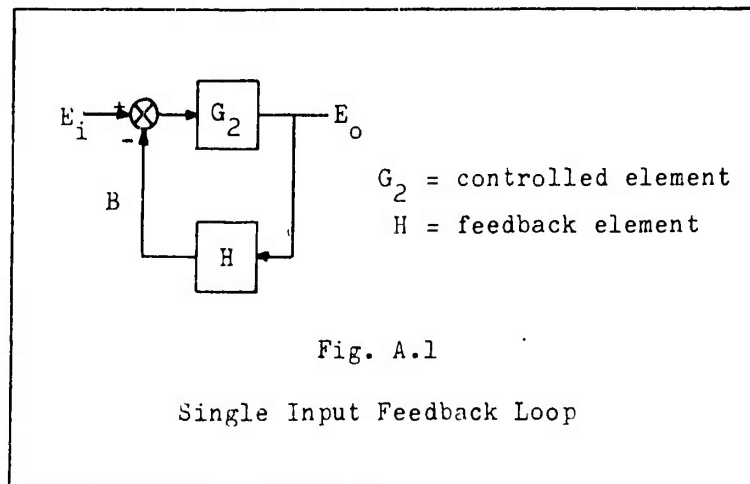
Bibliography

1. Black, H. S. "Stabilized Feedback Amplifiers." Electrical Engineering, 53:114-120 (January 1934).
2. Bode, H. W. Network Analysis and Feedback Amplifier Design. New York: D. Van Nostrand Co., Inc., 1945.
3. Boskovich, B., G. H. Cole, and D. L. Mellen. Advanced Flight Vehicle Self-Adaptive Flight Control System (Confidential). WADD TR 60-651, Part I. Wright-Patterson Air Force Base, Ohio: Aeronautical Systems Division, September 1960.
4. D'Azzo, J. J. and C. H. Houppis. Feedback Control System Analysis and Synthesis. New York: McGraw-Hill Book Co., Inc., 1960.
5. Hendrick, R. C. Automatic Gain Control of a Feedback Control System by Limit Cycle Amplitude Regulation. Thesis. Minneapolis, Minnesota: University of Minnesota, March 1961.
6. Horowitz, I. M. "Fundamental Theory of Automatic Linear Feedback Control Systems." IRE Transactions on Automatic Control, AC-4:5-19 (December 1959).
7. ----- "Plant Adaptive Systems Versus Ordinary Feedback Systems." IRE Transactions on Automatic Control, AC-7:48-56 (January 1962).
8. ----- Synthesis of Feedback Systems. New York: Academic Press, Inc., 1963.
9. Johannes, R. P. Study of a Self-Adaptive Control System Including Simulation and Effects of Variation of the System Dynamics. Thesis. Wright-Patterson Air Force Base, Ohio: Air Force Institute of Technology, March 1961.
10. Karplus, W. J. and W. W. Soroka. Analog Methods: Computation and Simulation (Second Edition). New York: McGraw-Hill Book Co., Inc., 1959.
11. Ostgaard, M. A., E. B. Stear, and P. C. Gregory. The Case for Adaptive Controls. Unpublished paper. Wright-Patterson Air Force Base, Ohio: Flight Control Laboratory, n. d.
12. Reed, M. W., J. A. Wolfe, and R. D. Mellen. Advanced Flight Vehicle Self-Adaptive Flight Control System. WADD TR 60-651, Part IV. Wright-Patterson Air Force Base, Ohio: Aeronautical Systems Division, June 1962.

Appendix A

Bode's Fundamental Feedback TheoremsUsing Control Theory Terminology

The following material is based on Bode's development in his text on feedback amplifier design (Ref 2:31-35). From Fig. A.1 without the feedback circuit (i.e. $H = 0$) the output voltage E_o



is related to the input voltage E_i by

$$E_o = G_2 E_i \quad (A.1)$$

When the feedback element is inserted, the following relationship exists between the output voltage and the sum of the input and returned voltage B :

$$E_o = G_2 [E_i + (-B)] = G_2 (E_i - B) \quad (A.2)$$

But the returned voltage is related directly to the output by

$$B = H E_o \quad (A.3)$$

With B eliminated from Equations (A.2) and (A.3)

$$E_o = G_2(E_i - HE_o) = \frac{G_2}{1+G_2H} E_i \quad (\text{A.4})$$

Comparison of Equations (A.1) and (A.4) leads to the first theorem:

Theorem 1: Feedback reduces the output of the circuit by the factor $1+GH$.

Where G is the total forward-branch transmission with respect to the input voltage E_i ($G = G_2$ in Fig. A.1). The factor $1+GH$ is analogous to Bode's general term "feedback" and later defined as "return difference" for a single-loop structure.

If Equation (A.4) is differentiated, keeping H and E_i constant, the following result is obtained:

$$\frac{dE_o}{E_o} = \frac{1}{1+G_2H} \frac{dG_2}{G_2} \quad (\text{A.5})$$

The quantities dE_o / E_o and dG_2 / G_2 represent the corresponding relative changes in the output voltage and the controlled element.

This leads to the second theorem:

Theorem 2: The relative change in the output voltage, caused by a relative change in the controlled element, is reduced by feedback in the ratio $(1+GH) : 1$.

This theorem implies that if the open-loop transfer function G_2H is much greater than unity, the output is almost independent of variations in the controlled element because of the nature of feedback.

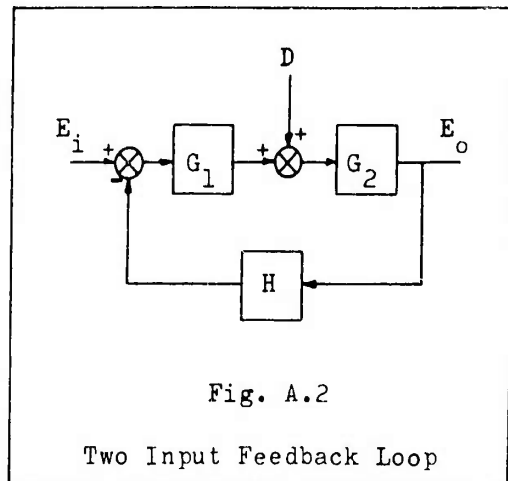
Equation (A.6) is obtained from Equation (A.4) and shows

$$\frac{E_o}{E_i} = \frac{G_2 H}{1 + G_2 H} \frac{1}{H} \quad (\text{A.6})$$

the effect of the feedback element on the output. Considering $G_2 H \gg 1$ implies $G_2 H / (1 + G_2 H) \approx 1$. This condition implies that the output can be considered to vary inversely with the transmission through the H element or, in other words, is approximately proportional to the H element loss. It further can be seen that for slight variations of the H element the output is greatly affected.

In Figure A.2, D represents the generation of noise or disturbance between the controlling element (G_1) and the controlled element (G_2). Let the input voltage (E_i) be zero. The output voltage is related to D by the following equation:

$$E_o = \frac{G_2}{1 + GH} D \quad (\text{A.7})$$



where G is the total forward-branch transmission ($G_1 G_2$) with respect to the input voltage E_i . Without the feedback branch the output is

$$E_o = G_2 D \quad (\text{A.8})$$

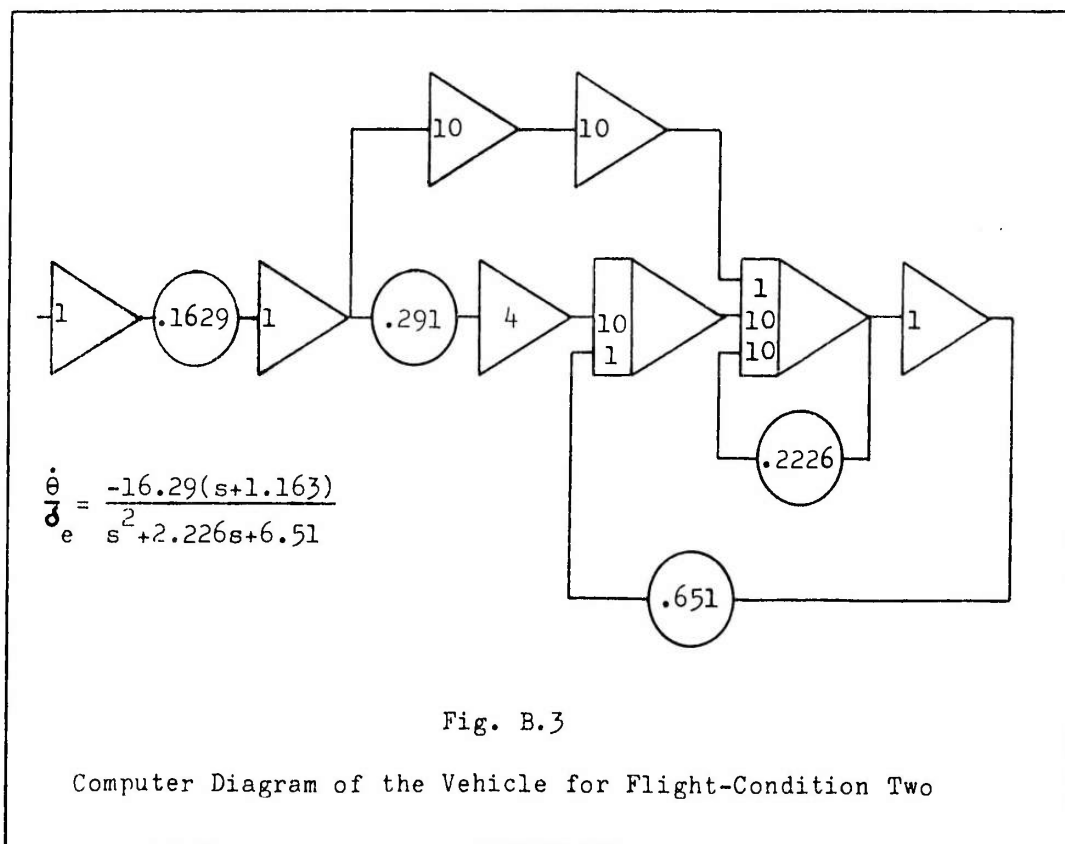
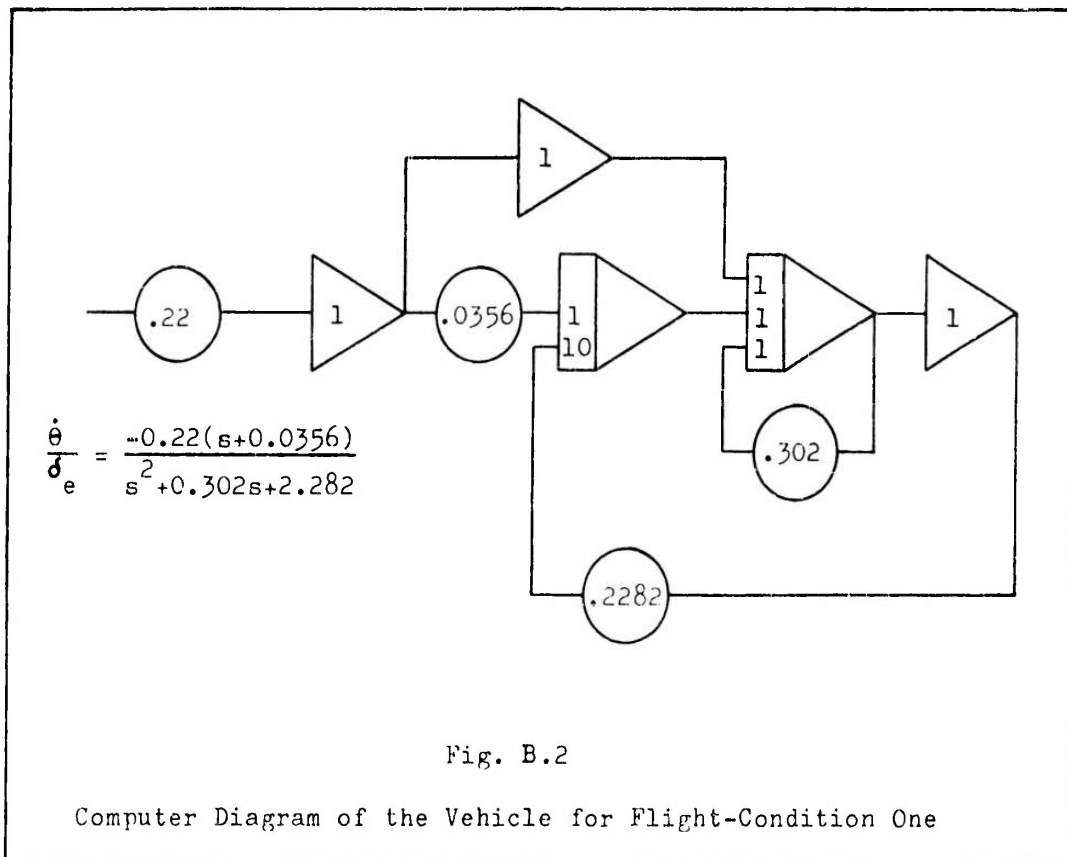
Equations (A.7) and (A.8) lead to the third theorem:

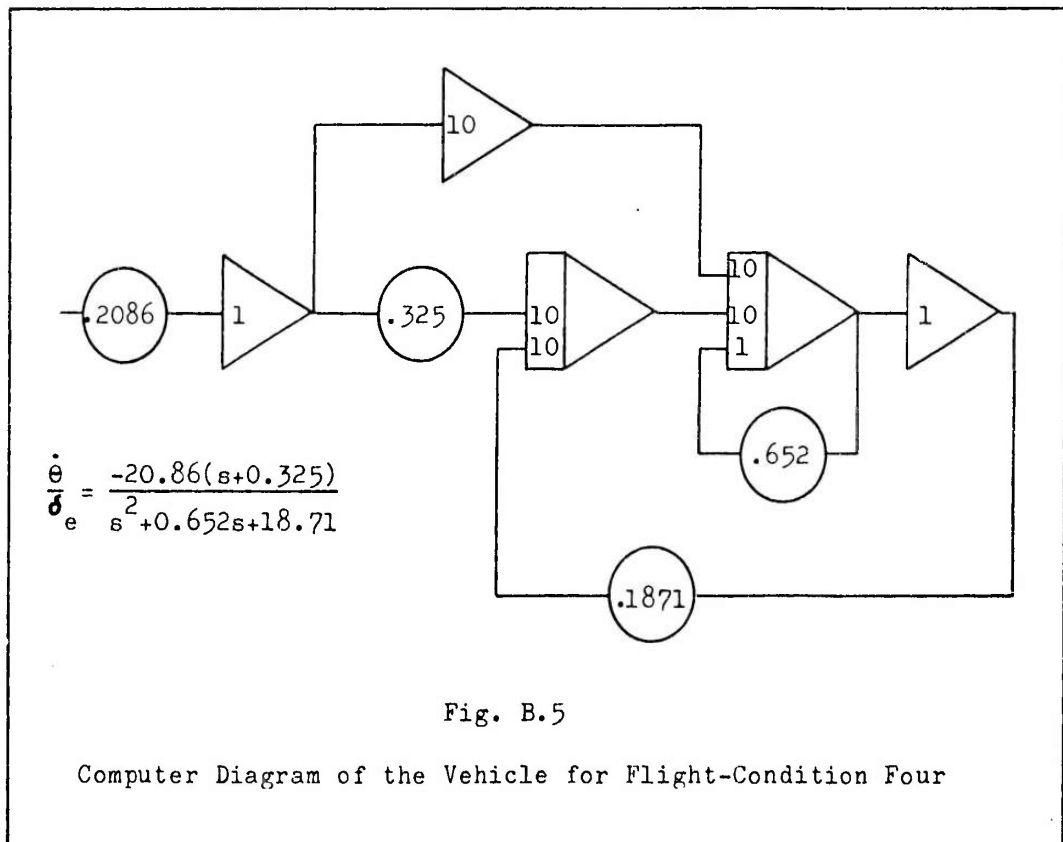
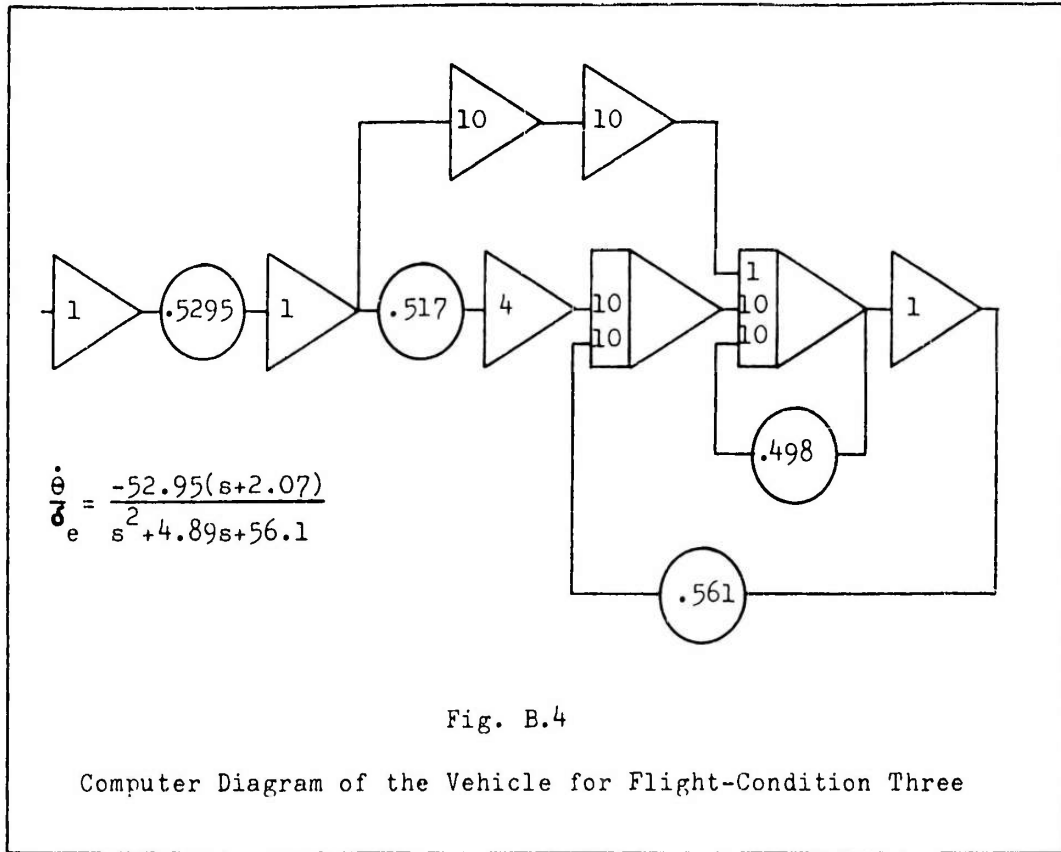
Theorem 3: The noise or disturbance level in the output of the circuit is reduced by feedback in the ratio $(1 + GH) : 1$.

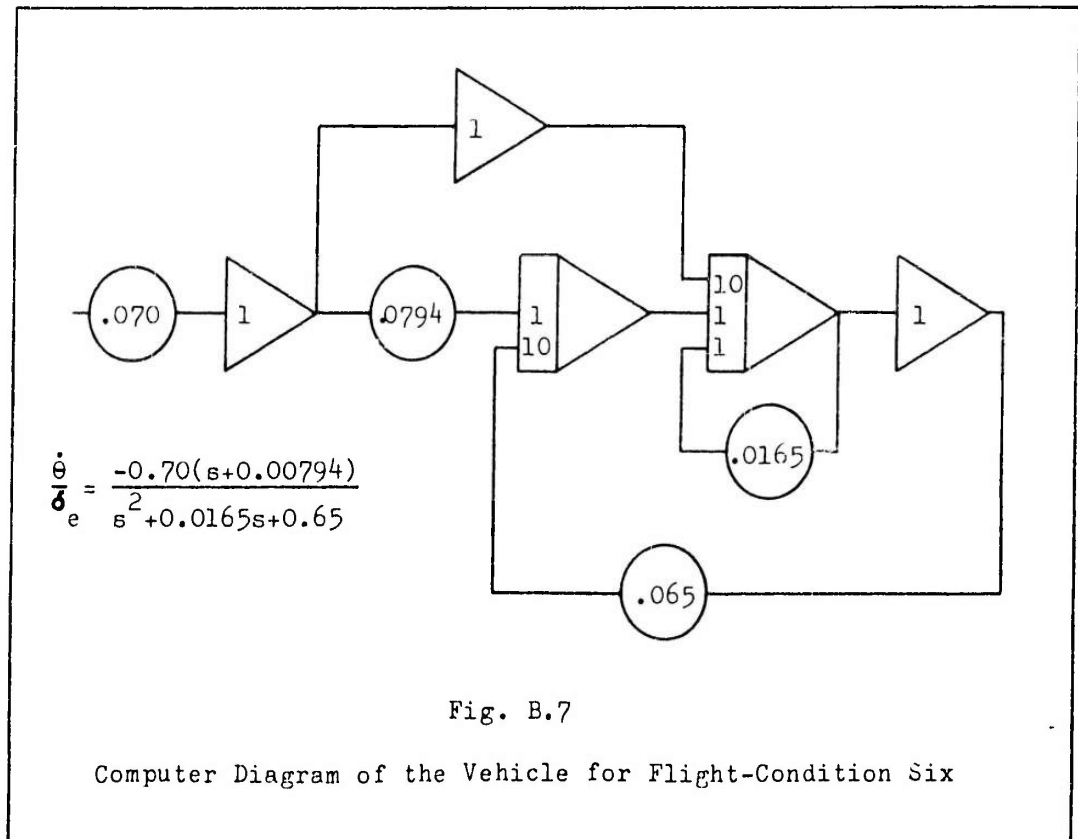
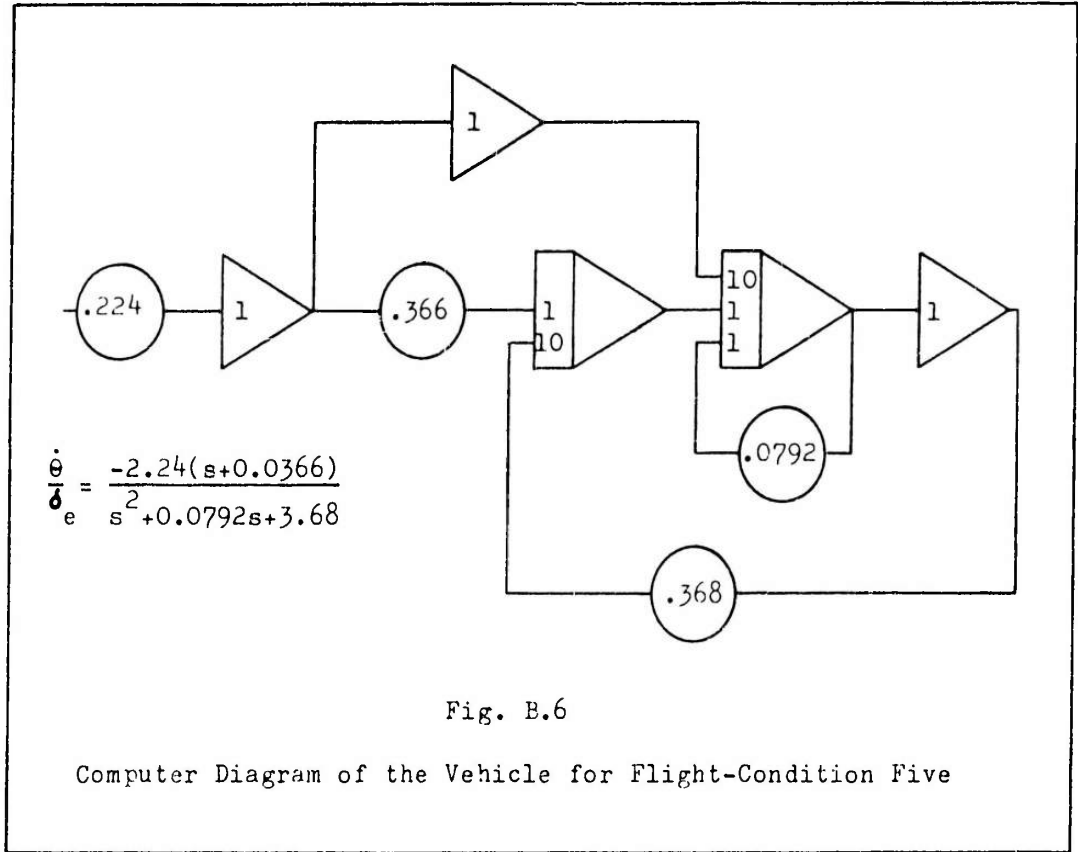
This theorem describes the important property of feedback in that it reduces the effects of noise and disturbances on the output.

GGC/EE/63-2

It should be understood that the blocks in the diagrams (i.e. G_1 , G_2 , and H) are circuits which have definite properties independent of one another. In other words, it is assumed there is no interaction or coupling between blocks except as shown by the connecting lines.







Appendix C

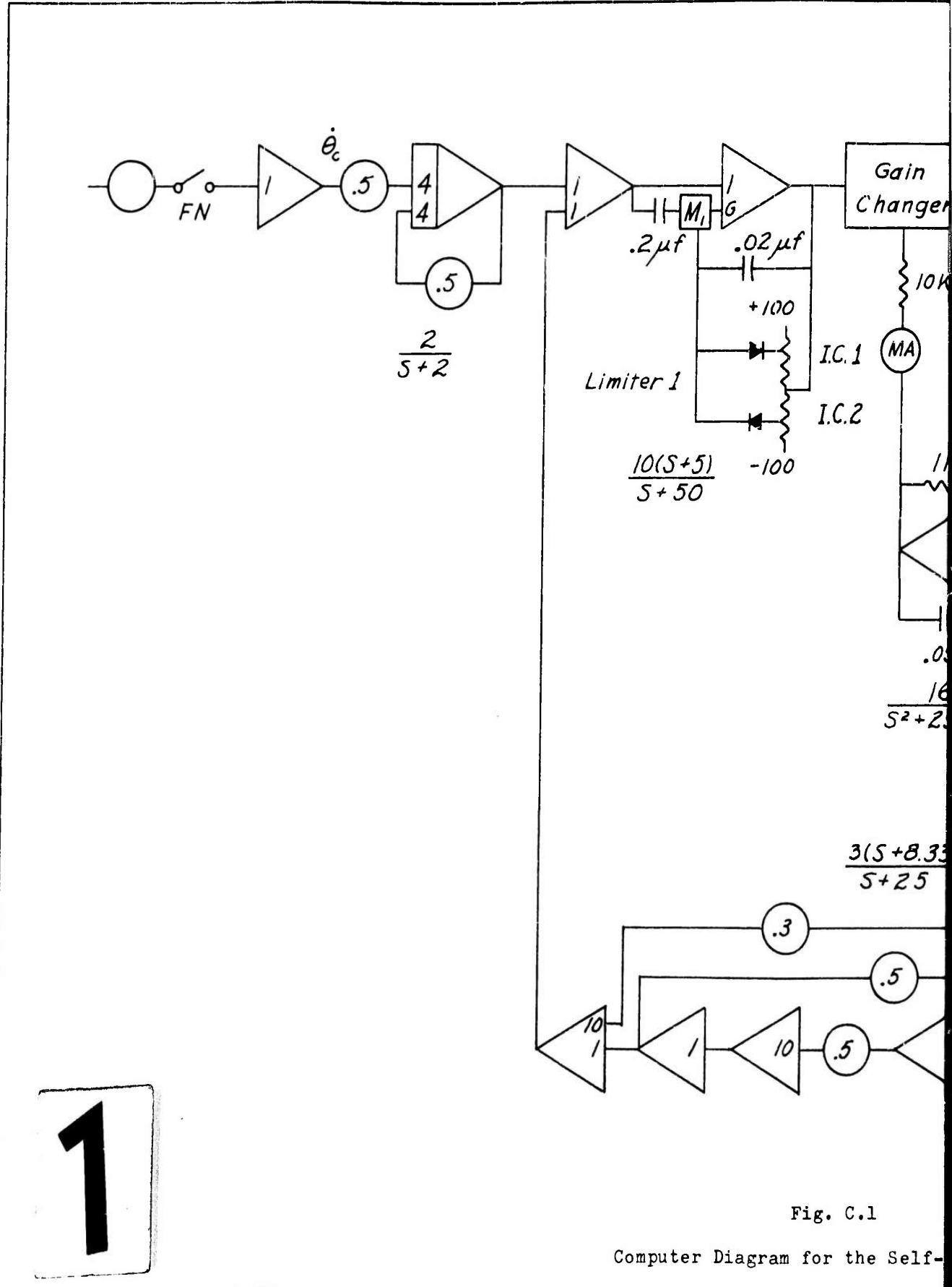
Analog Computer Circuit for Simulation of the
Self-Adaptive Pitch-Rate Control System

The computer circuit diagram for the self-adaptive system is Figure C.1. The transfer function of the various components of the system are shown below the computer circuit elements. The components may be determined by comparing this figure with Figure 11.

The gain changer used for the simulation is a battery-powered unit which operates in the same manner as the one used in the MH-96 system. The use of this gain changer requires that several unique features be added to the circuit. The ± 20 volt limiter is provided to limit the magnitude of the signal in the forward branch for large disturbance inputs. Since only small disturbance inputs were used in this thesis, the limiter did not have any effect on the performance of the system. The 10,000-ohm resistor on the output of the gain changer is for impedance matching. The load on the gain changer output must be in the 5,000 to 10,000-ohm range and, since the input impedance of the next amplifier is 100,000 ohms, the matching resistor must be added to the circuit. The circuit connecting the output of the proportional-plus-integral circuit to the bandpass input of the gain changer is essentially a filter. The four amplifiers form a bandpass filter with a center frequency at 33 radians. A limiter is placed on the first of these amplifiers to limit the amplitude of limit-cycle oscillations fed into the gain computer. This has the effect of limiting the decrease in gain of the system. The

Fig. C.1

Computer Diagram for the Self-Adaptive System



1

Fig. C.1

Computer Diagram for the Self-

GGC/EE/63-2

limiter is set at two to three times the amplitude of the nominal limit cycle. The amplitude of the limit cycle appearing at the output of the servo is established by setting the potentiometer (K) at a value which allows the current flowing into the bandpass input to be 0.5 milliamperes (rms) with a set-point voltage of 10 volts. The 10,000-ohm resistor in the lead to the bandpass input of the gain changer is also for impedance matching.

Appendix D

Location of Dominant Closed-Loop Poles
for the Fixed-Gain Design

To show that the dominant closed-loop poles determined from condition one lie farthest from the compensator zeros in the root-locus design of Chapter IV, a simplified root locus (Fig. D.1) will be analyzed. The pole-zero plot contains the vehicle dynamics for all six conditions, a pole at the origin, and a double zero at $s = -3$. A unit circle is drawn with the center at $s = -3$ and the point on the circle which satisfies the root locus angle condition is determined for each vehicle condition. These points represent the intersection with the circle of the locus from an aircraft pole to the compensator zero. The static loop sensitivity (K) at these points is calculated so that the change in K from that of condition one may be calculated. If the increase in control-surface effectiveness (which is also the increase in the static loop sensitivity of the fixed-gain system) is greater than the change in K on the circle, then the closed-loop pole for that flight condition lies closer to the compensator zero than the pole for condition one. Table D.I shows the ratio of the change in K and the ratio of the increase in control-surface effectiveness (M_d) for each flight condition. Table D.I shows conclusively that the closed-loop poles for condition one lie farthest from the compensator zeros.

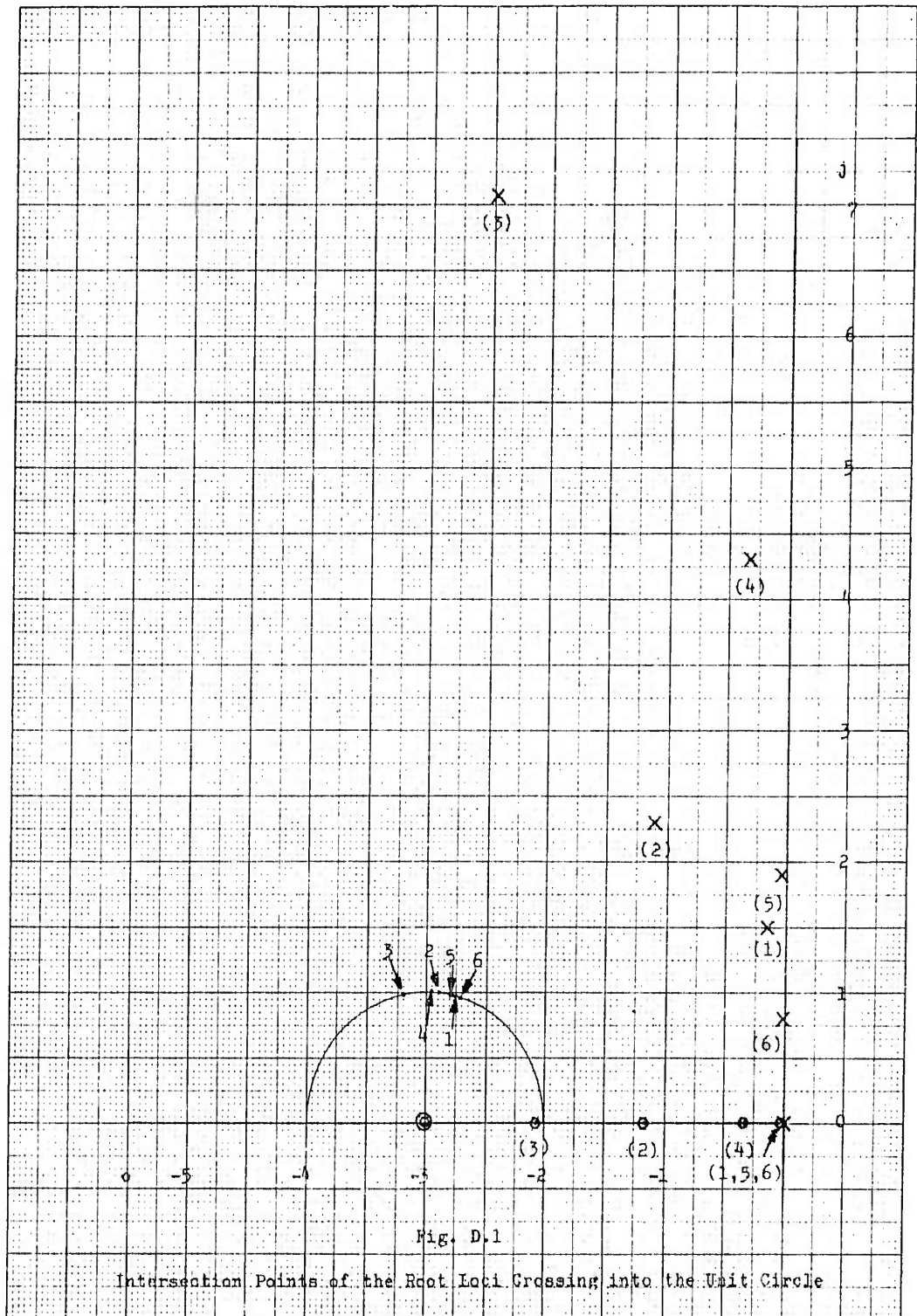


Fig. D.1

Intersection Points of the Root Loci Crossing into the Unit Circle

Table D.I

Ratio of Static Loop Sensitivity and Control Surface Effectiveness Compared to Flight Condition One

| Flight Condition | Ratio of the Change in K | Ratio of the Increase in M_δ |
|------------------|--------------------------|-------------------------------------|
| 1 | 1 : 1 | 1 : 1 |
| 2 | 0.86 : 1 | 74 : 1 |
| 3 | 11.25 : 1 | 240 : 1 |
| 4 | 2.84 : 1 | 95 : 1 |
| 5 | 1.17 : 1 | 10.35 : 1 |
| 6 | 0.90 : 1 | 3.17 : 1 |

Appendix E

Analog Computer Circuit for Simulation of the High-Gain-
Linear System from the Root-Locus Method of Design

The diagram for simulation of the system, based on Equation (44), appears in Figure E.1. Because of the noise generated by the elements used to simulate the feedback branch no data was taken using this circuit. In particular, the circuits with parallel capacitors in both the input and the feedback paths generated noise with peaks as high as 40 volts. When the entire circuit was connected, the amplifiers in the forward branch saturated causing a computer overload.

The pole and zero cancellations of the system were not simulated on the computer. For this reason, the transfer functions shown in Figure E.1 do not correspond directly to those shown in the block diagram of Figure 25.

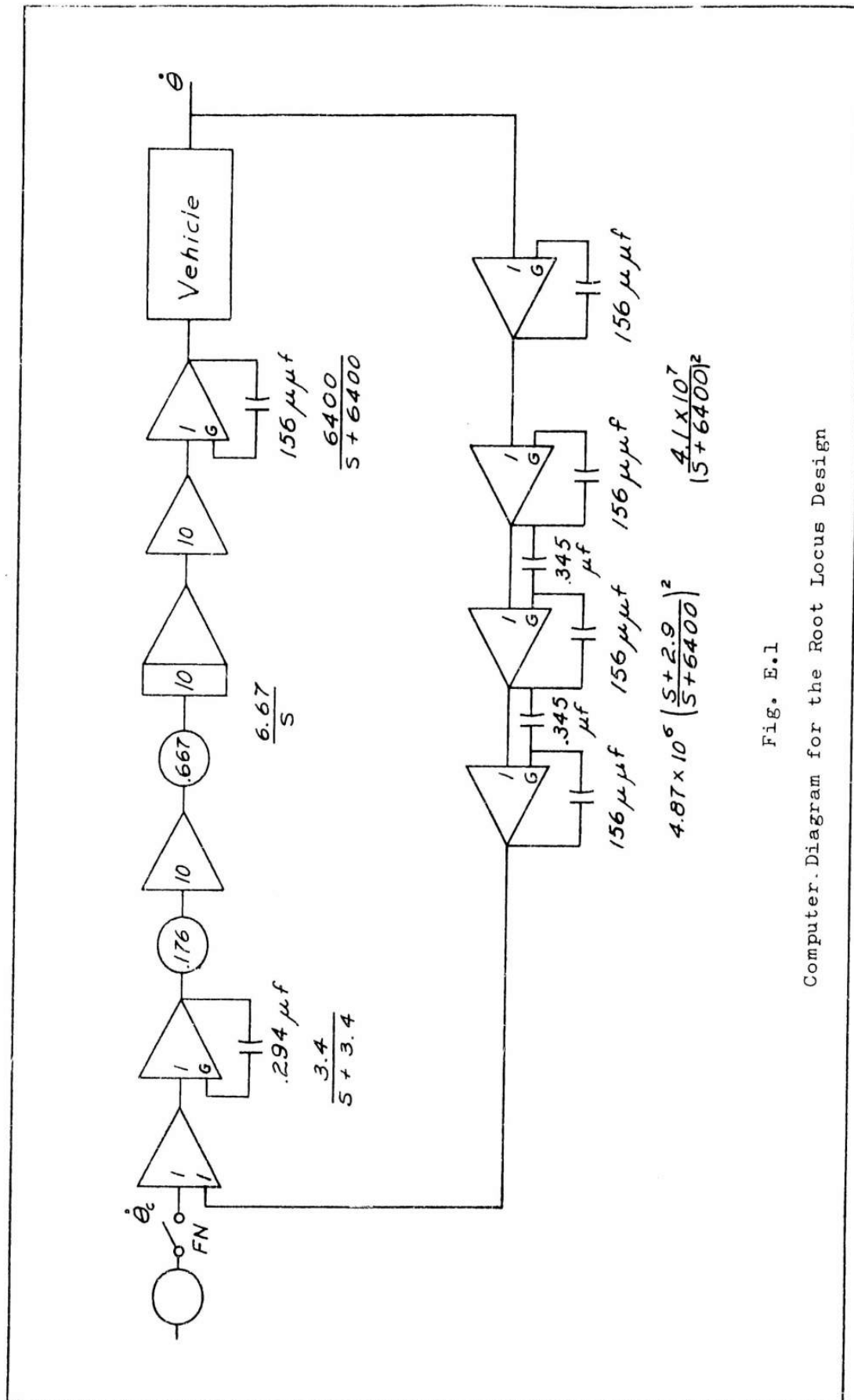


Fig. E.1

Computer Diagram for the Root Locus Design

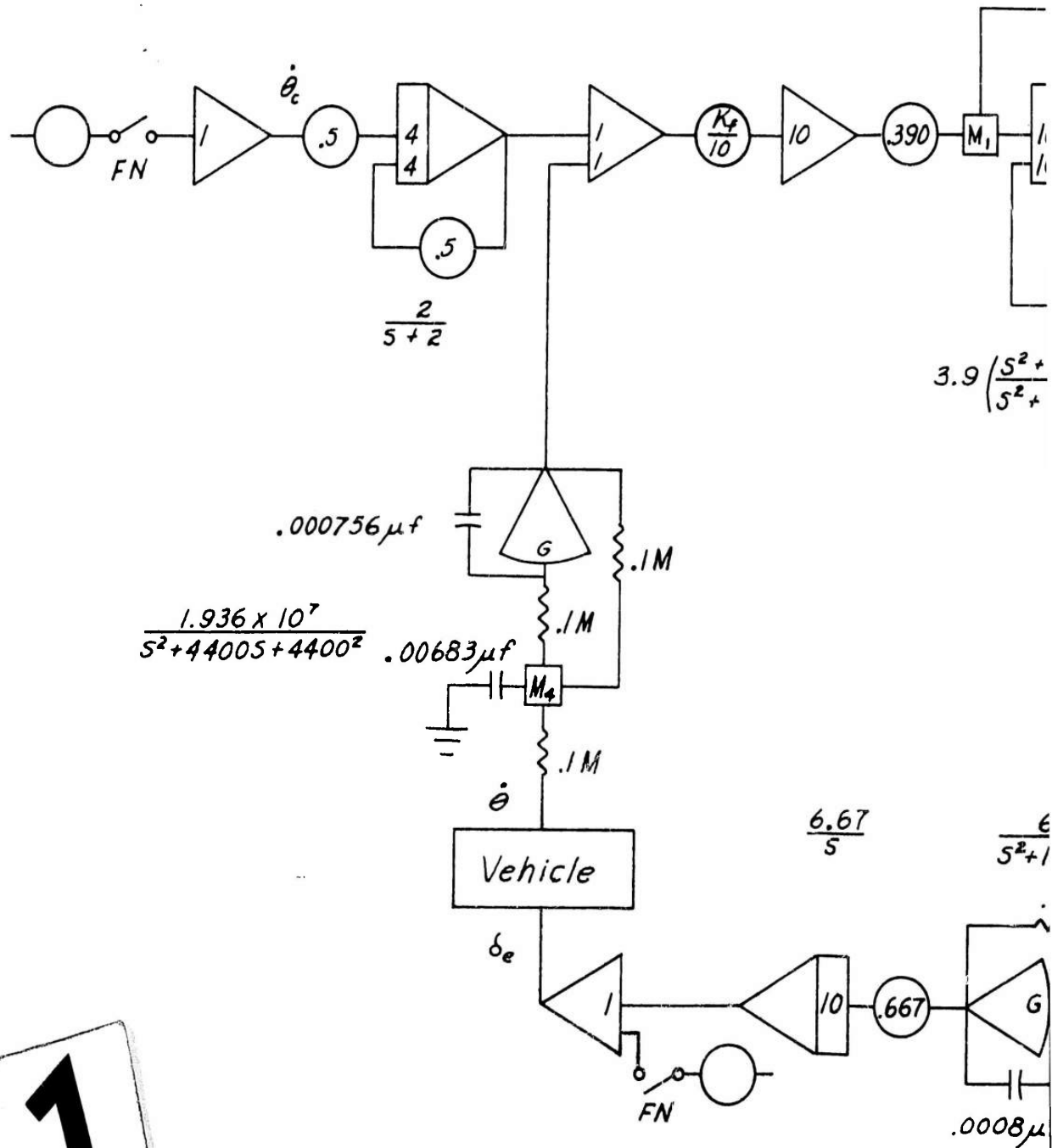
Appendix F

Analog Computer Circuit for Simulation of the High-Gain-Linear
System from the Frequency-Response Method of Design

The diagram of the computer simulation of the high-gain-linear system from which data was taken for this thesis is shown in Figure F.1. The simulation is based upon Equation (46) and since the cancellations that occur in the open loop transfer function are not simulated on the computer, the transfer functions shown on the computer diagram do not correspond directly to those shown in the block diagram of Figure 33.

Fig. F.1

Computer Diagram of the High-Gain-Linear System
Designed by the Frequency-Response Method



1

Fig. F.1

Computer Diagram of the High-Gain-L...
Designed by the Frequency-Respon...

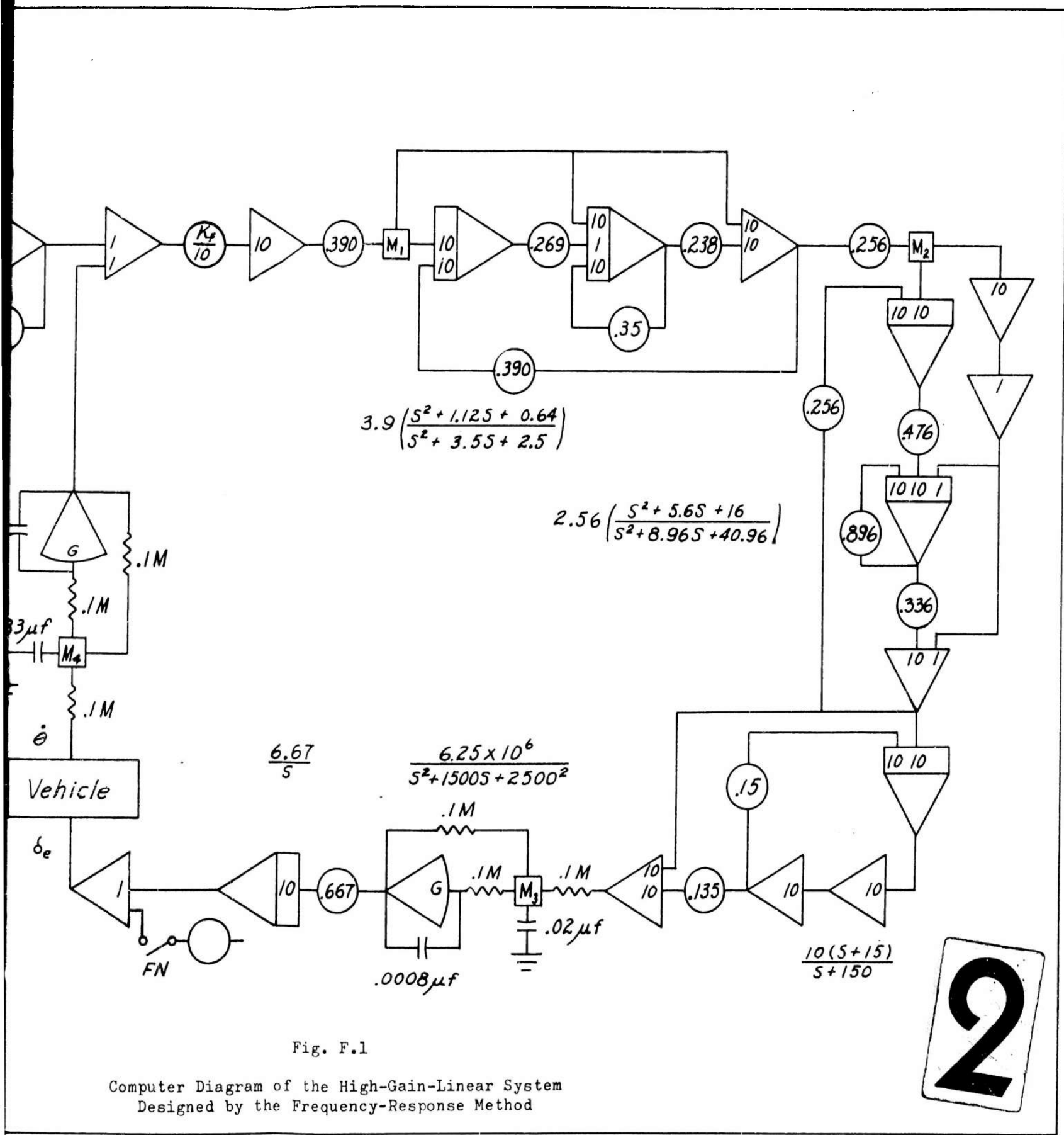


Fig. F.1

Computer Diagram of the High-Gain-Linear System
 Designed by the Frequency-Response Method

Vita

Captain Frazier Jackson Hellings

PII Redacted

He graduated from Ridley Park High School in 1951 and continued his education at the University of Miami, Coral Gables, Florida. In 1956, Captain Hellings graduated from the University of Miami and was awarded the degree of Bachelor of Science in Electrical Engineering. He worked as a Staff Engineer at Hycon Eastern, Inc., Cambridge, Massachusetts and in January 1957 he went on active duty with the United States Air Force. Prior to assignment to the Institute of Technology, Captain Hellings was a Communications and Electronics Officer at an Aircraft Control and Warning Squadron of the Air Defense Command.

Permanent address:

PII Redacted

